FLUVIAL ARCHITECTURE AND PALEOHYDRAULIC ANALYSIS OF ANCIENT RIVER DEPOSITS IN PLAN-VIEW AND 2-D VERTICAL OUTCROPS OF THE TURONIAN FERRON NOTOM DELTA, UTAH: FROM ALLOGENIC VALLEYS TO AUTOGENIC BARS

A Dissertation Presented to

the Faculty of the Department of Earth and Atmospheric Sciences

University of Houston

In Partial Fulfillment

of the Requirements for the Degree

Doctor of Philosophy

By

Mohammad Shahid Ullah

August 2015

FLUVIAL ARCHITECTURE AND PALEOHYDRAULIC ANALYSIS OF ANCIENT RIVER DEPOSITS IN PLAN-VIEW AND 2-D VERTICAL OUTCROPS OF THE TURONIAN FERRON NOTOM DELTA, UTAH: FROM ALLOGENIC VALLEYS TO AUTOGENIC BARS

_____

Mohammad S. Ullah

APPROVED:

_____

Dr. Joel Saylor, Chairman

_____

Dr. William R. Dupré, Committee Member

_____

Dr. Ian Evans, Committee Member

_____

Dr. Janok P. Bhattacharya, External Member
(McMaster University)

_____

Dr. Dan E. Wells, Dean
College of Natural Sciences and Mathematics

ACKNOWLEGEMENTS

My special thanks to my co-advisor Dr. Janok P. Bhattacharya for his enthusiasm, stimulating discussions, and for assisting with all aspects of the thesis project. His emphasis on critical thinking and his unwavering passion for geosciences has been always a great inspiration for me.

I thank Dr. Joel Saylor, my advisor and committee chairman for his unwavering support and guidance during the course of this research. I also thank Dr. William Dupré and Dr. Ian Evans for serving on my committee and for their valuable input and suggestions during the course of this research.

My special thanks to my dear friends Chenliang Wu and Benjamin Browning for contributing in my research, coauthoring my manuscript, and for all the help in preparing this dissertation. The research wouldn't be possible without their help in and outside the field. I also thank my fellow colleagues of the QSL Consortium, Yangyang Li and Ben Richards, for helping me in the fieldwork. I would like to thanks Macos Mendez for his outstanding assistance during the fieldwork in Utah.

My deepest gratitude goes to my loving wife Farin, who has tirelessly supported me, with a 5 month baby, while this work was underway. My deepest appreciation is to my mother,

whose love and blessing are always with me in whatever I pursue. To her and my lovely wife, Farin, I dedicate this work.

This research acknowledges project funding from QSL consortium supporting companies, which include BP, ExxonMobil, Shell, Nexen, EcoPetrol, Inpex, and Pioneer. Thank you for your support.

FLUVIAL ARCHITECTURE AND PALEOHYDRAULIC ANALYSIS OF ANCIENT RIVER DEPOSITS IN PLAN-VIEW AND 2-D VERTICAL OUTCROPS OF THE TURONIAN FERRON NOTOM DELTA, UTAH: FROM ALLOGENIC VALLEYS TO AUTOGENIC BARS

An Abstract of a Dissertation Presented to

the Faculty of the Department of Earth and Atmospheric Sciences

University of Houston

In Partial Fulfillment

of the Requirements for the Degree

Doctor of Philosophy

By

Mohammad Shahid Ullah

August 2015

ABSTRACT

This study documents the facies architecture of large valley-scale, intermediate bar-scale, and small bed-scale fluvial elements in a compound incised-valley fill in the Cretaceous Ferron Notom Delta in southeastern Utah, U.S.A. The results are based on aerial LiDAR surveys, 24 measured sections, photomosaics, and 1800 paleocurrent measurements based on both plan-view and cliff exposures of exhumed meander belts within a compound valley-system. Cross-sectional observations from outcrops and comparisons with modern rivers reveal that autogenic confluence scours have diagnostic fill facies composed of single set of large steep foresets, and produces a single-story body in which a fifth-order scour is filled with unit-bar foresets, which in turn are overlain by a fourth-order surface capped by compound-bar deposits.

Although the downstream persistence of fluvial sandy facies along the entire stretch of the incised valley suggests a greater upstream control, it could not entirely erase the imprint of downstream sea-level rise as indicated by the “backwater effect”. The backwater transition is observed in fluvial deposits at the most downstream location and is marked by thickening of channel belt deposits tied to channel deepening towards the river mouth, reduction in average channel belt width related to a reduced rate of lateral migration, increased proportion of finer grains in channel belt deposits tied to reduced bed material flux, and a vertical translation from fluvial to tidal facies in the valley deposits. Findings from this study support the idea that the backwater zone is a fundamental transition in coastal rivers, across which preserved sedimentary bodies

display predictable geometric changes that can be observed in ancient fluvial systems. Paleogeographic reconstructions of the meander plain from plan-view data in the upper part of the valley fill show the evolution of three channel belts formed by successive phases of dominantly lateral expansion. Three types of architectural facies or macroforms were identified in the point bars in the channel belts. They are classified as – Type A or small-scale macroforms, the amalgamation of which produce large-scale compound bars; Type B macroforms, which are interpreted as unit bars; and Type C macroforms, which consists of large, steeply dipping upper flow regime (UFR) planar beds. Plan-view bedding architectural analysis, therefore, can be a useful method to identify various fluvial macroforms.

Table of Contents

CHAPTER 1 Introduction

1.1 Overview

This dissertation describes the facies architectural elements of fluvial deposits in a compound incised-valley system in the Cretaceous Ferron Notom Delta in southeastern Utah, U.S.A. It describes the facies architectural elements from large-scale valleys to bed-scale features. The dissertation starts by defining the criteria to distinguish the allogenic compound incised-valley fills from autogenic confluence scour fills in 2-D outcrops and used it to demonstrate that the extensive fluvial incisions in the Ferron Notom fluvio-deltaic wedge are valley-scale features. This is followed by a discussion of the effects of allogenically controlled backwater effects on fluvial lithofacies and architecture in the valley upstream and downstream. The dissertation concludes with a paleogeographic reconstruction of the valley-top meander belts using plan-view data and a description of various plan-form macroform architectures and associated facies in the meander belts from both plan-view and 2-D outcrops.

1.2 Dissertation Organization

This dissertation is composed of five chapters. Chapters 2, 3, and 4 make up the main body of the dissertation. Chapter 2 is the manuscript of the paper - Ullah, M.S., Bhattacharya, J.P., Dupr′e, W.R., 2015, Confluence scours versus incised valleys: Examples from the Cretaceous Ferron Notom Delta, Southeastern Utah, U.S.A.: Journal

of Sedimentary Research, v. 85, p. 445–458. Chapters 3 and 4 form the basis for manuscripts that will be submitted to a peer-viewed journal.

Chapter 2 documents the identification criteria of large-scale autogenic confluence scours in ancient fluvial systems, as may be analyzed using outcrop, well-log, core, or seismic data, and how they may be distinguished from allogenically induced incised valleys. Confluence scours in braided rivers occur where channel threads join together, producing erosional relief that may be considerably deeper than average channel depth. Based on cross-sectional geometries, a number of confluence scour fills were interpreted on well-exposed fluvial outcrops in a Cretaceous compound incised-valley system in the Notom delta complex of the Ferron Sandstone Member, Utah. Cross-sectional observations from outcrops and comparisons with modern rivers reveal that confluence scours have diagnostic facies comprising a single set of large steep foresets. A confluence scour fill produces a single-story body in which a fifth-order scour is filled with unit bar foresets, which in turn are overlain by a fourth-order surface capped by compound bar deposits. The story thickness in the confluence scour does not represent the average channel depth because confluence scours allow preservation of the deepest parts of channels as well as fully preserved abnormally thick stories. Therefore, I argue that interpretation of incised valleys in an ancient system associated with sequence boundaries should not be based on the relative depth of the erosional surface versus the number of average preserved channel stories. Rather, it should be defined by the erosional relief that is significantly deeper than the thickest fully preserved stories, which in a braided stream are likely to represent confluence scour fills.

Chapter 3 focuses on the effects of backwater length, which is an important control on the effect of downstream base level on upstream fluvial valley deposits. The terminal segment of the river emptying into an ocean is called the backwater zone (L), and has a length scale approximated by "backwater length (L_{bw})", which is proportional to the mean channel depth (H) and inversely correlated to river slope (S). Estimation of backwater limits along an extensively exposed fluvial long profile preserved in the Ferron compound incised-valley fills were made from paleo-flow depth measurements in combination with measured changes in base-level, estimated tidal range, and fluvial slope. Three major erosional surfaces partition the compound-valley fill into three sequences (V3, V2, and V1), which were documented based on detailed outcrop studies, field correlation, field photomosaics, paleocurrent data, and 24 measured sections at angles approximating depositional strike and dip in both upstream and downstream areas. The maximum backwater lengths calculated for the V3, V2, and V1 rivers in the downstream Nielson Wash area were between 6 - 16 km, 3 – 9 km, and 5 – 13 km respectively. The Caineville area is almost 20 km southwest of the Nielson Wash, and is estimated to lie significantly landward of the backwater transition. This backwater transition in the valley rivers in the Nielson Wash is marked by: a) a thickening of V2 channel belt deposits tied to channel deepening towards the river mouth due to scouring during high discharge, b) a reduction in average V3 channel belt width that may be related to a reduced rate of lateral migration, c) an increased proportion of finer grains in channel belt deposits tied to reduced bed material flux, d) a clear change in fluvial style in V2 from upstream braided to downstream single-thread meandering system, and e) a vertical translation from fluvial

to tidal facies in all three incised-valleys, which corresponds to a systematic vertical decrease in overall grain size. Findings from this study thus support the idea that the backwater zone is a fundamental transition in coastal rivers, across which preserved sedimentary bodies display predictable geometric changes.

Chapter 3 is the basis for a manuscript to be submitted to Journal of Sedimentary Research, which is coauthored by me and my co-advisor Dr. Janok Bhattacharya. I have collected all the data, drafted all the figures, and written most part of the paper and Dr. Bhattacharya did primarily the editing of the paper.

The primary aim of Chapter 4 was to reconstruct the paleogeographic evolution of a number of meander belts in Valley 1 from extensive plan-view exposures and to describe their plan-view macroform architecture. Attempts were also made to reconstruct the depositional architecture and cross sectional geometries of large-scale 2-D macroforms from extensive plan-view exposures. Based on the orientation of planform paleoflows, accretion directions, locations, and their positions in the overall stratigraphic interval, the preserved fluvial sequences were divided into three channel belts, designated A, B and C from oldest to youngest. Paleogeographic reconstructions of the bars in Channel belt A and Channel belt C indicate that the meander belts were primarily formed by successive phases of dominantly lateral expansion that caused a gradual increase in channel sinuosity with time. Channel-belt B, on the other hand, did not produce any large meander bends and was formed by mostly smaller-scale alternate bars in a relatively straight channel reach. Bars in Channel belt A and C have lower length/width ratios, as a consequence of their relatively high channel sinuosity. Three types of architectural facies

or macroforms were identified within the large-scale point bars delineated from bedding architecture analyses integrated with cross sections and plan-views, as well from their lithofacies descriptions. Among these, Type A macroforms represent dune-scale and bar-scale cross sets that form amalgamated compound bars. Type B macroforms were interpreted as unit bars, which consist of moderate- to steeply dipping single large foresets. Type C macroforms represent the large, steeply dipping upper flow regime (UFR) planar laminations and/or beds. The concurrence of UFR planar beds along cut banks in upstream areas of the interpreted point bars, indicate that the large UFR planar bed facies in the study area form due to lateral accretion over the deep channel thalweg upstream of a bend apex. Incorporating established models for determining geometry and paleohydraulics of point-bar deposits into the reconstructed plan-view architecture of the macroforms, we infer that with progressively increasing sinuosity, Type B and Type C macroforms become thicker and steeper in a 2-D vertical section, due to the greater variations in point bar geometry.

Chapter 4 forms the basis of a manuscript to be submitted to Sedimentology that is co-authored by me, my co-advisor Janok Bhattacharya, William Dupr′e, Unal Okyay, Chenliang Wu, and Benjamin Browning. I have collected most of the data used in this paper and part of the data is from Chenliang Wu, and Benjamin Browning. Unal Okyay was responsible for the GIS mapping.

Chapter 5 highlights some of the findings from my dissertation and few concluding remarks about future work.

CHAPTER 2: Confluence Scours versus Incised Valleys: Examples from the Cretaceous Ferron Notom Delta, Southeastern Utah, USA

2.1 Summary

Confluence scours in braided rivers occur where channel threads join together, producing erosional relief that may be considerably deeper than average channel depth. Based on studies of the continental-scale Ganges-Brahmaputra river system, it has been observed that the maximum depth of confluence scours by autocyclic process may reach up to four to five times the average depth of the incoming channels. Considering the possibility of such massive scours in an ancient fluvial system, it was argued that allogenically produced incised valleys at sequence boundaries should only be properly defined in ancient systems if the erosional relief is more than five times average channel depth.

Based on cross-sectional geometries, a number of confluence scour fills were interpreted on well-exposed fluvial outcrops in a Cretaceous compound incised-valley system in the Notom delta complex of the Ferron Sandstone Member, Utah. Cross-sectional observations from outcrops and comparisons with modern rivers reveal that confluence scours have diagnostic fill facies (single set of large steep foresets) and do not produce multistory sand bodies. A confluence scour fill produces a single-story body in which a fifth-order scour is filled with unit bar foresets, which in turn are overlain by a fourth-order surface capped by compound bar deposits. The story thickness

in the confluence scour does not represent the average channel depth because confluence scours allow preservation of the deepest parts of channels as well as fully preserved abnormally thick stories. Therefore, I argue that interpretation of incised valleys in the ancient system associated with a sequence boundaries should not be based on the depth of the erosional surface versus the number of average preserved channel stories. Rather, it should be defined by the erosional relief that is significantly deeper than the thickest fully preserved stories, which in a braided stream are likely to represent confluence scour fills.

2.2 Introduction

The convergence of multiple threads in a river or at tributary junctions in a drainage basin often leads to significant erosion of the underlying riverbed and creation of an exceptionally deep scour for subsequent sediment deposition, which is referred to as a confluence scour (Fig. 2.1). Confluence scours are intrinsic or autogenic and are often described in braided rivers, which, in most cases, are considerably deeper than the average channel depth of incoming channels (Ashmore and Parker, 1983; Best, 1988; Best and Ashworth, 1997). Confluence scours reflect significant changes in downstream flow velocity and are generally the result of vortices caused by changes in hydraulic conditions (Mosley, 1976; Best and Roy, 1991; Ashmore et al., 1992).

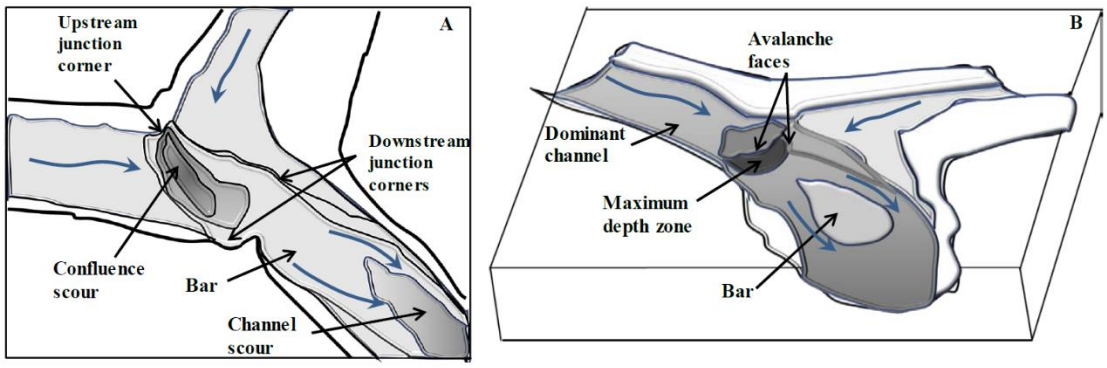

Figure 2.1 A) Vertical and B) oblique schematic diagram of a channel confluence showing various morpho-sedimentological zones and architectural elements.

There is currently some debate as to how to identify large-scale autogenic confluence scours in ancient fluvial systems, as may be analyzed using outcrop, well-log, core, or seismic data, and distinguishing them from allogenically induced incised valleys. Because confluence scours typically migrate both downstream and laterally and are filled by vertically and laterally extensive migrating bars, the entire channel belt could potentially be underlain by confluence scours. It has been hypothesized that large-scale confluence scours in outcrops, may resemble incised valleys, and may thus be interpreted as sequence boundaries formed during an allogenic fall in base level, as opposed to an autogenic scour (Salter, 1993). Best and Ashworth (1997) for example, described a scour at the confluence of the continental-scale Ganges – Brahmaputra River, Bangladesh, which is as large as 400 m x 2000 m and showed a downstream migration of 3.5 km in only 28 months. According to Best and Ashworth (1997), the maximum depth of this massive scour is about five times the average depth of the incoming Ganges and Brahmaputra Rivers. Several other studies involving numerical models and field data also demonstrated that the maximum depth of confluence scours could be up to four times the

average depth of incoming anabranch channels (e.g., Eilertsen and Hansen, 2008; Bridge and Demicco, 2008). Considering the possible occurrence of such laterally extensive, deep, migrating scours in ancient fluvial systems, it has therefore been argued that sequence boundaries, represented by incised valleys, should only be properly defined in ancient systems if the erosional relief is more than five times the average channel depth (Best and Ashworth, 1997; Fielding, 2007). These arguments also assumed that confluence scours have high preservation potential and should thus dominate the stratigraphic record of ancient braided streams. Therefore, it is important to distinguish large autogenic scours in alluvial channels from allogenic incisions associated with base-level change in the ancient record (Best and Ashworth, 1997; Fielding, 2007).

2.3 Geometry and Bed Morphology of the Scour Zone

The geometry of confluence scour zones depends mainly on the confluence angle of converging threads and on the relative width, depth, flow velocities, and discharge of the converging channels (Best, 1986, 1987). Confluence angles generally range from 15^{o} to 110^{o} and as they increase, confluence scours evolve from elliptical to more circular in plan-view. The shape of the scour also depends on the symmetry of thread orientation relative to the confluence direction. Contrast in discharge, flow velocity, and/or strength between incoming threads also results in variability of the scour shape and location of the deepest point. The dominance of one channel at a confluence can cause lateral migration of the scour (Ashmore and Parker, 1983). If the incoming channels have similar discharge,

the long axis of the scour tends to bisect the confluence angle; otherwise, the scour zone tends to be parallel to the direction of the channel with higher discharge.

At the scale of the confluence itself, Best (1986, 1987) and Ashworth et al. (1992) identified three morpho-sedimentological zones with distinct grain size, sediment structures, and bedform characteristics. These are: the upstream junction corner, the maximum depth zone, and the bar at the downstream junction corner (Fig. 2.1). The upstream junction corner, or the zone of flow stagnation, is characterized by finer-grained sediments on the river bed and a significant reduction of flow velocity, due to the divergence of incoming flows towards the outer bank of the channel (Best, 1988; Biron et al., 1993; De Serres et al., 1999). The maximum depth zone is characterized by an increase of grain size caused by a combination of factors, including flow acceleration due to the reduced area of the cross section, the reattachment of the secondary flows downstream of avalanche faces, and the influence of the mixing layer (Best, 1985). Steep avalanche faces form at the upstream end of the confluence and the sidewall of the maximum depth zone, which is parallel to the direction of the dominant incoming channel flow (Ashmore and Parker, 1983; Best, 1987, Eilertsen and Hansen, 2008). These avalanche faces dip into the scour zone, forming thick foreset deposits, together with a bar at one or both of the downstream corners of the junction (Mosley, 1976, Best, 1986).

2.4 Criteria for Identifying Confluence Scours

Confluence scours have not routinely been identified from cross-sectional analysis in ancient river deposits, in part because identification of braided rivers in 2-D

cross sections is not straightforward. The excess local accommodation created by a confluence scour on a riverbed is large enough for the channel to fill it up with a regular compound bar. Thus, when bars migrate across the confluence scour, they typically fill the scour pit with a unit bar consisting of a single set of large foresets (Bridge, 2006). The morphology of single large foresets in a confluence scour is similar to that of a Gilbert delta, where the height of the foresets is controlled by the depth of the scour. The unit bar in a confluence scour therefore does not scale to the average flow depth, but rather represents passive infilling of the entire scour by avalanching sediments. The left-over accommodation on top of the scour fill essentially represents the average channel depth, which would allow a compound bar to stack atop the underlying foreset-dominated unit bar. The compound bar represents return to background or non-scour condition and thus is not critical to the identification of the scour. Confluence scours therefore, produce an amalgamated two-tiered body comprising a deeper unit bar that actually fills the scour and a regular compound bar. Bristow and Best (1993) presented hypothetical models of confluence scours that also predict the presence of large-scale cross-stratification formed by progradation of the mouth bars of each incoming confluence channel in the scour zone.

In 2-D vertical cross sections, a confluence scour should be indicated by a single set of large foresets or cross-stratification, often at the angle of repose, which fills a scour zone. In most cases, a confluence scour fill produces a compound body in which the unit-bar foresets filling the scour are overlain by a compound bar deposit (Fig. 2.2). The thickness of the single-story unit bar should reach a maximum at the deepest part of the

scour zone, and its height should roughly scale to the confluence scour depth (Salter, 1993; Sambrook-Smith et al., 2005). Therefore, a confluence scour fill should not produce a multistory sand body. Rather, it will be marked by a fifth-order channel-base erosional surface (see Miall, 1985), filled with a single, oversize foreset deposit, capped by a secondary fourth-order macroform erosional surface that is overlain by the migrating compound-bar deposit (Fig. 2.2). Most importantly, the story thickness of the scour-filling unit bar would not represent the average channel depth, but would represent the scour depth.

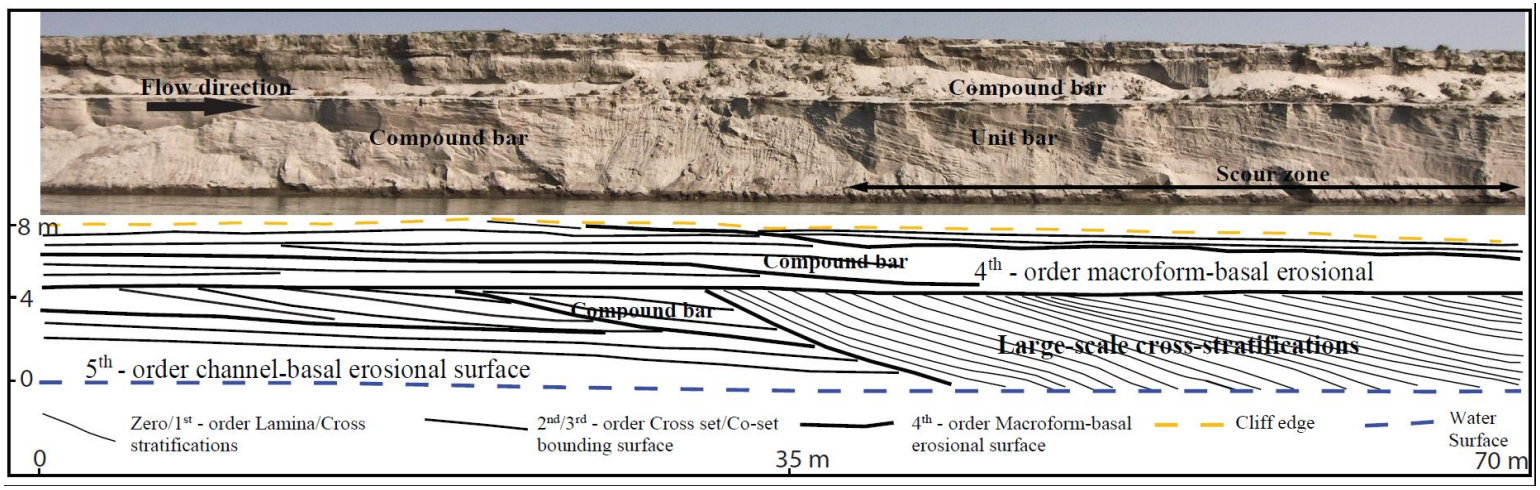

Figure 2.2 Example of a confluence scour fill in the Brahmaputra River, Bengal Basin, Bangladesh. As the compound bar system progrades over the confluence scour zone from left to right, it fills the scour with steep, large cross-stratification that form a single unit bar.

These criteria for identifying confluence scours are clearly demonstrated by a cross section of a confluence scour fill in the Brahmaputra River in Bangladesh, which is one of the largest braided river systems in the world (Fig. 2.2). As the compound-bar system progrades over the confluence scour zone from left to right, it fills the scour with large-scale, high-angle planar cross-stratification that form a single unit bar. The unit bar is characterized by a sand body that is at least 4 m thick above the water and is capped by a multistory compound bar consisting of dune scale cross sets. Although the base of the unit bar is submerged under water, extrapolation of the extent of this large-scale cross-stratification below the water surface provides some constraints regarding the depth of the confluence zone. The leeside slope angles of the foresets in the overlying compound bar range between 5 and 15^{o} before reaching the scour. This supports previous studies of Brahmaputra river bars, which demonstrated that the mean leeside slope angle of the dunes is 8.4° (Flood Action Plan 24, 1996b; Roden, 1998). It indicates that the majority of the dunes in the compound bars in the Brahmaputra do not dip at the angle of repose on their lee sides. However, these studies also showed that the maximum leeside slope angles of the dunes could be much higher than the mean leeside slopes (as high as 58°), due to intense eddying, which is also demonstrated in Figure 2.2. As the compound bar approaches the scour, the foresets become steeper and exceed the angle of repose, which results in the accretion of bar-margin slip-faces. This could result in sediment instability and might produce soft-sediment deformation structures. However, the slopes decrease gradually with a corresponding increase of foresets length as they prograde over the scour and fill it. Previous studies on the braided Brahmaputra River demonstrated

similarly steep, large planar cross sets produced by bar-margin slip-face accretion (Ashworth et al., 2000; Best et al., 2003). These studies described foresets up to 8 m from the thalweg to bartop and extend for 100 m as bars migrated both downstream and laterally into an adjacent deep thalweg.

A number of studies in ancient fluvial outcrops (e.g., Adams and Bhattacharya, 2005; Li et al., 2010), did not find any evidence of such deep confluence scours, despite their supposed high preservation potential. Moreover, these studies indicate that confluence scours do not extensively underlie entire channel belts, but are local features. In fact, very few studies of valleys in ancient fluvial outcrops show erosional relief greater than five times average channel depth (e.g., Korus et al., 2008). A number of studies demonstrate incised valleys that may only be 1.5 times to 3 times deeper than the formative channel (e.g., Adams and Bhattacharya, 2005; Feldman et al., 2005; Li et al., 2010; Reijenstein et al., 2011). These studies indicate that not all valleys associated with an ancient system are cut and initially filled by large-scale multithread braided rivers. Based on the comparison between large-scale macroforms and maximum scour depths in the modern Brahmaputra and the Hawkesbury River, Australia, Miall and Jones (2003) also concluded that the maximum depth of the scour is related to the scale of the river. Nevertheless, there remains disagreement on the scale dependence of confluence scours versus river size (Ashmore and Parker, 1983, Best, 1988, Best and Ashworth, 1997, Sambrook-Smith et al., 2005). This may reflect the fact that most examples of confluence scours described in the literature are based on small-scale laboratory experiments (Ashmore and Parker, 1983, Best, 1988) or on scours in modern large braided rivers

(Klaassen et al., 1988; Ashworth et al., 2000; Best et al., 2007). Well-documented examples of confluence scours and scour-filling sedimentary facies in ancient outcrops are lacking, in part because there have not been enough studies to that establish criteria to identify confluence scours in outcrop.

The aim of this paper is to describe and interpret confluence scours from 2-D cross-sectional exposures in a compound incised-valley fill at the top of the Cretaceous Ferron Sandstone Member of the Mancos Shale Formation in the Henry Mountains region, Utah, USA. The criteria for identifying confluence scours are first documented, based on cross-sectional geometry, sedimentary structures, and paleocurrent reconstructions, followed by a fuller explanation of confluence-scour scaling relationships. This will be used to develop criteria that can be applied to distinguish valley fill from deep confluence scours in ancient examples.

2.5 Regional Setting and Stratigraphy

The Ferron Notom delta was deposited from west to east into the Western Interior Seaway during the Middle to Late Turonian in the Late Cretaceous. This northwest flowing fluvial-deltaic clastic wedge was deposited in a rapidly subsiding retroarc foreland basin that formed by continued thrusting of the Sevier orogenic belt to the west (Fig. 2.3). The Notom delta complex was deposited in about 0.6 Myr, based on a biostratigraphic study by Peterson and Ryder (1975) and chronometric dating of volcanic sanidines by Zhu et al. (2012). The Ferron Sandstone Formation is bounded above by the

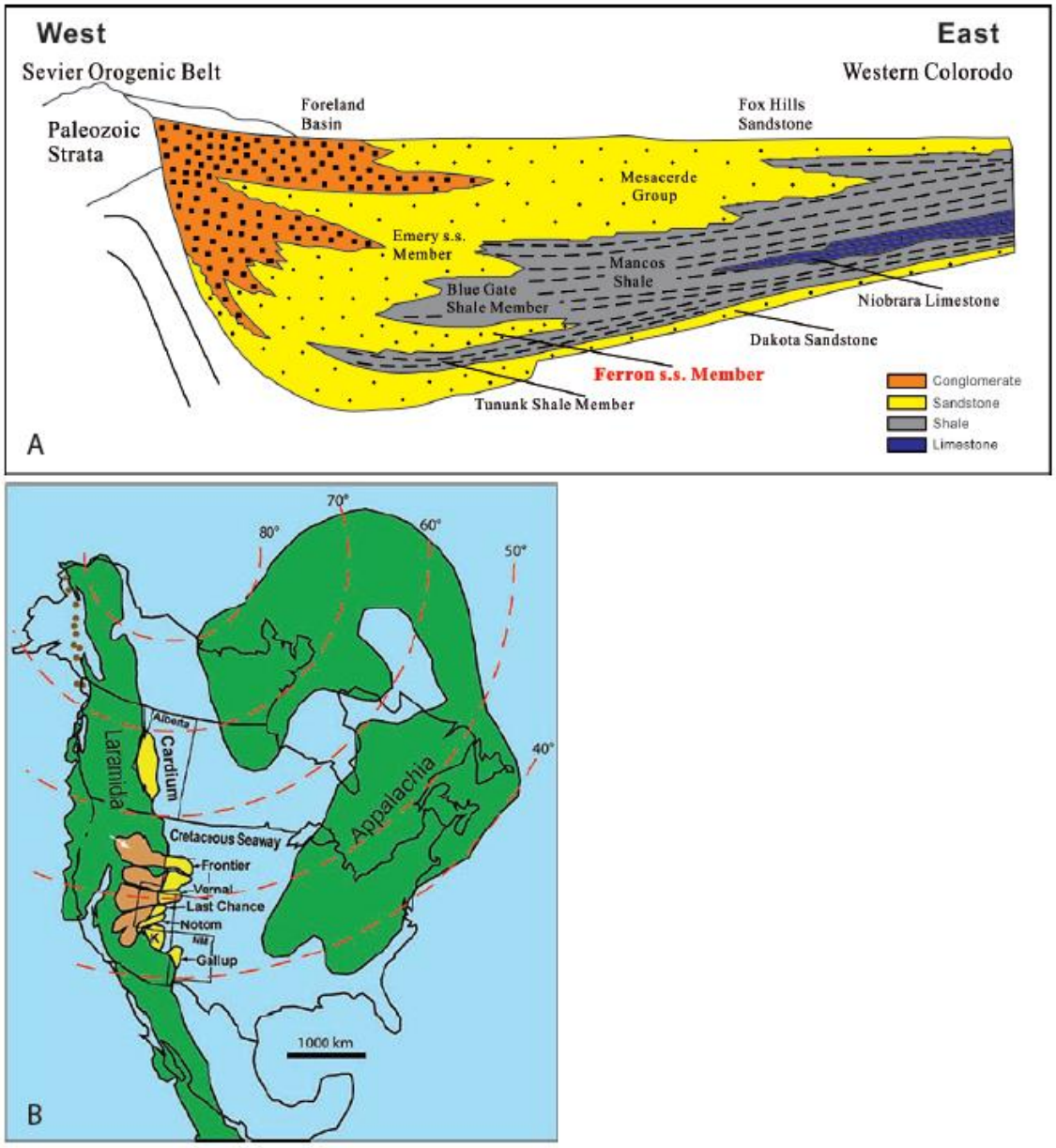

Figure 2.3 A) West-to-east Cretaceous wedge stratigraphy (from Barton et al., 2004, modified from Armstrong, 1968). B) Turonian paleogeographic reconstruction of the Western Interior Seaway showing the Ferron Notom Delta as one of the delta complexes along the western margin (from Bhattacharya and MacEachern 2009, after many other sources).

Blue Gate Shale and below by the Tununk Shale members of the Mancos Shale Formation.

Zhu et al. (2012) and Li et al. (2011) developed a high-resolution sequence stratigraphic framework of the Notom delta complex (Fig. 2.4). They divided the interval into 6 sequences, 18 parasequence sets, and 42 parasequences. $^{40}Ar/^{39}Ar$ dating of bentonite layers above and below the Ferron Sandstone reveals that the six depositional sequences occurred over a period of ~ 620,000 years (Zhu et al., 2012). Each sequence therefore, developed over ~ 100,000 years, roughly corresponding to 100-kyr Milankovitch-scale cycles, which were hypothesized to be glacio-eustatic in origin, but see Fielding (2010) for a contrasting view. Fluvial deposits in the upper incised-valley system (Sequence 1, Parasequence 3) are exposed on a triangular 3D outcrop belt extending between Caineville, Nielson Wash, and the Steamboat area in both strike-oriented and dip-oriented sections (Fig. 2.5). Previous work (Li et al., 2010, Zhu et al., 2012) documented a NE depositional dip direction and a southward long-shore current. The dominant depositional processes thus vary from river-dominated in the south to wave-dominated in the north, producing lateral facies variations in the same parasequences (Fig. 2.4).

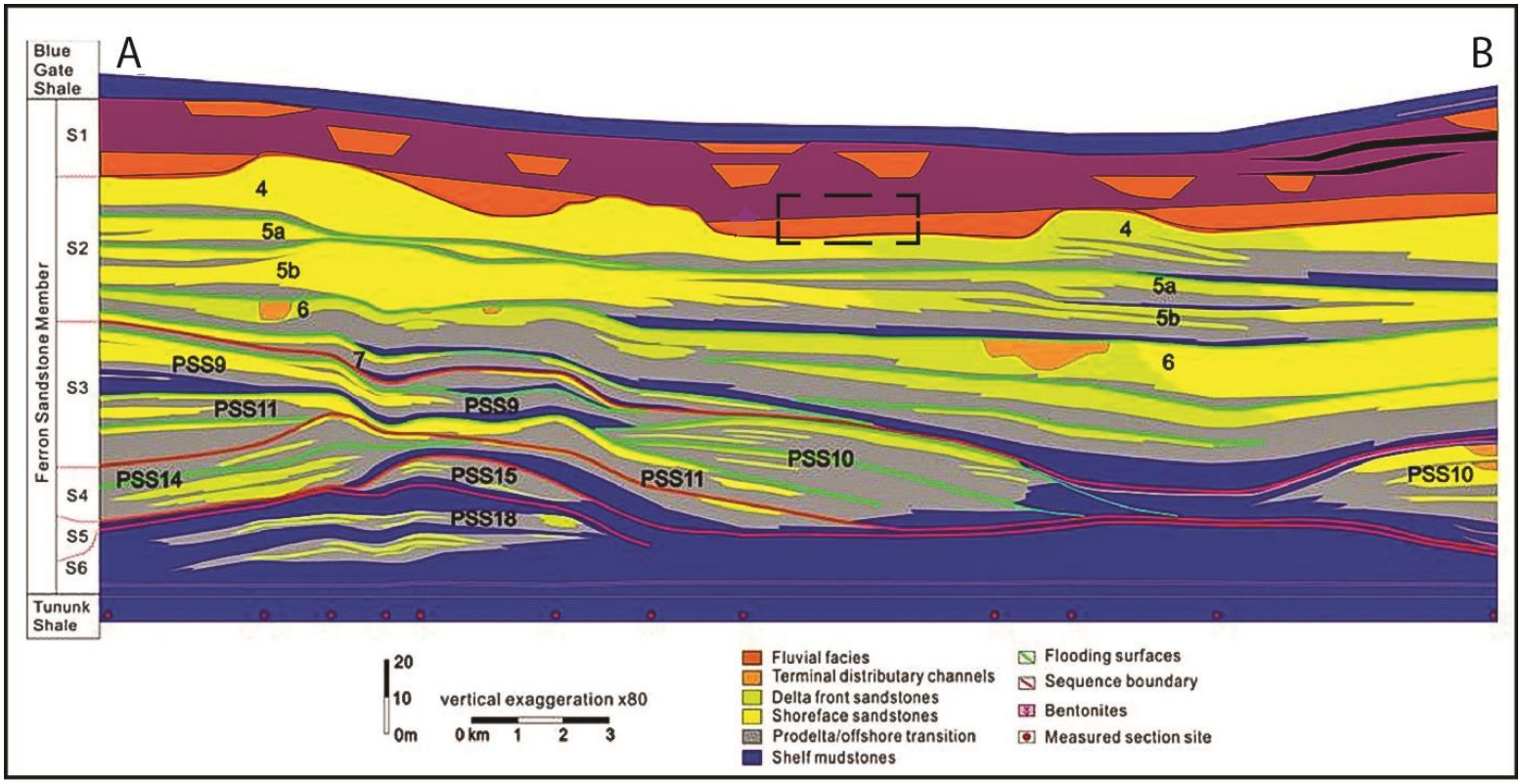

Figure 2.4 High-resolution depositional-strike sequence stratigraphic cross section of the Notom delta (from Zhu et al., 2012). The box outlines the approximate stratigraphic position of the compound incised valley investigated during this study. See Fig. 5 for the location of the profile.

Regional correlation and mapping show that Sequence 1 in the Ferron Notom system is floored by a compound valley with evidence of three separate cut-and-fill episodes (Li et al., 2010, Li and Bhattacharya, 2013; Hilton, 2013) each of which shows 20 to 30 m of erosional relief. Maximal channel story thicknesses of 5-7 meters (which suggest comparable flow depths) show that the regional erosional relief is 3-6 times maximum channel depths. This work focuses on documentation and interpretation of scour surfaces associated with individual channel stories in the regional valley fills.

2.6 Study Area and Methods

The outcrops chosen for fluvial scour analysis are located in the East Nielson Wash Canyon near Factory Butte, just north of Highway 24 (Fig. 2.5). These outcrops present exposures of the upper compound incised-valley system located at the top of the Ferron Notom wedge (Fig. 2.4). Field data from the scours were collected in outcrops along a nearly 1-km-long cliff face, which include exposures that are roughly perpendicular and parallel to depositional strike and dip. These physically accessible outcrops are highly suitable for detailed study to constrain the 3-D geometry of the channel and bar deposits.

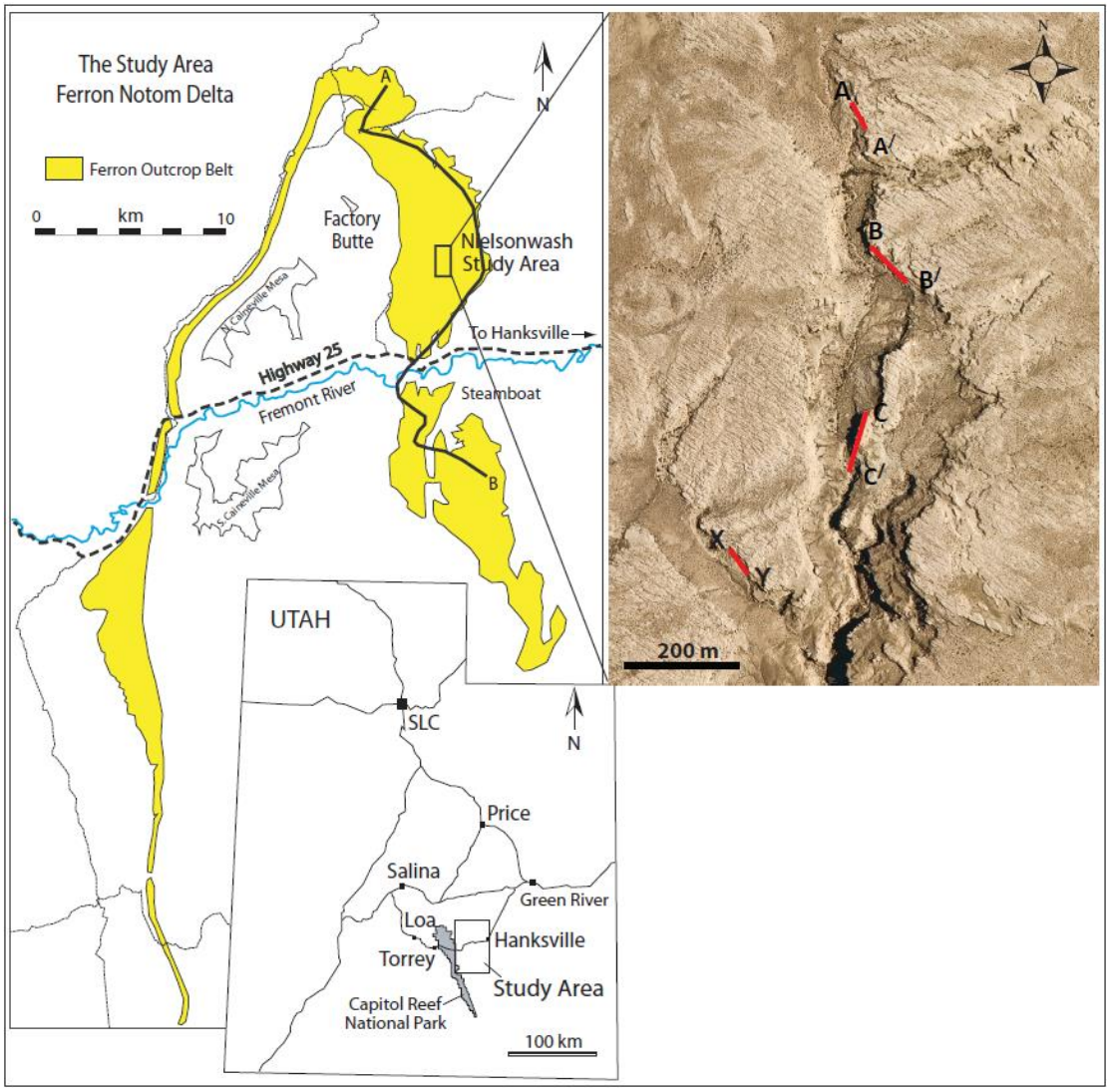

Figure 2.5 Shown in yellow is the outcrop of the Ferron Notom delta between Hanksville and Caineville, southeastern Utah. The black line represents the depositional-strike profile by Zhu et al. (2010; Shown in Figure 2.4). The black box outlines the Nielson Wash (study area). The red lines in the study area represent the locations of the bedding diagrams shown in Figures 2.7, 2.8, and 2.9.

Internal bedding and facies architecture of stacked bar and channel deposits were documented based on the correlation of bounding surfaces of different scales (zero to eighth order) through detailed bedding diagrams on photomosaics using the bounding-surface hierarchy of Miall (1985). The smallest-scale surfaces identified on the

outcrops are lamina and/or lamina-set bounding surfaces (zero and first-order surfaces). On photomosaics, these surfaces are typically unmappable, unless they form large single cross-strata in the channel scour fill. The smallest-scale surfaces correlated and mapped are centimeters to meters thick cross set and/or coset boundaries. These are interpreted to represent second-order and third-order surfaces that define bar-scale macroforms or inter-bar accretion surfaces, and either downlap onto channel floors or are truncated at the tops. The base of the macroforms, or bars, comprise a macroform-basal erosional surface and represents a fourth-order surface. Bar-top drapes are the best markers to identify and map bars on photomosaics (Adams and Bhattacharya, 2005). Changes in grain size and or cross-set thickness across an erosional surface also indicate successive bar deposits. The bases of major channels are identified as truncation surfaces, which define the fifth-order or channel-basal erosional surface. The sixth-order bounding surface, or the channel-belt-basal erosional surface, is defined as the contact between overlying rippled cross-bedded sandstones and underlying thick mudstones and/or siltstones.

Major fluvial erosional surfaces were identified as incised valleys (valley-base or seventh-order surface) based on field correlation, mapping, and detailed sedimentological descriptions. The bases of valleys are characterized by extraformational conglomerates and mud rip-up clasts, which are interpreted as valley lag deposits formed during relative fall and early low stand of sea level. The master valley basal erosional surface, or the sequence boundary (eighth-order surface), is mapped by onlapping fluvial deposits in the valley and truncation of underlying marine shoreface deposits (PS4 of Zhu et al., 2012).

The architecture of the compound valley fill and surfaces of incision were studied from photomosaics and cross sections along depositional strike and dip directions. Facies were recognized based on lithology, sedimentary structures, and fossil assemblage, and then arranged into facies associations. Paleocurrent data were collected mainly from dune-scale cross-strata and rib-and-furrow structures. Detailed analysis of bedding geometry of channel and bar deposits, with respect to paleocurrent data in strike-oriented exposures, was used to determine the plan-view morphology of paleo-channels. Depositional-strike views (perpendicular to flow) are a prerequisite to differentiate laterally accreting unidirectional point bars from bidirectional mid-channel braid bars (Miall, 1988; Bridge, 1993a; Bristow, 1993b; Holbrook, 2001). Braid-bar deposits typically show bidirectional downlap in strike sections, whereas single-thread meandering rivers typically show single laterally accreting sets.

Depths of confluence scours were estimated by mapping out the scour edge to the deepest part of the scour. Water depths were estimated from various empirically derived formulas based on studies of modern and ancient data (Bridge, 1993b; Leclair and Bridge 2001; Bridge 2003). According to Bridge (1993a) and Leclair and Bridge (2001) set thickness of the cross-strata can be used to calculate the height of formative dunes, which in turn scale to the flow depth. This technique, however, requires many set-thickness measurements to calculate the mean (S_m) and standard deviation (S_{sd}) of the set thicknesses. If the S_{sd}/S_m is approximately equal to 0.88 (±0.3), then the mean dune height (h_m) can be calculated using the following equation (Bridge and Tye, 2000):

$$h_m = 5.3\beta + 0.001\beta^2 \quad \text{where } \beta \approx s_m/1.8 \quad \text{.....} \quad (2.1)$$

Assuming that dunes and cross-strata formed during bankfull flow conditions, the maximum bankfull channel depth (*d*) has been empirically observed to be about 6 to 10 times mean dune height (Allen 1984, Bridge and Tye, 2000). Flow depths estimated from the cross-set thickness are also cross-checked with the thickness of fully preserved channel stories, which also roughly approximate channel flow depth (Bridge 2003). Flow depths can also be estimated independently from the height of bar accretion units, which typically scale to about 80-90% of flow depth (Bridge, 2003).

2.7 Examples of Scours in Cretaceous Systems

One of the first published examples of confluence scours in ancient fluvial deposits was shown in Adams and Bhattacharya (2005) based on detailed facies analysis of channels, bars, and bedforms in paleo-rivers of the Blackhawk and Castlegate Formations along Salina Canyon, Utah (Fig. 2.6). Although the Blackhawk Formation is believed to be an unconfined system, and the overlying Castlegate Formation is interpreted to be deposited in a valley (Van Wagoner, 1995), the study by Adams and Bhattacharya (2005) showed a similar braided fluvial style in both formations. Moreover, the braided channels in the Blackhawk and Castlegate Formations are similar in scale and produced scours of the same depth. Figure 2.6 shows examples of two modestly developed interpreted confluence scours in the Blackhawk Formation. Average flow

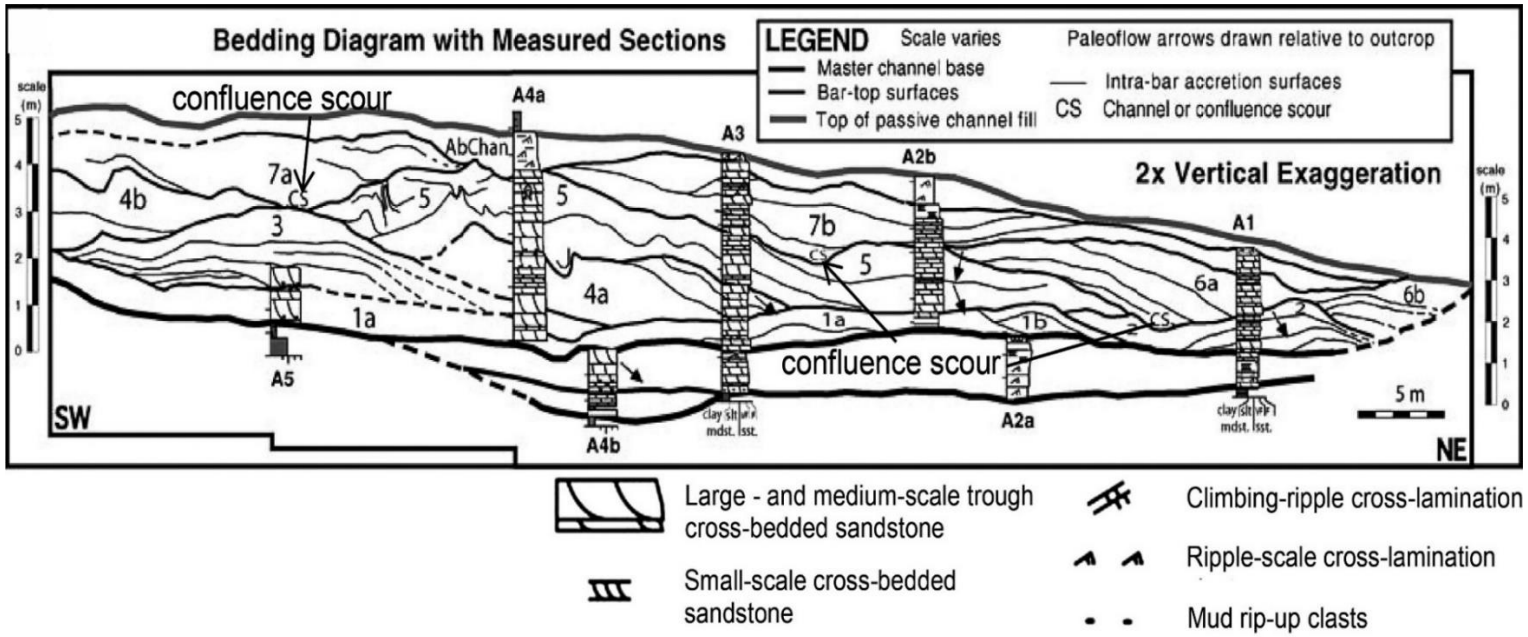

Figure 2.6 Strike-oriented bedding diagram showing interpretation of bars and channels in the Blackhawk Formation. Mounded shape braid bars are numbered 1 to 7. Arrows represent paleocurrents. Note the occurrence of confluence scours (CS) at the base of bars 7b and 6a (Adams and Bhattacharya, 2005).

depth of the channels calculated from story thickness and cross-bed sets is about 3-5 m, which is greater than the erosional relief produced by the scour. Li et al. (2010) conducted a similar study and documented the detailed bedding architecture of bar and channel deposits in a compound incised-valley fill at the top of the Cretaceous Ferron Sandstone Member. Detailed analysis of bedding geometry of channel and bar deposits with respect to paleocurrent data in this strike-oriented exposure indicates that the lowermost channel (Ch1) and the uppermost channel (Ch5) are braided (Fig. 2.7). They interpreted the bedding architecture at the base of Ch1 as small-scale chutes and fills without any noticeable confluence scours. The bedding diagram shows a 1.5–2 m thick distinct solitary unit with well-developed avalanche faces in the upper right of the profile in Ch5 (CCB in Fig. 2.7). These large single cross-strata dip parallel to the cliff face, at a high angle to regional flow. Li et al. (2010) interpreted these strata as the product of an advancing cross-channel unit bar in a braided river and thus may represent a confluence scour. It is clearly not a particularly over-deep feature. There are also a number of other scour features, overlain by single bars throughout the cross section, but there are no observed outsize scours.

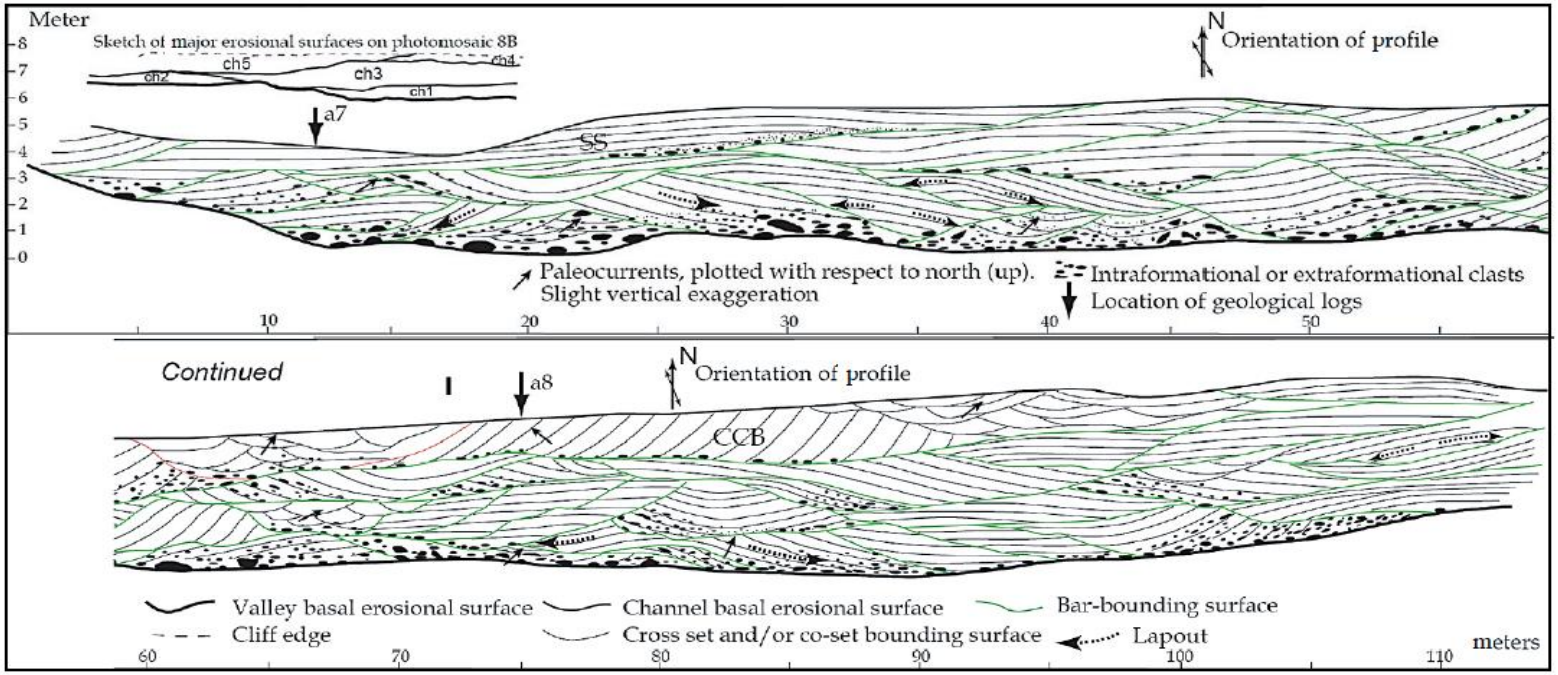

Figure 2.7 Strike-oriented bedding diagram showing interpretation of bars and channels within a compound incised-valley fill at the top of the Cretaceous Ferron Sandstone Member. The large single set of cross-strata with well-developed avalanche faces in the upper right of the profile in Ch5 (CCB) is interpreted as an advancing cross-channel unit bar in a braided river (Li et al., 2010).

The studies by Adams and Bhattacharya (2005) and Li et al. (2010) reveal the existence of interpreted confluence scours in braided channels in two different ancient deltaic systems. The examples of confluence scours described in these studies show geometry similar to that of the confluence scour fills in the modern Brahmaputra River, as shown in Figure 2.2. However, none of these confluence scours described in the ancient system are anywhere close to five times average channel depth. At best, they appear to represent maximum braid-bar and channel depths based on the previous studies. Our study also identified a number of fluvial scours in the upper incised-valley fills at the top of the Cretaceous Ferron Sandstone Member of the Mancos Shale Formation in the Henry Mountains region, Utah (Fig. 2.4). According to Li et al. (2010) and Hilton (2013), Ferron rivers were classic dirty rivers, capable of producing hyperpycnal flow that never exceed about 6 m in water depth (Bhattacharya and MacEachern, 2009). The examples of confluence scours in these much smaller Cretaceous rivers thus provide an ancient perspective of confluence scour fills and their scaling relationships, compared to their modern counterparts.

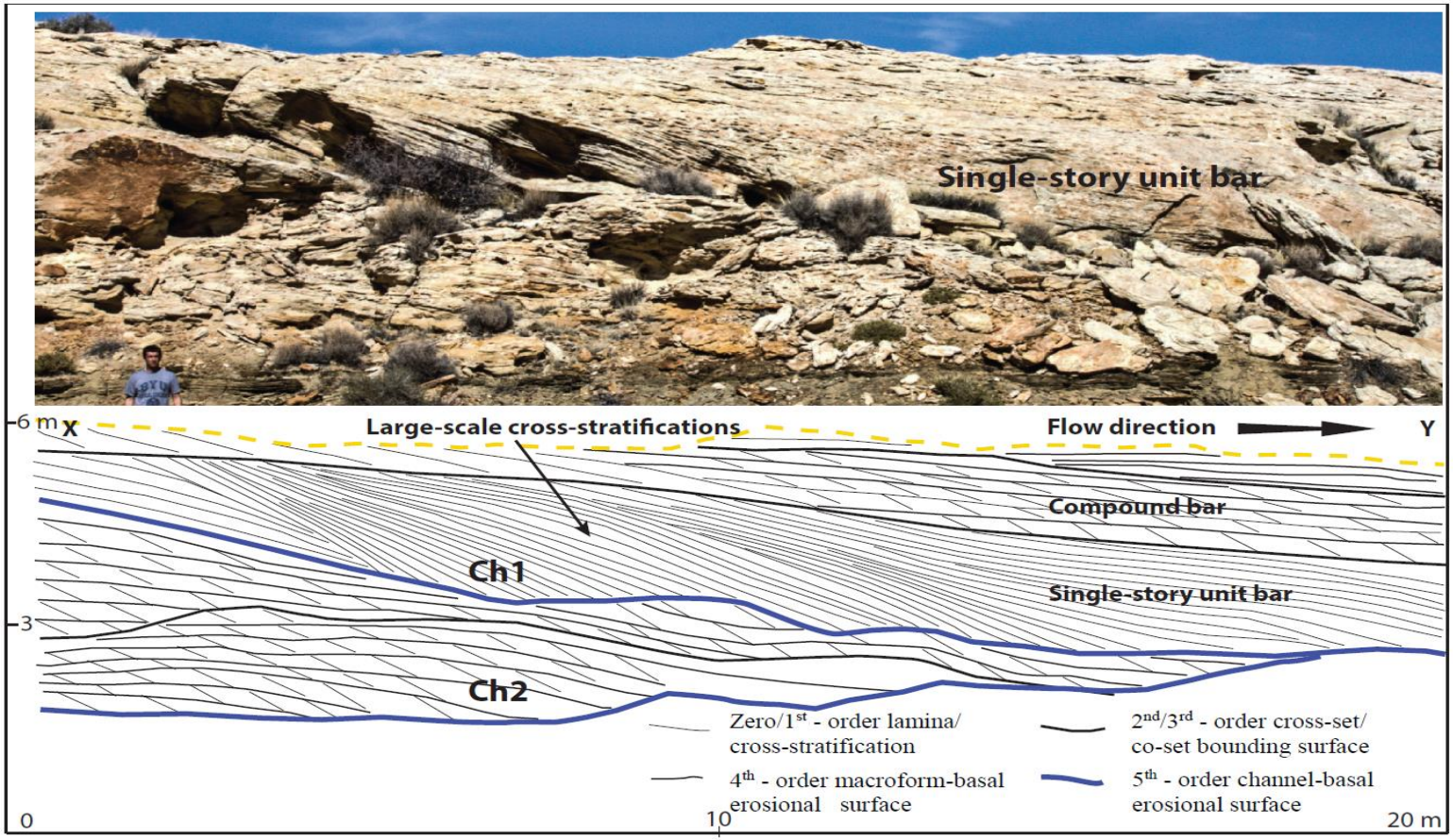

Figure 2.8. Example of a channel scour fill in Cretaceous Ferron Notom Delta that has a geometry similar to the scour fill in the Brahmaputra River (Figure 2.2). The scour at the base of the upper channel (Ch1) eroded down into the lower channel (Ch2) and later filled by a single-story unit bar formed by the progradation of large-scale cross-stratification over the scour base. The single large foresets, which fill the scour, gets longer and less steep as they advance through the scour.

Figure 2.8 shows an example of a channel scour fill, similar to the scour fill in the Brahmaputra River (Fig. 2.2) but at a much smaller scale. Fifth-order surfaces mark the bases of the two channels (Ch1 and Ch2), which are indicated by truncation of large-scale accretionary beds. Large-scale foresets, about 2 m thick, overlie a surface exhibiting significant relief, indicating a basal scour. The large foresets in Ch1 apparently steepened, then became shallower as they prograded across the scour and filled it in a direction parallel to flow. The smaller-scale cross sets lie above the base of the bar defining a fourth order surface on top of the larger-scale foresets. The large-scale foresets are interpreted as a unit bar, filling an initially deep scour. As the scour filled, the foresets apparently flattened and were eventually overlain by dune-scale cross-bedded sandstones, interpreted as a downstream-accreting compound bar. These elements are interpreted to represent the upstream scour fill and downstream compound bars associated with a confluence scour.

Figure 2.9 shows the detailed bedding architecture, facies, and paleocurrents from three vertically stacked sandstone bodies at the base of the incised-valley fill (see Fig. 2.5 for location). Fifth-order surfaces, or channel basal erosional surfaces, mark the base of these sand bodies (Ch1, Ch2, Ch3), which are indicated by the truncation of bar-scale macroform or inter-bar accretion surfaces (second-order and third-order surfaces). The lowermost channel sand body (Ch3) overlies a surface exhibiting significant relief (~ 2 m) and truncates hummocky cross-stratified marine shoreface deposits. This fluvial erosional surface is interpreted as the master valley basal erosional surface (i.e., a sequence boundary). There is a distinct change in bar geometry in Ch3, from slightly dipping sets

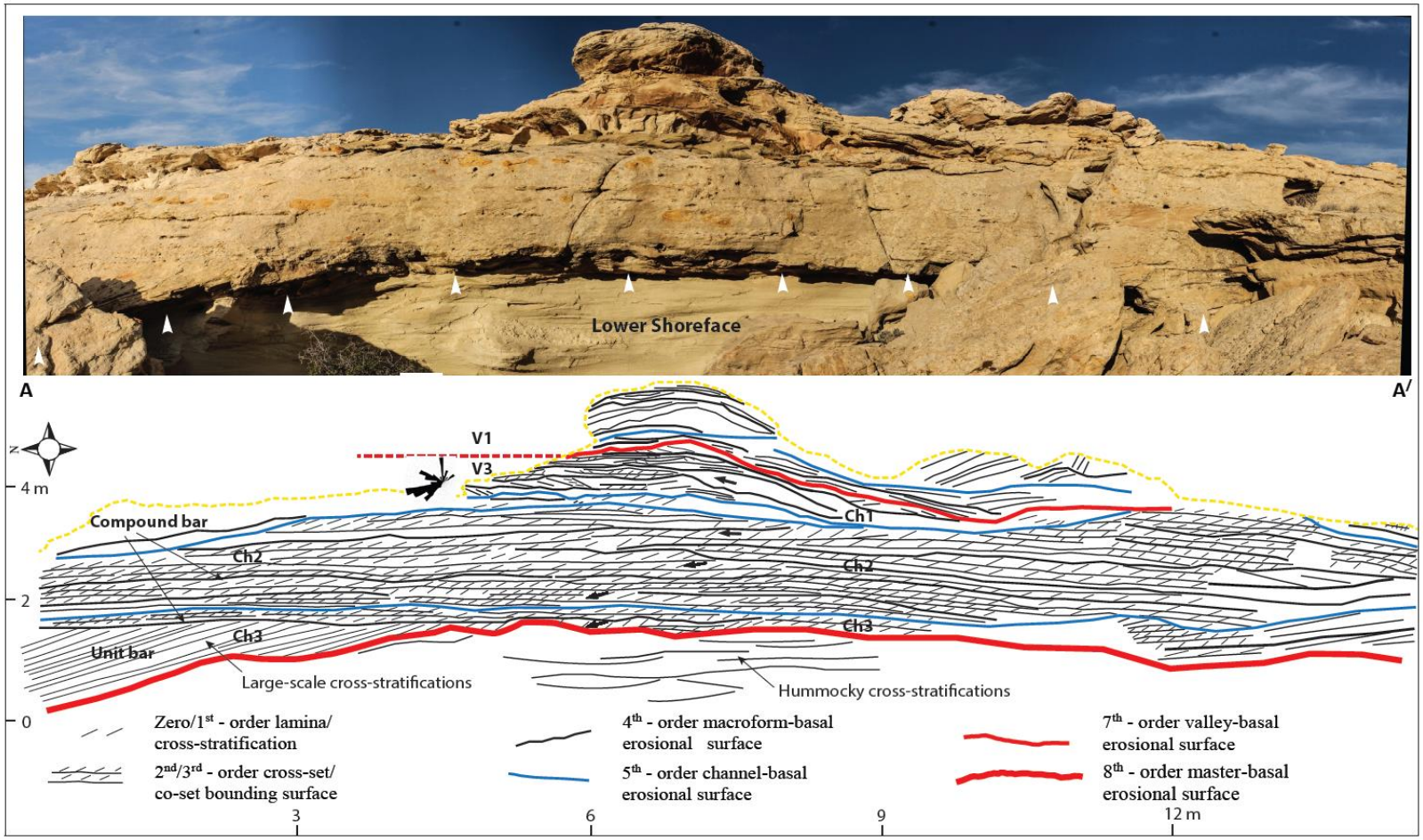

Figure 2.9 Shown a fluvial scour in marine shoreface with an interpretation of valley-basal (white arrows) and channel-basal erosional surfaces (see Fig. 2.2 for outcrop location). In the bottom-most channel body, there is a distinct change in bar geometry from horizontal cross sets to steeply dipping single large-scale cross-stratification as the bar progrades over the scour. Arrows represent paleocurrents.

of cross-strata to a steeply dipping set of large-scale cross-strata as the bar fills the zone of maximum relief. This set of large-scale cross-strata is more than 4 m long and dips at the angle of repose. The maximum preserved thickness of the unit bar is 1.6 m. These large foresets are in turn overlain by smaller horizontal set of dune-scale cross-strata. The paleocurrent directions (arrows) in these cross sets suggests that the outcrop is oriented approximately parallel to the flow direction, and that the third-order and fourth-order bar accretion surface in the channel bodies accreted mostly downstream.

The single large foresets in Ch3 are interpreted as a unit bar, filling a deep basal scour cut into marine shoreface deposits at the base of an incised valley. The overlying cross-bedded sandstones indicate a compound bar. The heights of the sets of cross-strata in the compound bar, upstream of the scour pit, are between 15 and 20 cm, suggesting an average flow depth of 2.7 m to 3.6 m (using techniques from Bridge and Tye, 2000, and Leclair and Bridge, 2001). Once the scour is filled by the unit bar, the smaller-scale cross sets of a compound bar build across the now-filled scour. Similar to the previous examples in Figures 2.2 and 2.8, the scoured surface is thus overlain by a single-story sand body with an internal erosional surface formed as the compound bar truncates the underlying unit bar. This erosional base of the compound bar as indicated by a sudden jump in grain size, and abrupt truncation of the underlying single large foresets does not represent a second story, but rather an erosional diastem within a single channel.

Figure 2.10 shows an example of a compound incised-valley system along a roughly north-south-oriented outcrop in the study area (see Fig. 2.5 for location). At least three channel belts are recognized in the middle valley (V2), the top of which (Cb1 and

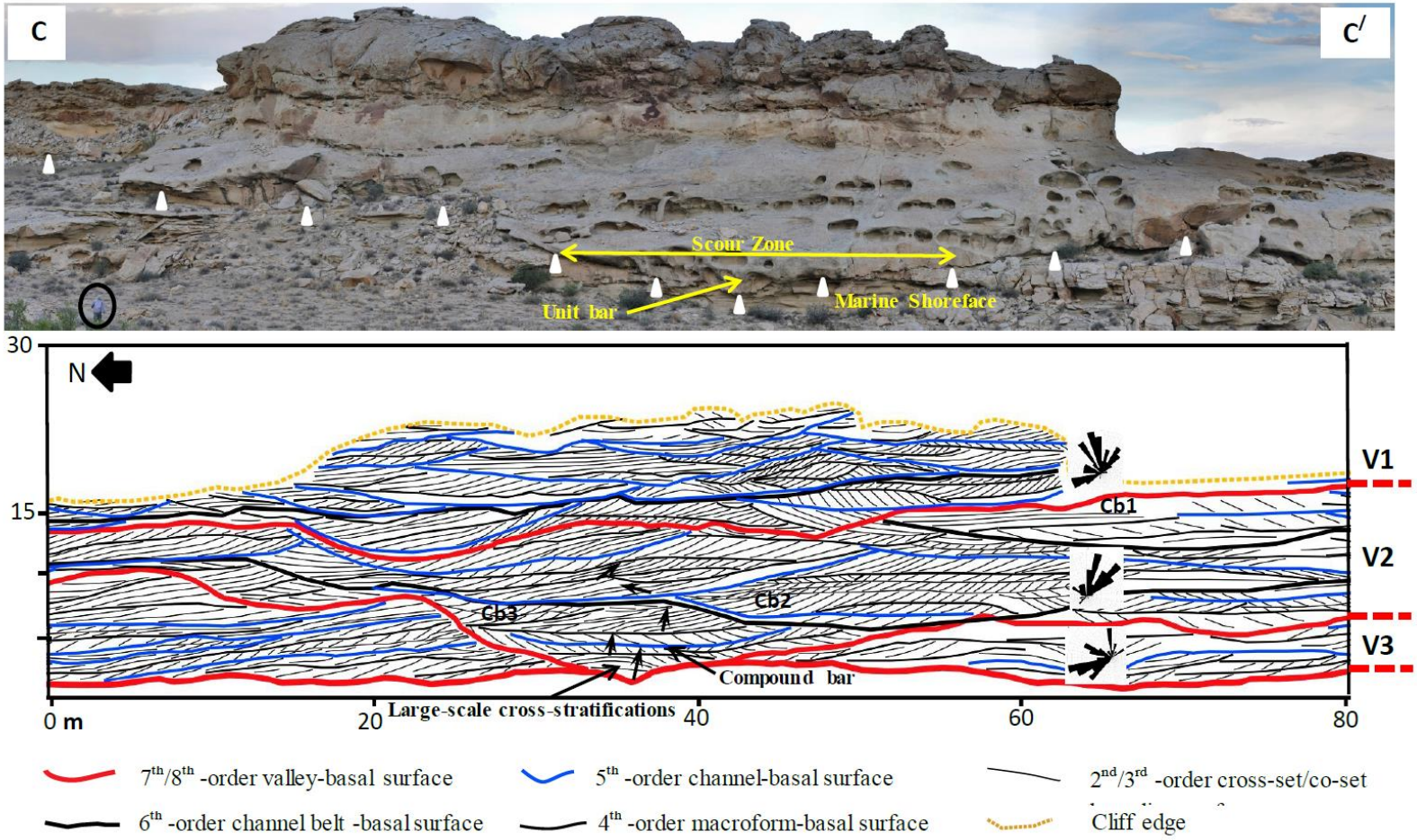

Figure 2.10 Shown an example of a compound incised-valley system along a roughly north-south-oriented outcrop (see Fig. 2.2 for outcrop location). The simple unit bar and cross-channel compound bar in the lower most channel story in the channel belt 3 (Cb3) represent the filling of a clear U-shaped scour at the base of V2 (white arrows) that occurs at the confluence of multiple channel threads in a braided system. Arrows represent paleocurrents.

Cb2) shows distinct dipping foresets. Bedding geometry combined with paleocurrent data (red arrows), shows that bars in these channel belts had distinct unidirectional accretion towards the channel cut bank, indicating that the formative rivers were single-thread meandering rivers with laterally accreting point bars. Underlying these channel belts are two vertically stacked medium to coarse-grained fluvial channel bodies in channel belt 3 (Cb3), which not only cut out all of the older valley 3 (V3) deposits in the middle part of the outcrop, but also further incised into the highly bioturbated marine facies. This deep incision into distal marine shoreface sandstones indicate an erosion surface that violates Walther's Law, and is thus interpreted as a sequence boundary caused by a drop in base level. Although the margin of this valley has not been mapped locally, regional correlation and mapping suggests that it has about 20 m of erosional relief (Hilton, 2013).

Paleocurrents and accretion directions in the channel stories in the lower channel belt (Cb3) are roughly perpendicular to the cliff face at an angle of 100^{o} and 90^{o} respectively relative to the north. Bedding geometry, combined with paleocurrent data, shows that the bars in the lowermost channel story accreted mostly downstream, as indicated by distinct mounded shapes with bilateral downlap accretion surfaces. This is interpreted as a mid-channel unit bar in a braided system built by a large, single set of trough cross-stratification in the core of the unit. The overlying cross-strata that dip parallel to the cliff face, at a high angle to the overall paleoflow direction, mark both sides and top of the unit bar, and probably indicate the advancement of a cross-channel compound bar. This simple unit bar and cross-channel compound bar in the lower channel story most probably represent the filing of a U-shaped scour that is interpreted to

have occurred at the confluence of multiple channel threads in a braided system. The erosional relief of this scour is approximately 5 m, as measured on the outcrop, and is filled by a 2.5-m-thick unit bar at the base of the valley (Fig. 2.10). The average cross-set thickness of the lower channel story measured in the outcrop is 13.5 cm, excluding the scour fill. Using the technique of Bridge and Tye (2000) and Leclair and Bridge (2001), formative water depth were likely between 2.4 and 4.0 m. The scour, therefore, is about two times deeper than the average depth of the channels, which fed the scour. The larger-scale regional erosional surfaces is many kilometers in width and about 20 m deep, and it is inconceivable that it could be produced as a simple autogenic confluence scour in a system in which maximum channel depths were on the order of 5 m.

2.8 Scours in an Ancient Meandering System

Most of the examples of scours described in the sedimentological literature are focused on braided rivers (Klaassen et al., 1988; Ashworth et al., 2000; Best et al., 2007). However, scours in meandering systems are common, as tight river bends can be characterized by a deep thalweg scour in the cut bank. The maximum channel thalweg depth in a meandering river can be significant, and may be much deeper than the average channel depth in a wide braided river. This overall variation of depth between meandering and braided rivers can produce different ranges of scour modification that need to be considered in interpreting the ancient record.

Figure 2.11 shows an example of a scour in a meandering river in valley 3, along with an interpretation of valley-base and channel-base erosional surfaces. Detailed

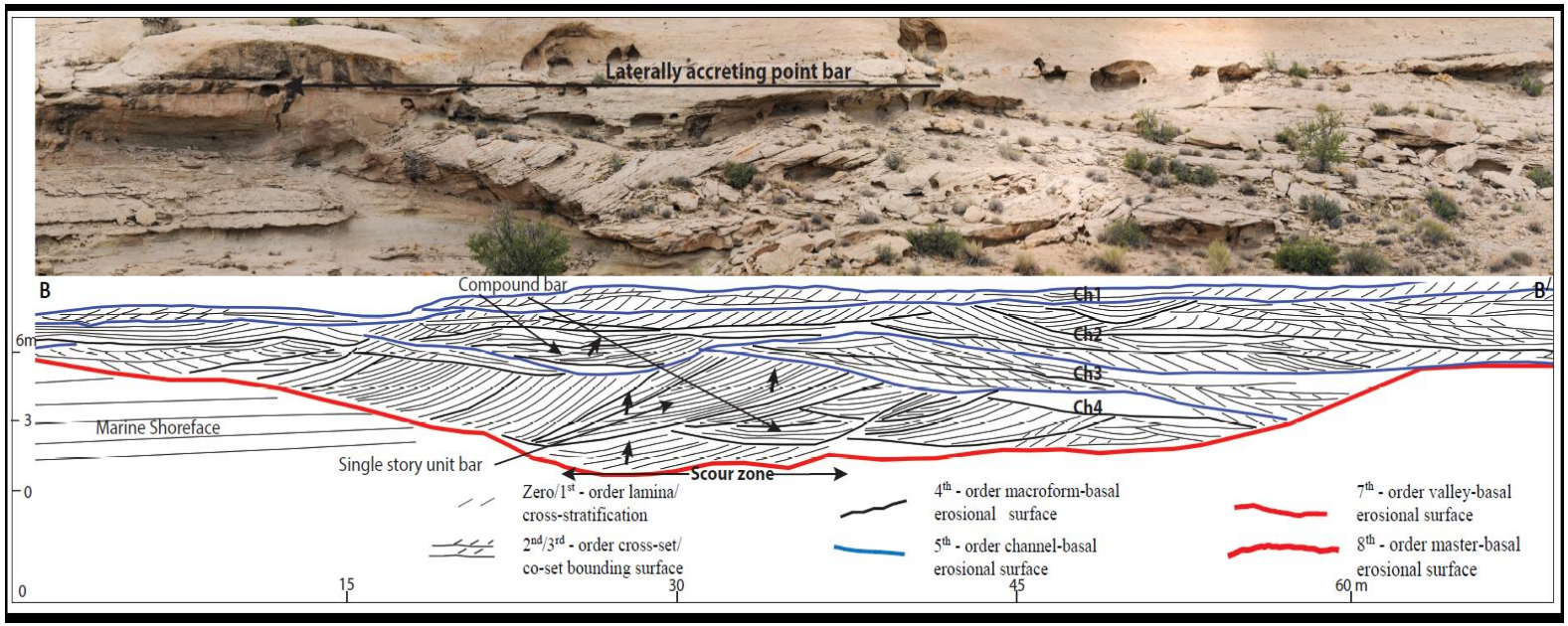

Figure 2.11 Shown an example of scour in a meander system along with an interpretation of valley-basal (white arrows) and channel-basal erosional surfaces (top). In the lowermost channel body (Ch4), bars show distinct unidirectional accretion towards the channel cut bank (see Fig. 2.12 for paleogeographic reconstruction), indicating that the formative river was a single-thread meandering river with laterally accreting point bars. The cut bank at the river bend is most probably characterized by a deep thalweg scour. Arrows represent paleocurrent.

bedding architecture, along with paleocurrent information along the cliff face, is also shown (see Fig. 2.5 for outcrop location). Four channel bodies (Ch4, Ch3, Ch2, and Ch1) are recognized in valley 3. Fifth-order surfaces mark the base of these channels, which are indicated by the truncation of the bar-scale macroform or inter-bar accretion surfaces (second-order and third-order surfaces). Each of top the three channel stories (Ch1, Ch2, and Ch3) show distinct inclined sets or cosets of trough cross-strata, which downlap onto channel floors or are truncated at the tops. Paleocurrent measurements (red arrows) from these cross-strata indicate that the paleoflow direction is into the outcrop. The direction of accretion of the cross-strata, however, is perpendicular to the paleoflow. Bars in these channel bodies therefore show distinct unidirectional accretion towards the channel cut bank, and the formative rivers are interpreted as single-thread meandering rivers with laterally accreting point bars.

The lowermost channel sand body (Ch4) overlies an extensive fluvial erosion surface that exhibits significant local relief of more than 4 m. The underlying nearly horizontal marine shoreface deposits show toplap truncation against this surface. This major fluvial erosional surface at the base of valley 3 represents the same master valley basal erosional surface or the sequence boundary shown in Figures 2.9 and 2.10. The zone of maximum relief on this surface (in the middle of Figure 2.11) shows accretion of single large-scale cross-strata, which are between 5 and 15 m long and dip at an angle greater than the angle of repose. However, the second-order and third-order coset boundaries at both the side and the top of the scour show relatively low-angle dips of the cosets, which are a few tens of centimeters thick. The paleocurrent directions in these

cross-strata suggest that the third-order and fourth-order bar accretion surfaces in Ch4 accreted laterally.

The large-scale, steeply dipping foresets in Ch4 can therefore be interpreted as a unit bar, filling a deep basal scour into a marine shoreface at the base of an incised valley. The cross-bedded sandstones in the sand bodies at both sides of the scour are interpreted as compound bars. The scour most probably represents a deep thalweg at the cut bank near the interpreted river bend (Fig. 2.12, top). In the inner bank, gently dipping sets of cross-strata form the core of compound point bars that show distinct unidirectional accretion towards the channel cut bank. However, as the river migrated laterally over the scour, it filled the scour with a set of steeply dipping thick foresets interpreted as multiple unit bars (Fig. 2.12, bottom).

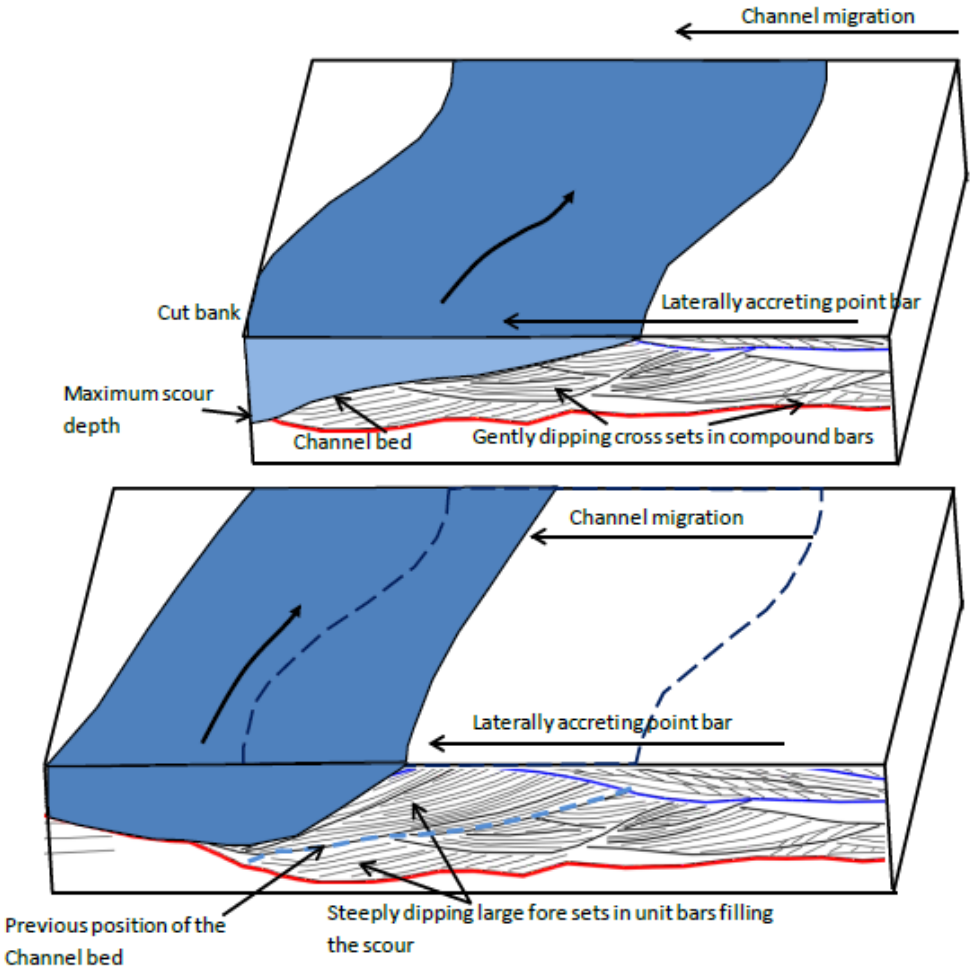

Figure 2.12. Paleogeographic reconstruction of the lowermost channel (Ch4) shown in Figure 2.11. At the inner bank, gently dipping cross sets form the core of the compound bars, which show distinct unidirectional accretion towards the channel cut bank (top). As the river migrates laterally over the scour, it filled the scour with steeply dipping large single foresets that form multiple unit bars (bottom).

The maximum preserved thickness of the channel body is 4 m, right above the thalweg scour. However, the thickness of this channel body is zero at the river margin (Fig. 2.12). This shows that the rock record contains variably thick channel bodies that range from maximum thickness, recording the thalweg depth, to zero thickness at the river margin. Therefore, the thickness of a channel story is highly variable depending on

its position on the channel cross section (Hirst et al. 1993). The average channel depth in a meandering river is typically about 35% of the maximum channel thalweg depth. Therefore, the average thickness of a fully preserved channel story in a meandering river (assuming no top erosion by younger channels) does not necessarily represent the deepest part of the river for any single location. By analogy, if a confluence scour in a braided river really is five times deeper than the average channel depth, this does not necessarily require the confluence scour to be filled by five channel stories. In outcrop, the maximum story thickness of a single story basically conforms to the maximum depth of the channel, not the average depth. Of course, where an outcrop samples channel-margin deposits, the story thickness at that place cannot be thicker than the depth of the channel at that locale.

2.9 Discussion

Distinguishing Confluence Scours vs. Incised Valleys in Ancient Outcrops

Certain criteria can be used in identifying allogenically formed incised valleys from autogenically stacked channel bodies in a confluence scour at the base of a valley. The relief on a regional erosional surface associated with an incised valley must be large enough to confine the uppermost fluvial valley deposits within that surface. The relief associated with an incised valley can be estimated by mapping the interfluves at or in between the valley margins and then taking the elevation difference from the deepest part of the valley floor. Li et al. (2010) and Hilton (2013) mapped rooted shoreface deposits (parasequence 4 in Fig. 2.4) associated with valley interfluves and documented nearly 30 m of overall regional valley erosional relief in the Ferron Notom compound

incised-valley system. However, their study found a maximum channel depth of about 5-6 m with an average 3-4 m, which is similar to the findings from this study. Therefore, the valley-scale erosion is up to ten times average channel depth in the Ferron Notom compound incised-valley system.

Consequently, if the maximum erosional relief of the valley is much greater than the thickness of the thickest single story, or even multiple stacked vertical stories at a confluence scour, the erosional surface represents the base of an incised valley or in some cases a sequence boundary. This is clearly demonstrated in Figure 2.10. The relief at the base of individual stories in the scour never exceeds about 5 m (Table 2.1), despite that fact that up to 17 m of relief has been documented associated with the regionally mapped valley 2 (Li et al., 2010). Therefore, the maximum relief of valley 2 is about four times the maximum preserved story thickness in the study area. Our study also shows that modal story thickness in Valley 2 is about 2 m (Table 2.1). The valley relief in the Notom delta is therefore certainly more than five times the average story thickness.

Moreover, the base of valley 2 truncates underlying highly bioturbated mudstone or very fine-grained marine shoreface sandstone deposits. This observation of more proximal facies truncating distal facies, across extensive erosional surfaces, also helps identify valleys versus autogenic channel scours.

Valley	Stats	Hilton 2013	Griffin 2013	Campbell 2013	Li et al. 2010	SUM TOTAL	THIS STUDY
V1	MEAN (m)	1.4	-	1.5	2.2	1.8	1.7
	MIN (m)	0.5	-	0.1	0.8	0.5	0.5
	MAX (m)	3.4	-	3.4	4.3	4.3	3.0
	STDEV	0.7	-	0.6	0.9	0.8	0.6
	n	95.0	-	20.0	118.0	233.0	52.0
V2	MEAN (m)	0.8	-	1.0	1.8	1.0	2.0
	MIN (m)	0.4	-	0.3	1.3	0.3	0.5
	MAX (m)	2.0	-	1.7	2.7	2.7	4.1
	STDEV	0.4	-	0.3	0.6	0.4	0.6
	n	20.0	-	61.0	5.0	86.0	52.0
V3	MEAN (m)	2.1	2.8	1.8	-	2.1	1.3
	MIN (m)	0.9	1.2	0.5	-	0.5	0.4
	MAX (m)	3.5	3.7	3.1	-	3.7	2.9
	STDEV	0.6	0.4	0.5	-	0.6	0.5
	n	73.0	16.0	27.0	-	116.0	46.0

Table 2.1 Compilation of preserved channel story thickness in a compound incised-valley fill at the top of the Cretaceous Ferron Sandstone Member of the Mancos Shale Formation in the Henry Mountains region, Utah.

Scaling Relationships of Confluence-Scours

The confluence scour found at the base of valley 2 (Fig. 2.10) in the study area has a depth of less than five times average channel depth. In fact, examination of the ancient record simply does not provide examples of individual confluence scours that are about five times average channel depth. In a recent study on scours in modern distributary channels in the Øyeren delta, Norway, Eilertsen and Hansen (2008) demonstrated a scour depth/upstream channel depth ratio (S/C ratio) of between 1.4 and 3.3. Interestingly, the confluence scours described in Eilertsen and Hansen (2008) are not

substantially deeper than the meandering-river-bend scours on the same delta plain. The wide range of S/C ratios in modern and ancient rivers is attributed to the confluence angle by a number of laboratory and field studies, where it was shown that the scour depth increases nonlinearly with the confluence angle for a given relative discharge (Best, 1987, 1988). This relationship between confluence angle and scour depth was shown mathematically by Klaassen and Vermeer (1988), and can be used for a reasonable estimation of scour depth (Sarker, 1996):

$$h_{cs}/h = 1.292 + 0.037\theta \quad \ldots\ldots\ldots\ldots\ldots\ldots\ldots\ldots\ldots\ldots (2.2)$$

where h_{cs} is the confluence scour depth, h is the mean flow depth of the upstream channels, and θ is the junction angle. According to this equation, a confluence angle of 45^o, 60^o, and 90^o can produce scours which are 3, 3.5, and 4.5 times average channel depth respectively. This equation also demonstrates that to produce a scour more than five times the average flow depths of the upstream channels, the confluence angle has to be more than 100^o. This confluence angle–scour depth relationship is also supported by laboratory experiment, where scour depth is found to increase systematically at higher junction angles (Best, 1988). Data collected on 14 confluence scours in the braided Jamuna River also support these mathematical and laboratory experiments (Flood Action Plan, 1996a; Best et al., 2007). These studies showed that scours produced with confluence angles up to 60^o during the flood season are 2-3.5 times the average flow depths of incoming braided threads. However, only two of those produced scours four times deeper than the incoming confluence channels and in both cases, the confluence angles were more than 80^o.

The contrast in discharge between the incoming threads can also control the scour depth, along with the confluence angle, as the scouring processes associated with unequal depth channels are different from those at confluences with channels of equal depths (Best, 1988, Biron et al., 1993). Based on the study in the sand-bed Bayonne-Berthler River confluence, Quebec, under varying flow conditions, Biron et al. (1993) showed that the morphology of the confluence zone is generally characterized by an absence of scour. Both rivers upstream of the junction in this study had similar widths (~ 8 m), and the junction angle was 65 °. The maximum depth of the incoming rivers was 1.99 and 2.81 m respectively with a maximum discharge ratio of 1.33 during a sample period of 30 days. In contrast, for a given confluence angle the maximum scour depth increases as the discharge in the entering channels tends to equality.

It is therefore highly unlikely to find frequent scours at ancient sequence boundaries, let alone the scours that are more than five times deeper than the average channel depths. Nevertheless, Best and Ashworth (1997) suggested that it is not uncommon to have confluence scours that are five times average channel depth, and therefore erosional surfaces that have relief less than or equal to five times average channel depth could be confluence scours and do not have to be sequence boundaries. Our study clearly shows that confluence scours have diagnostic fill facies (single large steep foresets) and do not produce multistory sand bodies. Moreover, the rock record indeed is biased towards recording the deepest parts of channels, since the thalweg scour or confluence scour creates its own accommodation. Therefore, the story thickness at the

confluence scour does not represent the average channel depth, as confluence scours allow preservation of the deepest parts of channels as well as fully preserved stories.

Bedding diagrams and paleogeographic reconstructions presented in our study suggest that braided or meandering streams in the lower part of the valley fills were at most 3-4 m deep. Previous studies also showed that the average preserved channel story thickness in the compound incised-valley fill is probably about 1-2.5 m (Table 1). The interpreted confluence scour shown in Fig. 10 is 5 m deep, which is up to five times the average or minimum story thickness. However, these 1-2.5 meter thick stories are neither fully preserved nor represent the much deeper thalweg. Therefore, we argue that interpretation of incised valleys in an ancient system associated with a sequence boundaries should not be based on the depth of the erosional surface versus the number of average preserved story thickness. Rather, it should be defined by an erosional relief that is significantly deeper than the thickest fully preserved stories, which in a braided stream are likely to represent confluence scour fills.

2.10 Conclusions

1. Confluence scours are caused by erosional processes that are intrinsic or autogenic and often occur in braided rivers where separate channel threads join together and erode an exceptionally deep scour. The excess accommodation created by a confluence scour on a riverbed is large enough for the average channel depth to fill it up with a single unit bar. Thus, when bars migrate across the confluence scour, they typically fill the scour pit with a single set of large, steeply dipping foresets

that form a unit bar. In most vertical cross sections, a confluence scour fill produces a single-story body in which a fifth-order scour is filled with unit-bar foresets, which in turn are overlain by a fourth-order surface capped by compound-bar deposits.

2. The average thickness of a fully preserved channel story in a meandering river does not necessarily represent the deepest part of the river. In an ancient outcrop, the maximum thickness of a single story should conform to the maximum depth of the channel rather than to the average depth.

3. The rock record is biased towards recording the deepest parts of channels, since the thalweg scour or confluence scour creates its own accommodation. Therefore, the story thickness at the confluence scour does not represent the average channel depth, since confluence scours allow preservation of the deepest parts of channels as well as fully preserved stories.

4. If the maximum erosional relief of an erosional surface is significantly greater than the thickness of the thickest single story, or even multiple stacked vertical stories at a confluence scour, then such an erosional surface likely represents the base of an incised valley and may be a sequence boundary. In the Ferron examples, the maximum relief of valley 2 (17 m) is about three times the maximum story thickness (5 m) in the study area. However, numerous well-documented valleys may form erosional surfaces that are only 1.5-2 times

maximum channel depth, especially if the valley is cut by a meandering stream and thus lacks confluence scours.

5. Interpretation of allogenically formed incised valleys in ancient systems associated with sequence boundaries are thus best defined by erosional relief that is significantly deeper than the thickest fully preserved stories, which in a braided stream are likely to represent autogenic confluence scour fills. Examples of autogenic modification of allogenically formed incised valleys in this paper indicate that both allogenic forcing and autogenic feedback can act simultaneously in fluvial systems. This demands attention to a more balanced approach in terms of defining allogenic vs. autogenic mechanisms in ancient and modern fluvial outcrops. Observations of cross-sectional geometries from confluence scour fills in this study indicate that autogenic processes can produce unique patterns that are similar across a large range of scales (space and time) and thus can be characteristic of autogenic processes.

CHAPTER 3: Interpreting Backwater Effects on Fluvial Style and Architecture in a High-gradient Compound Incised-valley Deposit: Examples from the Cretaceous Ferron Notom Delta, Southeastern Utah, U.S.A.

3.1 Summary

Non-marine sequence-stratigraphic models for incised valley fill predict systematic changes in fluvial style with changing system tracts, assuming a constant rate of marine transgression. Downstream base-level influence on fluvial style however, can be highly variable, and may produce less predictable patterns depending on the upstream extent of the backwater, which is proportional to river flow depth and inversely correlated to river slope. It has been hypothesized that the backwater length controls the ability of the effects of base-level changes to propagate upstream. Previous studies on the modern Mississippi River valley demonstrated that most of the channels experience predictable morphological and sedimentological changes as they enter their backwater length, and are characterized by rivers that are aggradational, avulsive, and distributive in nature.

This paper tests the effects of backwater length on channel facies in an ancient system using detailed facies architectural analysis of channel and bar deposits from vertical measured sections. Estimation of backwater limits are made from paleo-flow depth measurements in combination with measured changes in base level, estimated tidal range, and fluvial slope. The outcrop belt occurs along an extensively exposed fluvial long profile preserved within a Cretaceous compound incised-valley fill at the top the

Ferron Notom Delta, Henry Mountain region, southeast Utah. Three major erosional surfaces partition the compound-valley fill into three sequences (V3, V2, and V1), which were documented based on detailed outcrop studies, field correlations, field photomosaics, paleocurrent data, and 24 measured sections in both upstream Caineville and downstream Nielson Wash areas. The maximum backwater lengths calculated for the V3, V2, and V1 rivers in the downstream Nielson Wash area were between 6 - 16 km, 3 – 9 km, and 5 – 13 km respectively. The Caineville area is almost 20 km southwest of the Nielson Wash, and is estimated to lie significantly landward of the effect of backwater. Evidence for backwater effects at the downstream Nielson Wash location includes: a) a thickening of V2 channel belt deposits tied to channel deepening towards the river mouth due to scouring during high discharge, b) a reduction in average V3 channel belt width that may be related to a reduced rate of lateral migration, c) an increased proportion of finer grains in channel belt deposits tied to reduced bed material flux, d) a clear change in fluvial style in V2 from upstream braided to downstream single-thread meandering system, and e) a vertical translation from fluvial to tidal facies in all three incised-valley fills accompanied by a systematic vertical decrease in overall grain size. Findings from this study support the idea that the backwater zone is a fundamental transition in coastal rivers, across which preserved sedimentary bodies display predictable geometric changes.

3.2 Introduction

A number of non-marine sequence stratigraphic models (e.g., Shanley et al., 1992; Shanley and McCabe, 1994; Van Wagoner, 1995) hypothesized that a lowstand fluvial

system should consist of amalgamated low-sinuosity, high-gradient braided channel deposit confined in an incised valley, whereas transgressive to highstand system tracts should contain mostly mud-dominated floodplain facies that contain isolated single story meander belts. These models however, are often over simplified and do not account for incised valley systems that have mixed wave/tidal/fluvial influence (Boyd et al., 2006). Incised valleys are intrinsic components of all these non-marine sequence stratigraphic models, and are hypothesized to originate during periods of falling sea level, resulting in fluvial incision and sedimentary bypass (e.g., Posamentier and Vail, 1988; Wright and Marriott, 1993; Shanley and McCabe, 1994, Zaitlin et al., 1994). Some of these conceptual models show a similar downstream transition of fluvial style from braided to meandering, assuming a constant sediment supply and rate of base-level rise (Zaitlin et al., 1994; Boyd et al., 2006). There are many field examples that test these models of how fluvial styles change in incised valleys relative to base-level change (e.g., Shanley et al. 1992; Martinsen, 1994; Shanley and McCabe 1994; Van Wagoner, 1995; Adams and Bhattacharya, 2005). There are also numerous studies that attempt to distinguish the signatures of upstream climate versus downstream base-level change in fluvial rock sequences. Most of these studies focus on Quaternary incised-valley fills (e.g., Blum, 1992; Blum et al., 2006), as the signatures of the base-level change in ancient systems are often convolved with shorter time-scale autogenic processes that control ultimate preservation (Blum et al., 2006).

Base-level exerts a first order control on the lower reaches of fluvial systems, referred to as the "backwater effect". Paola and Mohrig (1996) first proposed the concept

of backwater effect defined as the length scale that controls the upstream distance over which open-channel flow is affected by changes in the elevation of standing water in the receiving basin (Fig. 3.1). The terminal segment of the river emptying into an ocean is called the backwater zone (L), and has a length scale approximated by "backwater length (L_{bw})" , which is proportional to the mean channel depth (H) and inversely correlated to river slope (S) or gradient of the water surface within the normal flow reach (Parker, 2004). Thus, theoretically, backwater zones occur in all rivers that enter a receiving basin, and are most extensive in deep rivers with a very gentle slope. For a continental-scale low-slope river like Mississippi, ($S \leq 10^{-5}$, H = 10–40 m), the backwater reach can extend hundreds of kilometers upstream (Fig. 3.1).

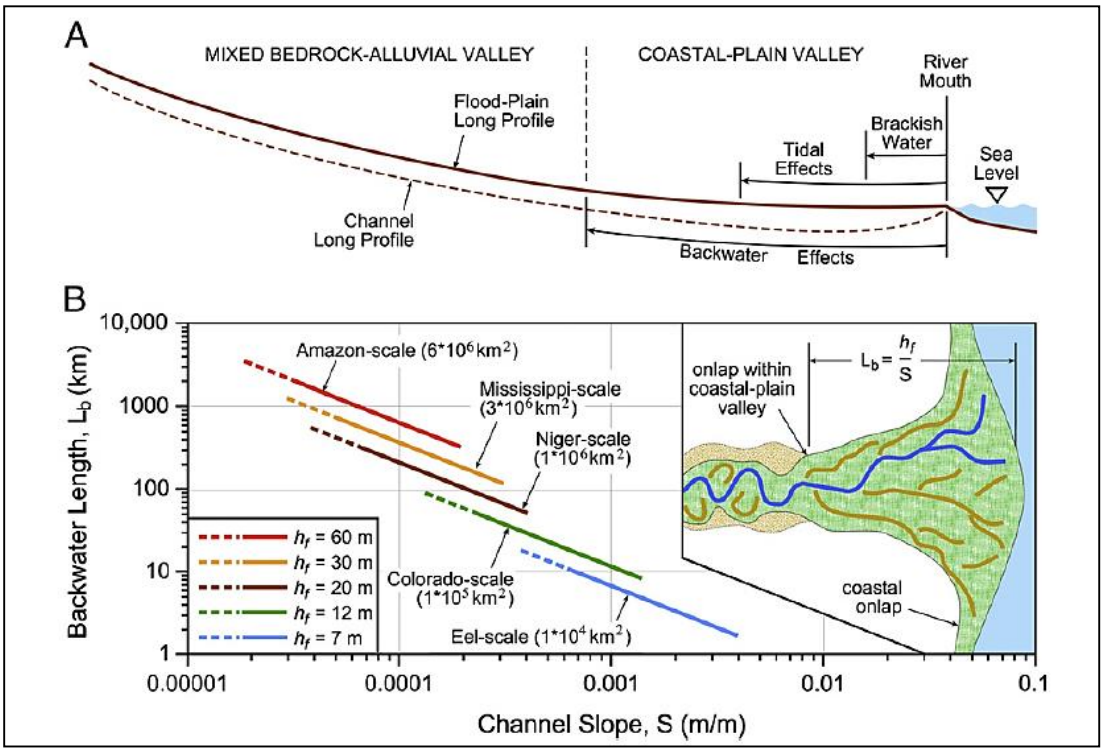

Figure 3.1 A) Cartoon showing a river entering an ocean with various zones of interest. B) The backwater effect is most extensive in deep rivers with a very gentle slope (Blum et al., 2013).

It was shown that within the backwater length (L_{bw}), the elevation of the channel bed lies below mean sea level, causing a deviation of the water surface slope from the bed surface slope (Fig. 3.1 A). Consequently, gravity-driven normal flow conditions, which dominate upstream of the backwater zone, is also affected by pressure gradients within the backwater zone. This results from the proximity of the static body of water in the ocean or lake, which causes the flow to decelerate due to a gradual downstream deepening of the channel (Parker, 2004; Nittrouer et al., 2012). Blum and Tornqvist (2000) and Blum et al. (2013) further hypothesized that the backwater length theoretically controls the ability for downstream effects (e.g., sea-level or lake-level changes) to propagate upstream. This hypothesis developed from their observations of upstream limits of onlap of Holocene flood-plain strata onto steeper-gradient late Pleistocene channel belt sand-bodies within the Mississippi coastal-plain incised valleys (Fig. 3.1). Blum et al. (2013) demonstrated that most of the Texas coastal-plain alluvial valleys are well within their backwater limits and are thus characterized by rivers that are largely aggradational, avulsive, and distributive in nature. Several other workers who studied the lower Mississippi coastal plain (e.g., Hudson and Kesel, 2000; Allison et al., 2012; Nittrouer et al., 2012), made similar observations on morphological and sedimentological changes due to fundamental transformations in flow and sediment transport as channel and channel belts enter their backwater lengths. For example, flow deceleration in the backwater zone causes extraction of larger particles, resulting in rapid downstream fining of bed materials when channels enter their backwater lengths. Hudson and Kesel (2000) and Nittrouer et al. (2012) showed that extraction of larger particles might cause channels

to become narrower and deeper after reaching the backwater length. These morphological and sedimentological changes, therefore, can induce a downstream transition of fluvial style from braided to meandering, as suggested by the traditional non-marine sequence stratigraphic models. Therefore, the sinuosity and planform fluvial style can also be affected by the backwater effect independent of base-level change and can produce similar observations in the geological record by these two different mechanisms.

This paper examines the morphological and sedimentological changes in ancient fluvial deposits that crop out in a long, continuously exposed section within a Cretaceous compound incised-valley fill at the top of the Ferron Notom Delta, north of the Henry Mountain region, southeast Utah. The main purpose of this paper is to document backwater effects on fluvial style and facies architecture in an ancient incised-valley fill, and to determine the extent that backwater effects can be traced upstream from a paleo-shoreline. Key observations that are used include detailed facies-architectural analysis of channel and bar deposits from vertical measured sections along the outcrop belt, estimations of backwater limits from paleo-flow depth estimations, and estimates of tidal range and slope of the fluvial profile.

Detailed facies and architectural studies of bed-scale fluvial deposits in ancient compound valley systems in outcrop are important in documenting the internal hierarchy and heterogeneity of fluvial aquifers and hydrocarbon reservoirs, especially if that heterogeneity is controlled by backwater effects (e.g., the degree of downstream fining and position and extent of tidal facies).

3.3 Regional Setting and Stratigraphy

The Ferron Notom Delta prograded into the Cretaceous Western Interior Seaway from west to east during the middle to late Turonian in response to the Sevier Orogeny (Fig. 3.2A) (Dickinson, 2004; DeCelles, 2004). This northeast growing fluvial-deltaic clastic wedge was deposited in a rapidly subsiding retroarc foreland basin (Peterson and Ryder, 1975; Zhu et al., 2012). The Ferron Sandstone Member is one three deltaic clastic wedges bounded above by the Blue Gate Shale and below by the Tununk Shale, members of the Mancos Shale Formation (Fig. 3.2B).

The Notom Deltaic wedge is exposed in south-central Utah, west of Hanksville (Fig. 3.3). Li et al. (2011) and Zhu et al. (2012) developed a high-resolution dip-sequence stratigraphic framework of the Ferron Notom wedge, sub-dividing the interval into 6 sequences, 18 parasequence sets, and 42 parasequences (Fig. 3.4). These topset-preserved (e.g., floodplain coals etc.) laterally extensive, dip-oriented sequences suggest sediments accumulated during a period of relatively high accommodation, compared to other Cretaceous interior formations (e.g., Frontier Formation). These 6 sequences were deposited over a period of ~ 620,000 years, based on $^{40}Ar/^{39}Ar$ dating of bentonite layers above and below the Ferron Sandstone. Each sequence on average is thus estimated to be deposited in approximately 100,000 year intervals, which roughly correspond to 100-kyr Milankovitch-scale glacio-eustatic cycles (Zhu et al., 2012). Previous work (e.g., Li et al., 2010; Li et al., 2011; Zhu et al., 2012; Fielding, 2015) described overall basinward and down-stepping parasequences forming a forced regressive systems tract. The dominant

depositional processes vary from river-dominated in the SW to wave-dominated towards the NE, producing lateral facies variations within the same parasequence (Fig. 3.4).

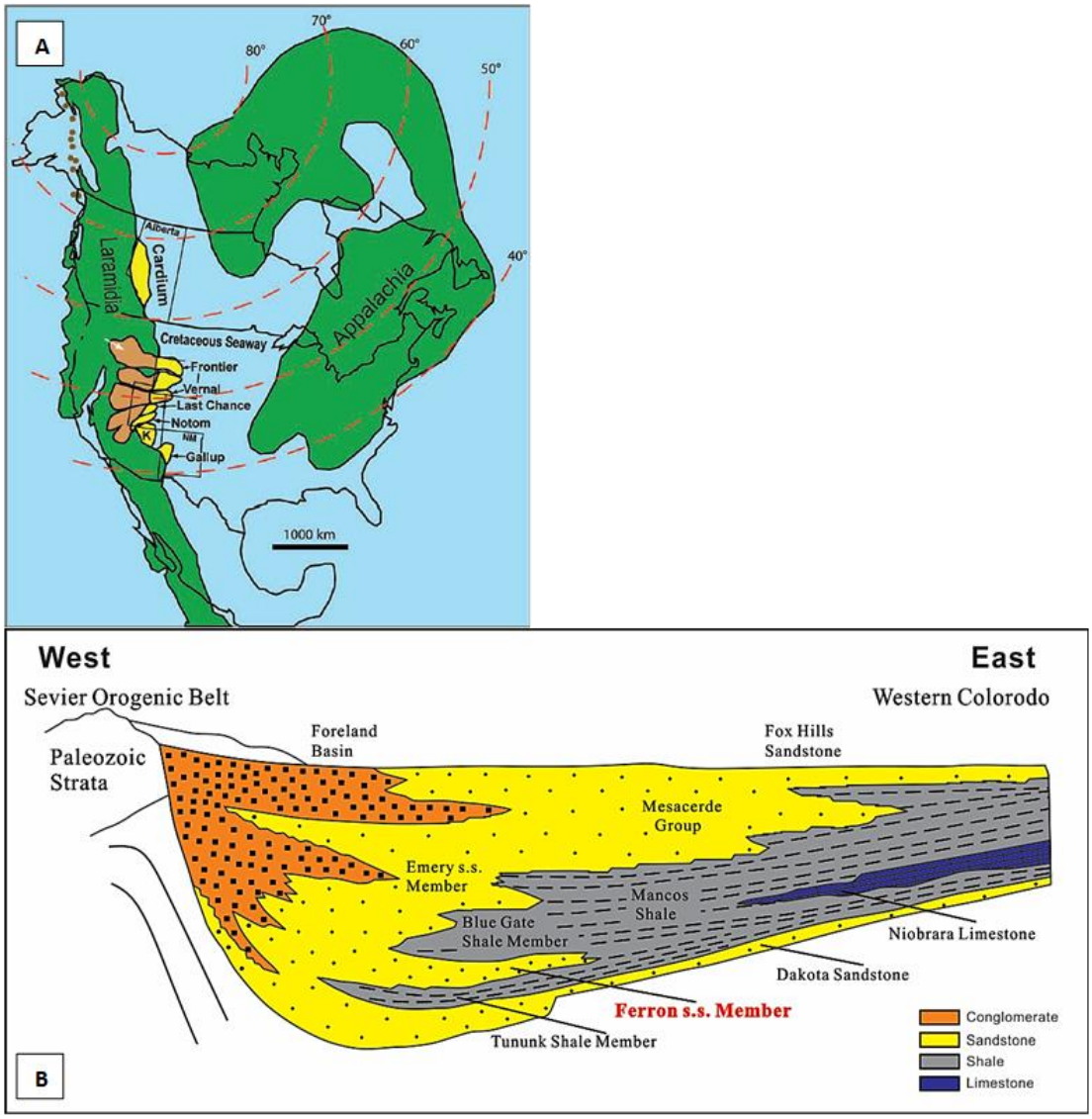

Figure 3.2 A) Turonian paleogeographic reconstruction of the Western Interior Seaway showing the Ferron Notom Delta as one of the delta complexes along the western margin (from Bhattacharya and MacEachern 2009, after many other sources). B) West-to-east Cretaceous wedge stratigraphy (from Barton et al., 2004, modified from Armstrong, 1968).

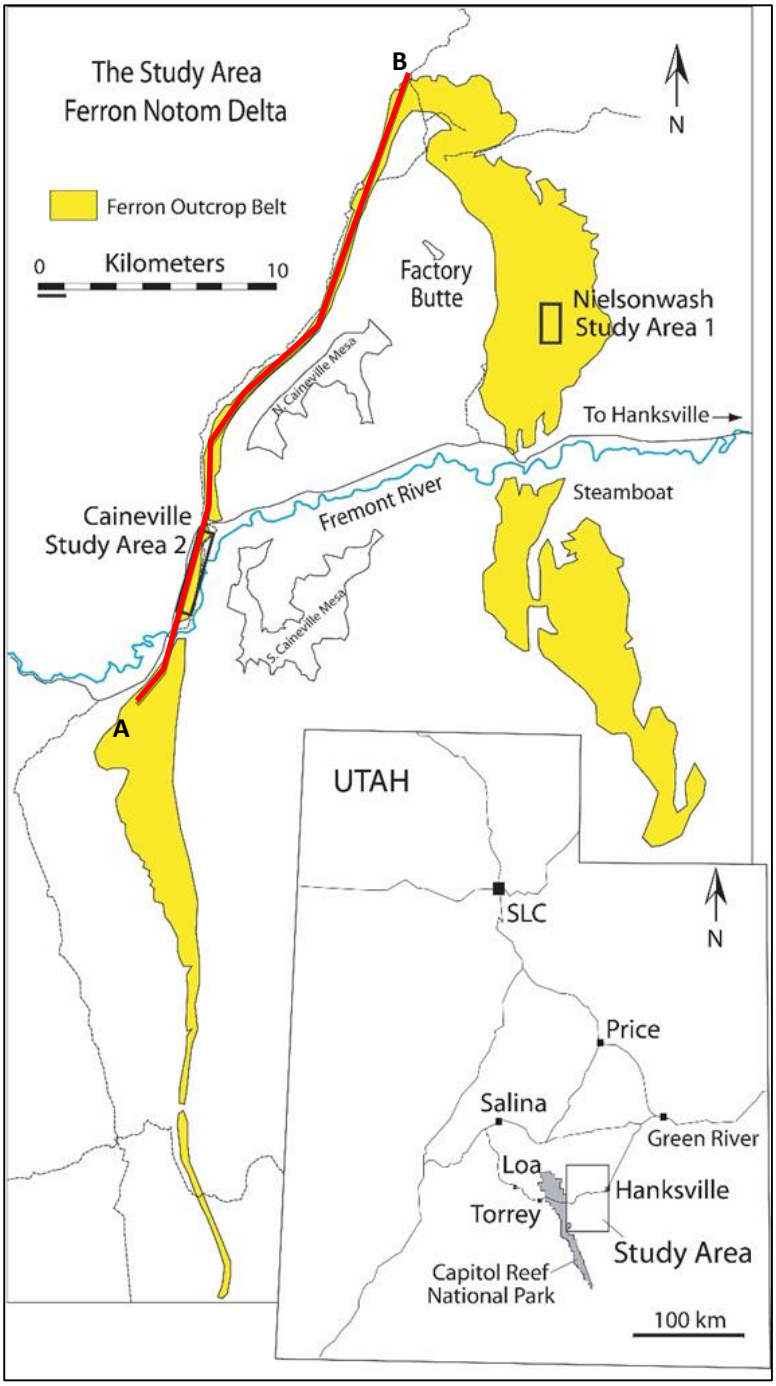

Figure 3.3 Shown in yellow is the outcrop of the Ferron Notom delta between Hanksville and Caineville, southeastern Utah. The red line represents the depositional-dip profile by Zhu et al. (2010; Shown in Figure 3.4). The black box outlines the Nielson Wash East (study area 1) and Caineville (study area 2). SLC = Salt Lake City.

Extensive fieldwork documented a well-developed regional scale compound incised-valley system exposed in both strike and dip directions in the Sequence 1 (Li et al., 2010; Li and Bhattacharya, 2013; Hilton, 2013) (Fig. 3.4). The base of this compound incised-valley system delineates a composite, time-transgressive surface or highly diachronous sequence boundary (Li et al., 2011). Detailed correlation of major erosional surfaces from field mapping, measured sections, and photomosaics reveal the presence of at least three cut-and-fill episodes in Nielson Wash, east of the Factory Butte area, each of which shows 20 to 30 m of erosional relief (Li et al., 2010; Hilton, 2013). The compound nature of this regional scale incised-valley system is also supported by the presence of interfluve terraces (Zhu et al., 2012; Hilton, 2013; Bode, 2014). Maximal channel story thicknesses of 5-7 meters in Nielson Wash show that the regional erosional relief of the individual valleys is 3-6 times maximum channel depths (Li et al., 2010; Hilton, 2013; Ullah et al., 2015).

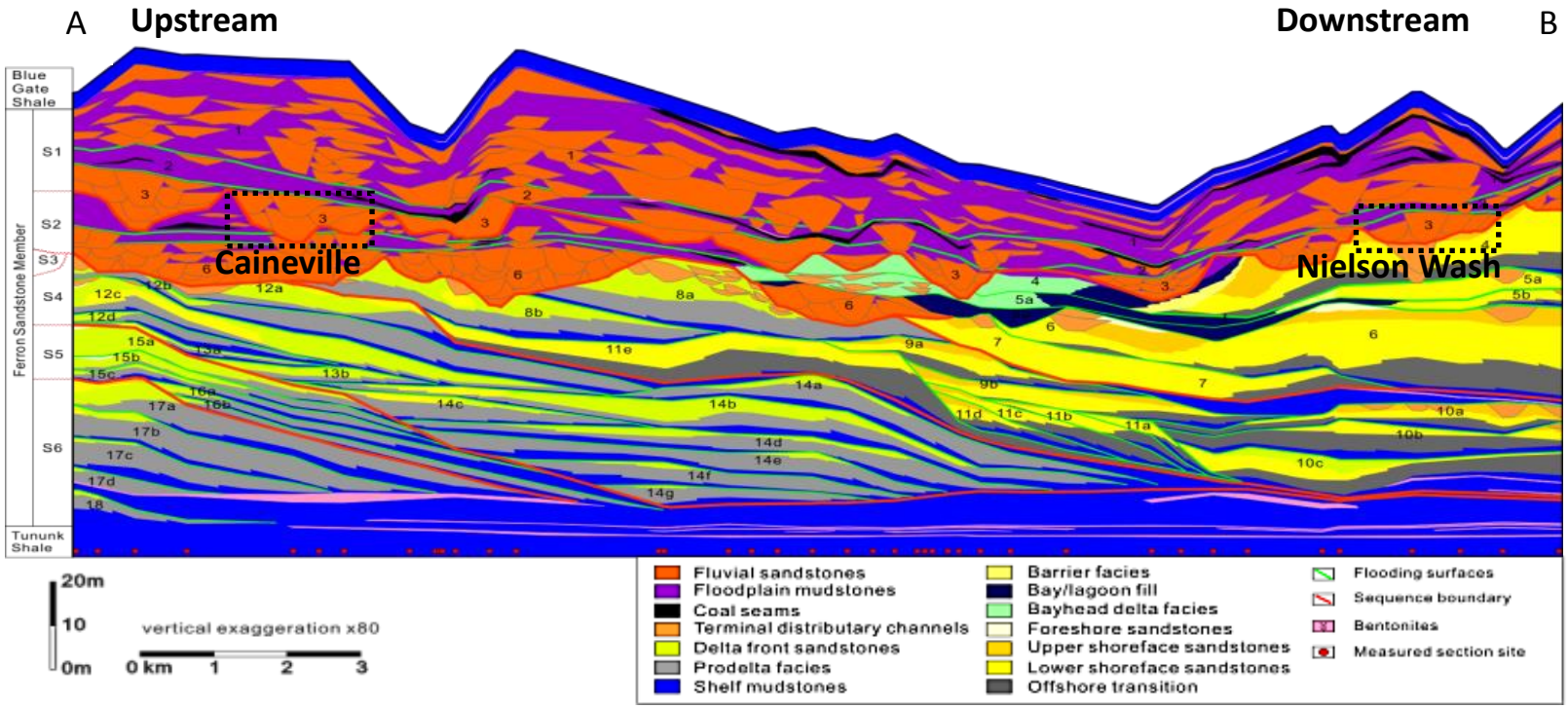

Figure 3.4 High-resolution depositional-dip sequence stratigraphic cross section of the Notom delta (from Zhu et al., 2012). The box outlines the approximate stratigraphic positions of the compound incised valley investigated during this study. See Fig. 3.3 for the location of the profile. The numbers in the figure represent the18 parasequence sets described by Li et al. (2011) and Zhu et al. (2012).

3.4 Study Area and Methods

Fluvial deposits in the upper compound incised-valley system (Sequence 1, Parasequence 3) are exposed in a triangular shaped outcrop belt in a series of cliff and mesa exposures extending between Caineville, Nielson Wash, and the Steamboat area in both strike- and dip-oriented sections (Fig. 3.3). Field data from the distal part of the valley fill were collected from outcrops along a nearly 1.5 km-long cliff face in East Nielson Wash Canyon near Factory Butte, north of Highway 24 (Fig. 3.5). The proximal part of this same incised-valley system is well exposed along a 4 km-long dip-slope dissected cliff exposure near Caineville 15 km southwest of the Nielson Wash (Fig. 3.5, 3.6). Field observations from 24 vertical measured sections along accessible cliffs were used to document lithologies, sedimentary structures, and stratal architecture to compare the proximal Caineville to distal Nielson Wash segments of the valley fill. The architecture of the compound valley fills and surfaces of incision were physically traced by walking them out in conjunction with photomosaics and cross-sections constructed from the measured sections.

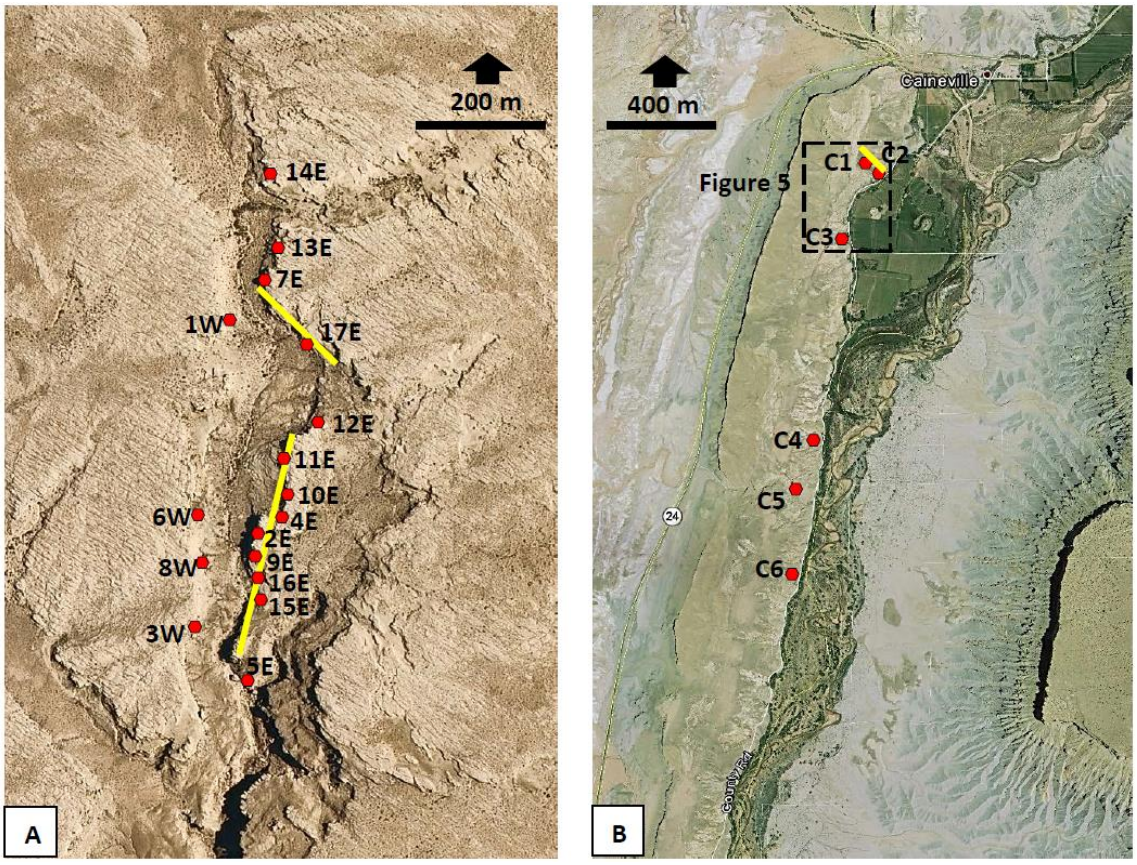

Figure 3.5 Satellite image of the Nielson Wash (A) and Caineville area (B). The yellow lines in the study area represent the approximate locations of the bedding diagrams shown in Figures 3.17, 3.19, and 3.20. The red dots represent the locations of the measured sections in the Nielson Wash East and Caineville area. The outcrops within the boxed area in Fig. 3.5B are shown in fig. 3.6.

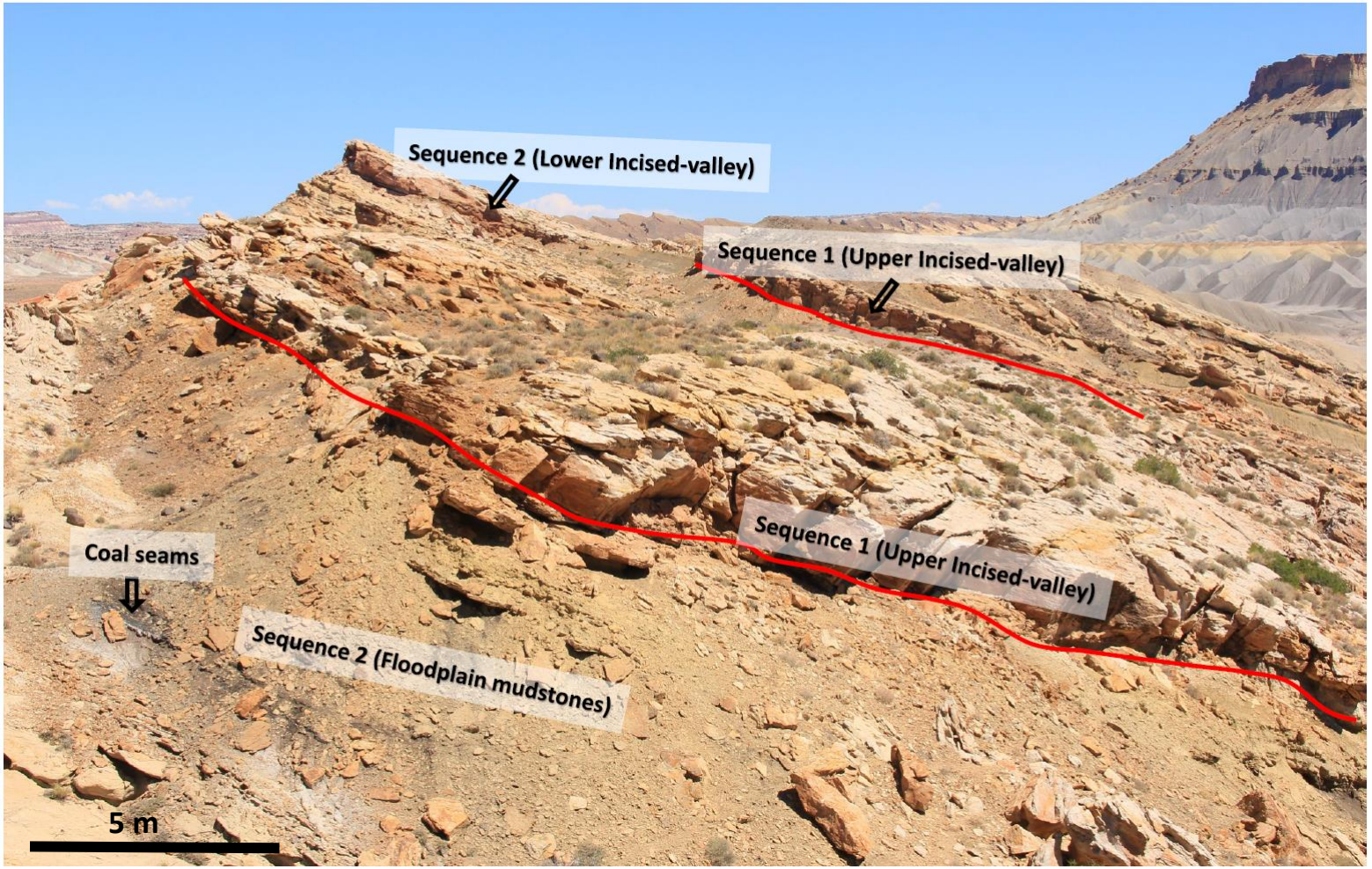

Figure 3.6 Proximal part of the Upper incised-valley system (sequence 1) is well exposed along dip-slope dissected cliff exposures in Caineville area. The contact between the upper incised-valley fill and the underlying floodplain mud of the lower incised-valley system (sequence 2) is marked by red lines (Sb1a).

Internal bedding and facies architecture of stacked bar and channel deposits were documented based on the correlation of bounding surfaces of different scales (zero to eighth order) using the bounding surface hierarchy of Miall (1985). The smallest-scale surfaces correlated and mapped were centimeters to meters thick cross-set and/or coset boundaries, represented by second and third-order surfaces that define bar-scale macroforms or inter-bar accretion surfaces. The base of the macroforms, or bars, represented a fourth-order surface. The bases of major channels define the fifth-order or channel-basal erosional surface. Valley-base or seventh-order surface were defined based on field correlation, mapping, and detailed sedimentological descriptions. The master valley basal erosional, or the eighth-order surface (sequence boundary) was marked by truncation of underlying marine shoreface deposits by overlying fluvial deposits (PS4 of Zhu et al., 2012).

Facies were recognized based on lithology, sedimentary structures, and fossil assemblages using Miall's 1996 classification scheme. Grain sizes were estimated in the field using a hand lens and a grain-size card. The length and thickness of cross sets were also recorded and classified as small- (<10 cm), medium- (< 25 cm), and large-scale (> 1 m) sets to match their vertical thicknesses to that of their formative bedforms (i.e. dune-scale vs. bar-scale) (Bridge, 2003). Plan-view morphology or the paleogeographic reconstructions of the paleo-channels and channel belts were done based on detailed analysis of plan-view architecture of channel and bar deposits, in combination with paleocurrent and sediment accretion data. Sediment transport and mean flow directions

were estimated from dune-scale cross strata in 2-D strike-oriented exposures and where possible, verified based on the nearest rib-and-furrow structures in plan-view.

Channel depth and slope were estimated using the outcrop data (see appendix), and then used to calculate backwater lengths. Paleohydraulics (e.g., slope, velocity, discharge) were calculated from the sedimentological parameters collected in the field (mainly median grain size (D_{50}), bedform-type, cross-set thickness, and water depth). These data were extracted from preserved channel stories using various empirically derived formulas based on studies of both modern and ancient data (Bridge, 1993b; Paola and Mohrig, 1996; Leclair and Bridge, 2001; Bridge, 2003; Holbrook and Wanas, 2014). Channel and channel belt apparent widths were estimated in this study using the techniques of Bridge and Mackey (1993). Paleo-discharge was estimated using the techniques of Bhattacharya and Tye (2004) and Bhattacharya and MacEachern (2009).

3.5 Ferron Compound Incised-valley System

We used two primary criteria to distinguish allogenically formed incised valleys from large-scale autogenic channel scours. The first criterion was the relative relief associated with an erosional surface as identified by stratal truncation below and onlap above. If the maximum erosional relief of an erosional surface is significantly greater than the thickness of the thickest single story, or even multiple stacked vertical stories at a confluence scour, then such an erosional surface likely represents the base of an incised valley, and may be a sequence boundary (Ullah et al., 2015). The second criterion was the observation of more proximal fluvial facies truncating more distal marine facies. Li et al.

(2010) and Hilton (2013) mapped rooted zones developed on shoreface deposits (Parasequence 4 in Fig. 3.4) associated with valley interfluves, and documented nearly 30 m of overall regional valley erosional relief. Their studies documented maximum channel depths of about 6 m with an average depth of 3-4 m. Therefore, the valley-scale erosional surfaces are up to ten times average channel depth.

Caineville Area

Detailed correlation of major erosional surfaces from field mapping, measured sections, and photomosaics revealed the presence of at least two cut-and-fill episodes in the upstream part of the studied compound-incised valley system (sequence 1) in the Caineville area (Figs. 3.6 & 3.7). The bases of valleys are characterized by pebbly coarse- to very coarse-grained extraformational sandstones and minor conglomerate with mud rip-up clasts, interpreted as valley lag deposits formed during base-level fall and early lowstand. These extraformational conglomerates and lag deposits at the valley base were traced laterally at least three kilometers upstream in the Caineville outcrop belt. In some areas, the base of the valleys contained fossilized wood. The maximum preserved compound valley-fill thickness in Caineville is 14 m and is partitioned into two separate valleys floored by two unconformities Sb1a and Sb1b. Sb1a marks the base of the older Valley 3 (V3) and Sblb the base of the younger Valley 2 (V2) (Fig. 3.7). The base of the lower V3 (Sb1a) truncates underlying fluvial floodplain deposits of an older incised-valley system associated with Sequence 2 of the Ferron Notom wedge (Fig. 3.6, 3.7). The maximum preserved thickness of V3 deposits, as measured in the Caineville

area, is ~ 8 m. The base of the upper V2 (Slb1b) erodes into either V3 or floodplain deposits of the underlying older incised-valley system of sequence 2 (Fig. 3.7). The maximum preserved thickness of V2 deposits in the Caineville area is 10 m.

These two erosional surfaces (Sb1a, Sb1b) in the upstream Caineville can be traced 15 kilometers downstream along cliff faces to the Nielson Wash area (Figs. 3.8 and 3.9) . A major change in the paleogeography from V3 to V2 in both areas is supported by more than 100^{o} eastward shift in flow direction. The mean paleoflows of the channels in V2 is SE and shows a similar orientation between the Caineville and Nielson Wash areas (Fig. 3.10); however there is a slight divergence of paleocurrents among the V3 channels in the two areas. The mean paleoflow direction of the V3 channels in the Caineville area is 12^{o} and is 335^{o} in the Nielson Wash East area (Fig. 3.10), indicating a 30^{o} westward shift of the mean flow direction downstream. The paleoflow directions of the V3 channels in the Nielson Wash area show greater variability compared to their upstream parts. Compared to the V3 channels, the paleoflow directions of the V2 channels in Caineville show a wider range with a mean flow direction of 116^{o} (E-SE).

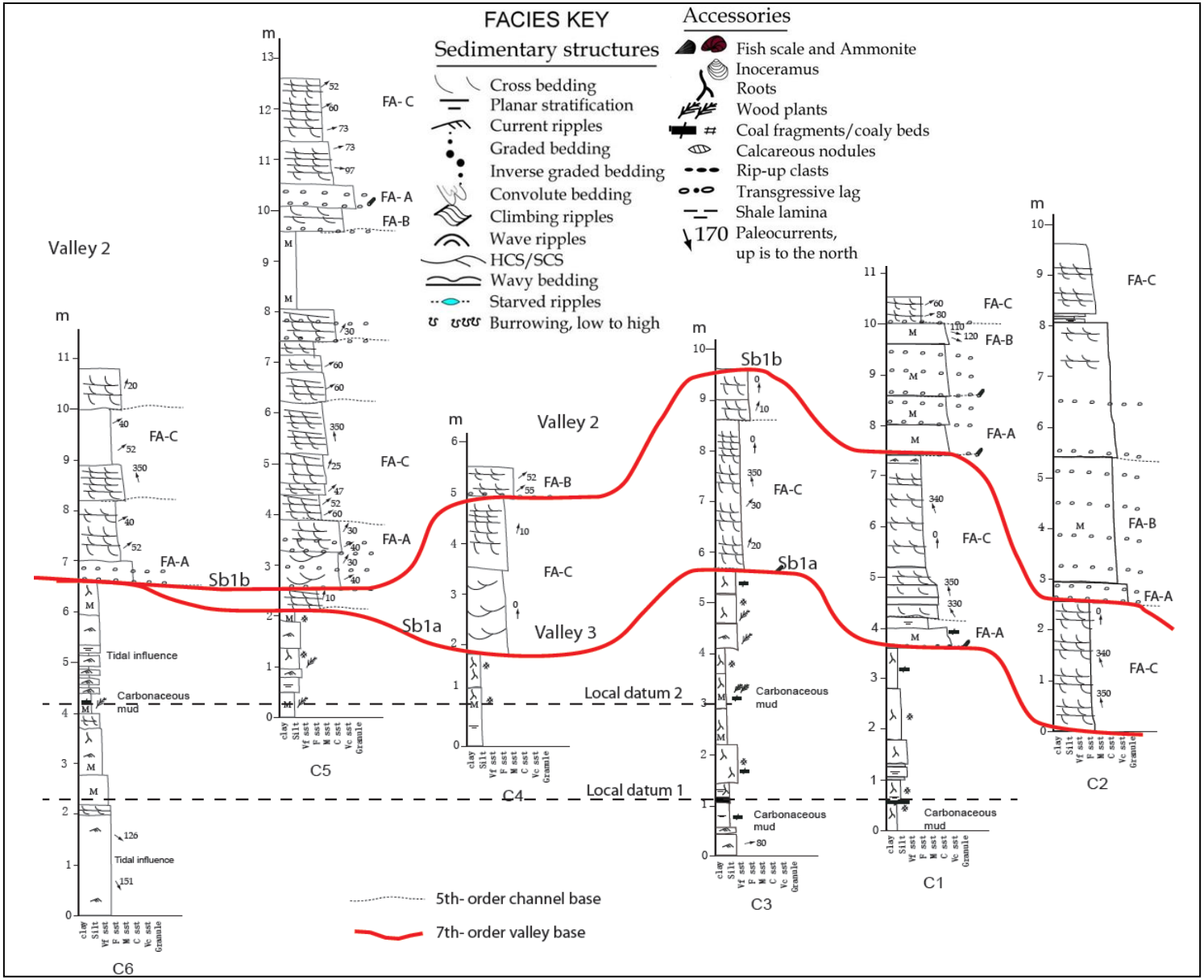
FACIES KEY
Sedimentary structures
Cross bedding
Planar stratification
Current ripples
Graded bedding
Inverse graded bedding
Convolute bedding
Climbing ripples
Wave ripples
HCS/SCS
Wavy bedding
Starved ripples
Burrowing, low to high
Accessories
Fish scale and Ammonite
Inoceramus
Roots
Wood plants
Coal fragments/coaly beds
Calcareous nodules
Rip-up clasts
Transgressive lag
Shale lamina
170 Paleocurrents, up is to the north
Valley 2
Valley 3
Sb1b
Sb1a
Local datum 1
Local datum 2
Tidal influence
Carbonaceous mud
FA-A
FA-B
FA-C
5th- order channel base
7th- order valley base
C1
C2
C3
C4
C5
C6

Figure 3.7 (opposite page) Measured sections showing facies and stratal bounding surfaces in incised valleys in the upstream Caineville area along section C-C/ in Figure 3.5. Thick solid red lines mark the valley basal erosional surfaces, Sb1a and Sb1b.

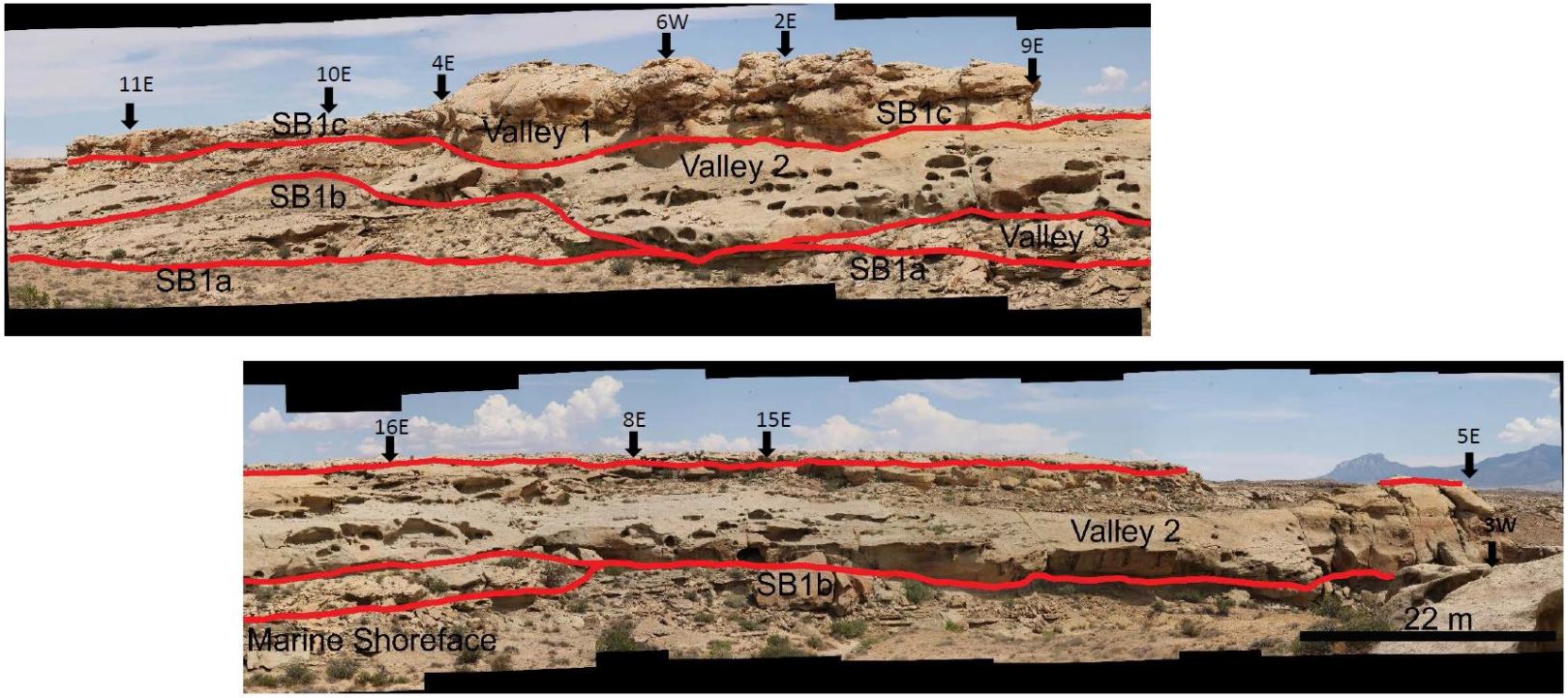

Figure 3.8 Photomosaic showing the valley systems and stratal bounding surfaces in incised valleys in the Nielson Wash area. The black arrows mark the locations of the measured sections shown in Fig. 3.9.

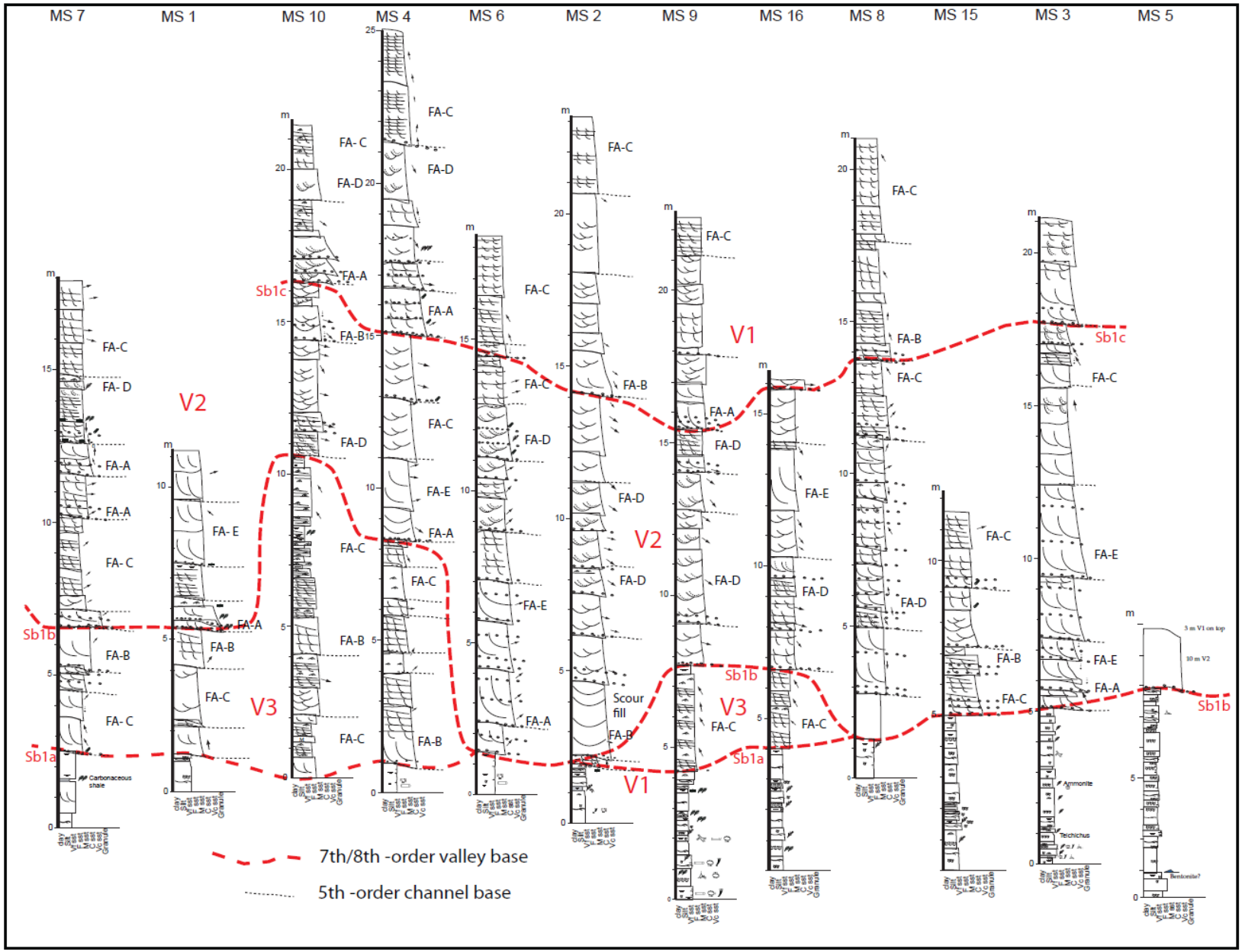
MS 7
MS 1
MS 10
MS 4
MS 6
MS 2
MS 9
MS 16
MS 8
MS 15
MS 3
MS 5
Sb1a
Sb1b
Sb1c
V1
V2
V3
Scour fill
Carbonaceous shale
Ammonite
Teichichus
Bentonite?
7th/8th -order valley base
5th -order channel base

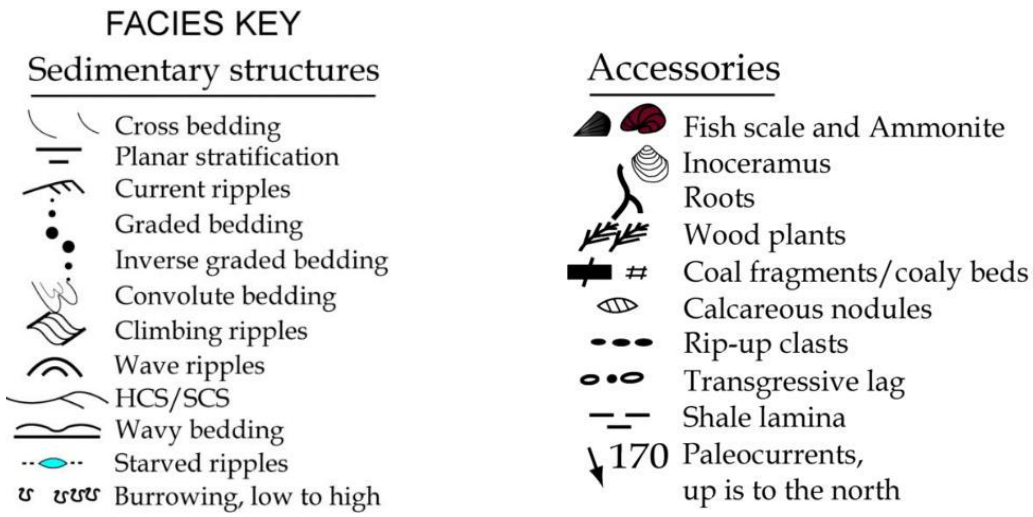

Figure 3.9 Measured sections showing facies and stratal bounding surfaces in incised valleys in the downstream Nielson Wash area. Please see Figure 3.5 for the locations of the measured sections. Thick solid red lines mark the valley basal erosional surfaces, Sb1a, Sb1b, and Sb1c. The sections are not equally spaced in the outcrop.

Nielson Wash Area

Previous studies (e.g., Li et al. 2010; Li and Bhattacharya 2013; Ullah, et al., 2015) demonstrated an additional episode of cut-and-fill in the upstream part of the valley in Nielson Wash. This youngest V1 is floored by another extensive erosional surface (Sb1c, Fig. 3.8 and 3.9). Compared to the bottom two valleys, the paleoflows within the V1 channels in Nielson Wash show much more variability with a mean of 61^{o} (Fig. 3.10). This marks a 60^{o} northward shift of mean flow direction from the underlying V2 channels (mean 120^{o}), and represents the third and final cut-and-fill episode in the downstream Nielson Wash area.

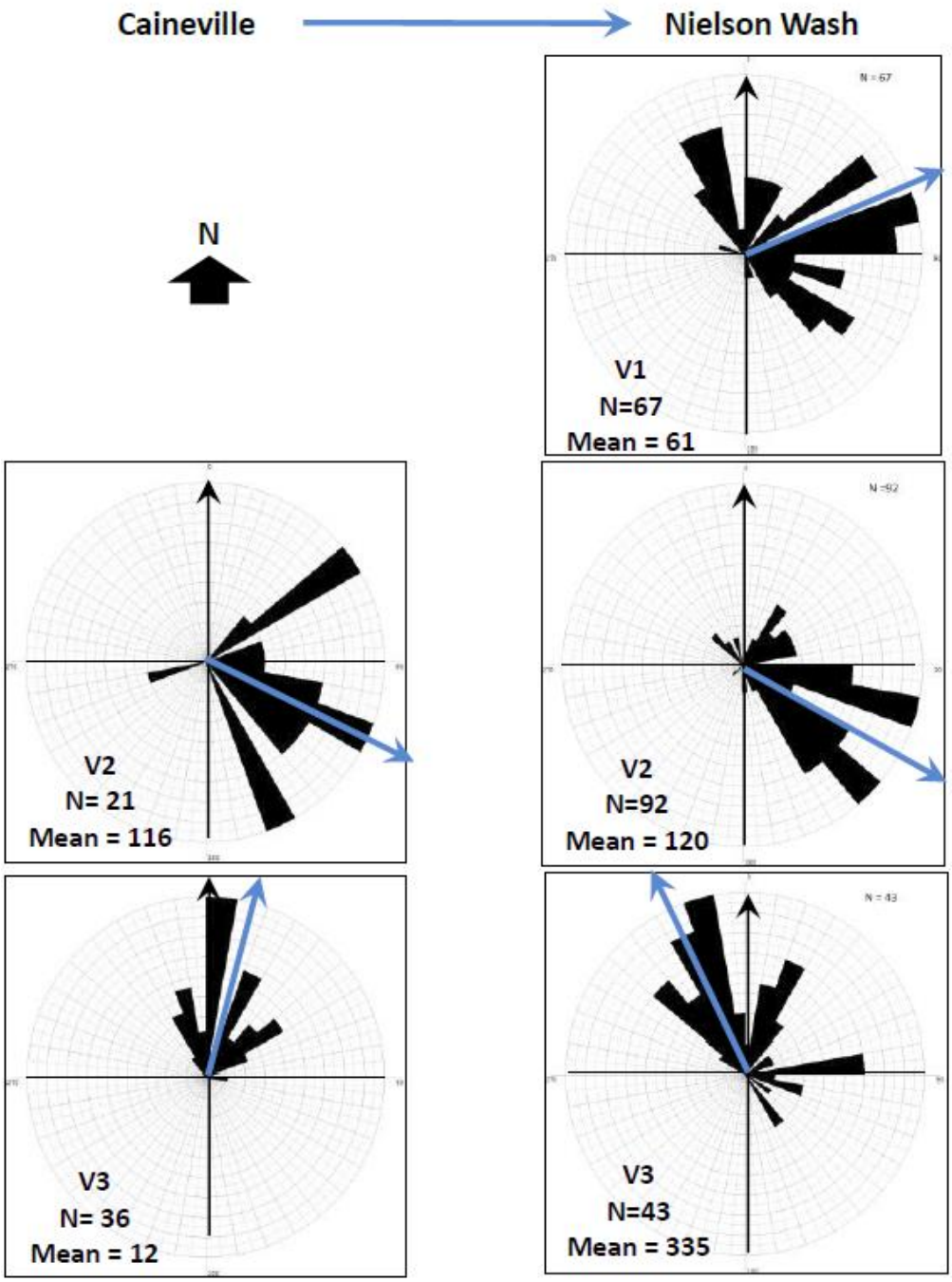

Figure 3.10 Rose diagrams showing paleoflow directions in the incised valleys (V1, V2, and V3) in the Caineville (left) and Nielson Wash area (right). Paleocurrent data were collected from dips of dune-scale cross strata in fluvial sandstone facies from measured sections. The blue arrows represent the mean flow direction in each valley.

V2 channels in the Nielson Wash shows similar mean paleoflow direction as in Caineville area, however, but with much less variability. The base of the valleys in Nielson Wash were traced over a distance of 1.5 kilometers on the outcrop, and in most cases are marked by granule to very coarse-grained sandstone with abundant lag materials and fossilized wood fragments. Maximum cumulative thickness of all the valley-fills from the correlations of the measured sections in the Nielson Wash area was recorded as 25 m in this study (Fig. 3.8, 3.9). However, elevation differences calculated using a Digital Elevation Model (DEM) of the lowest and highest points in the valley fill, (Chapter 4) show that the actual valley thickness (~32+ m) is much higher than the previous estimates.

The correlation of stratal bounding surfaces in the compound incised valley exposed along a cliff face in the Nielson Wash area is shown in Figure 3.9. The base of the lowermost valley V3 (Sb1a) truncates either highly bioturbated marine mudstone or very fine-grained marine shoreface sandstone deposits of Parasequence 4 (PS4 in figure 3.4). The maximum preserved thickness of V3 in the Nielson Wash area is 12 m. Although partially eroded by the youngest valley V1, V2 valley fill is much thicker in the downstream part of the valley in Nielson Wash compared to the upstream exposures in Caineville. In Nielson Wash, V2 erodes either partially into V3 or it completely cuts it out, superimposing fluvial deposits of V2 onto highly bioturbated marine shoreface deposits of Parasequence 4 in sequence 2 (Fig. 3.8). The maximum erosional relief and the maximum preserved thickness of V2 deposits measured in the Nielson Wash is 11 m and 15 m respectively (Fig. 3.8, 3.9). V1 erodes into either V2 or V3 in the Nielson Wash area

(Fig. 3.8). The maximum erosional relief associated with V1 is 9 m. The thickness of the V1 deposits is generally 6-12 m, and is mostly consists of vertically stacked fining-upward fluvial deposits.

3.6 Facies Analysis

Based on lithology, grain size, scale and abundance of sedimentary structures, bedding thickness, and bounding surfaces, five main channel-fill lithofacies associations were documented in the Caineville and Nielson Wash areas (Table 3.1). These are: A. Valley/ Channel Basal Lag Deposits (FA- A), B. Coarse-grained Fluvial Sandstone (FA- B), C. Fine-grained Fluvial Sandstone (FA- C), D. Tidally Influenced Fluvial Sandstone (FA- D), and E. Large, Steeply Dipping, Laterally Accreting Single Foresets (FA- E) (see Figs. 3.11 – 3.14). The distribution of these facies and correlation of their stratal bounding surfaces contained within the incised valleys exposed along two cliff faces in the upstream Caineville and downstream Nielson Wash area are shown in the cross sections in Figure 3.7 and 3.9. These facies not only show noticeable variations between the upstream vs. downstream valley fills but also exhibit considerable lateral and vertical variations throughout a single phase of valley fill.

Table 3.1 Five main channel-fill lithofacies associations documented in the Caineville and Nielson Wash area.

Facies Association	Facies Description	Bounding surface	Interpretation	Valleys
A: Valley/ Channel Basal Lag Deposits	Trough/planar cross-Bedded (Gt/Gp) or massive sand matrix-filled basal channel pebbles; scour-fill Sand lithofacies Ss; frequent mud rip-up clasts, intra-basinal overbank clasts.	5^{th}- order channel or 6^{th} – order valley erosional surface at the base.	Coarsest fraction of the bed-load sediments retained during relative sea level fall and early lowstand	V1, V2 in Nielson Wash; V2, V3 in Caineville
B: Coarse Fluvial Sandstone	Highly amalgamated medium to coarse grained dune/bar -scale trough cross-bedded sands (St) and planar cross-bedded sands (Sp).	1^{st} and 2^{nd} – order internal bounding surface; $4^{th}/5^{th}$ order surface at the base.	Channel-fill or bedform deposits representing most of the bed-load sediment.	V1 (basal part), V2 in Nielson Wash; V2, V3 in Caineville
C: Fine Fluvial Sandstone	Very fine to medium-grained dune and bar-scale trough cross-bedded sands (St) and planar cross-bedded sand (Sp), upper plane horizontally bedded Sand (Sh) current ripple cross-laminated sand (Sr) and climbing ripples.	1^{st} and 2^{nd} – order internal bounding surface; $4^{th}/5^{th}$ order surface at the base.	Channel-fill or bedform deposits in mostly lateral accretional depositional units; Levee and bank deposits.	V1, V2 (upper part), V3 in Nielson Wash; V2 (upper part), V3 in Caineville.
D:Tidally Influenced Fluvial Sandstone	Very fine- to fine grained sandstones often interbedded with thin clays and siltstones. Current ripple cross-laminations, climbing ripples, planar and flaser beddings, and dune-scale cross stratifications; presence of brackish water fossils.	1^{st} and 2^{nd} – order internal bounding surface.	Late lowstand to transgressive deposits as indicated by comparatively finer grained, less amalgamated sand bodies.	Middle and top part in V1 and V2, basal part in V3 in Nielson Wash; not observed in Caineville.

Table 3.1. Continued

Facies Association	Facies Description	Bounding surface	Interpretation	Valleys
E: Moderate - steeply dipping, laterally accreting large-single foresets	Large-scale single foresets, dipping at or greater than the angle of repose. The individual foresets are between 1.5 and 4 m in height and can extend more than 20 m laterally. They are comprised of 0.5 - 1 cm thick, alternating very fine- to medium sandstone.	5^{th} -order channel erosional surface at the base, 4^{th} – order surface at the top; no internal bounding surface.	Distinct unidirectional accretion towards the channel cut bank as the river migrated laterally over the deep thalweg near the river bend filling a scour.	V1, V2, and V3 in Nielson Wash; rarely observed in Caineville.

Facies Association A: Valley/Channel Basal Lag Deposits

Valley/channel basal lag deposits (FA -A) comprise a few decimeters to meter-thick, poorly sorted trough-and planar cross-bedded (Gt/Gp in Miall, 1996) or massive (Gm) sand matrix-filled, basal channel pebble conglomerates. Sometimes they are interbedded with plane-bedded granules. They have a 5^{th}- order channel or 6^{th} – order valley-basal erosional surface at the base. Basal lag deposits are also characterized by large mud rip-up and smaller intra-basinal overbank clasts, and Fe-concretions, and represent the coarsest bedload deposits (Fig. 3.11). Valley/channel basal lag deposits also locally contain Scour-Fill Sandstones, (Ss lithofacies of Miall, 1996) consisting of poorly sorted, coarse- to very coarse-grained sandstone with poorly defined cross stratification.

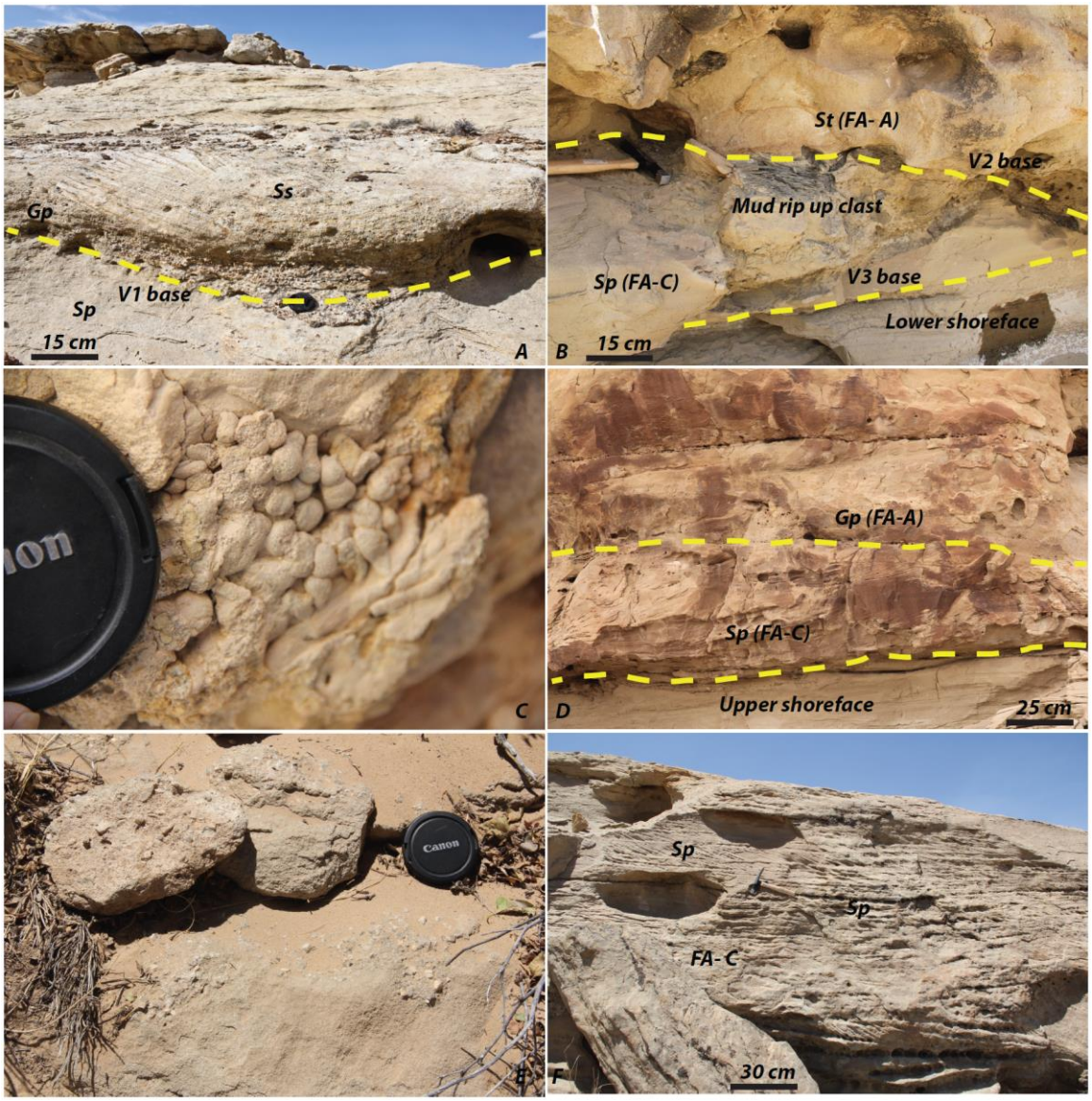

Figure 3.11 Various lithofacies in valley-filling fluvial deposits in Nielson Wash: A) Planar cross-bedded basal channel pebble (Gp) overlain by poorly sorted coarse-to very coarse-grained sandstone (Ss) at the base of V1. B) Widespread occurrence of extrabasinal pebbles and large mud rip-up clasts at the base of V2. C) *Teredolites longissimus* at the base of V3 indicating flood-dominated tidal facies (FA- D). D) Multistory valley fill in V1 and V3. The fluvial sandstones in V3 have a sharp, erosional contact (marked by yellow line) with the shoreface facies below. E) Wide occurrence of poorly sorted extrabasinal pebbles at the base of V2 (FA- A). F) Cosets of decimeter-thick planar cross sets on a 2-D outcrop.

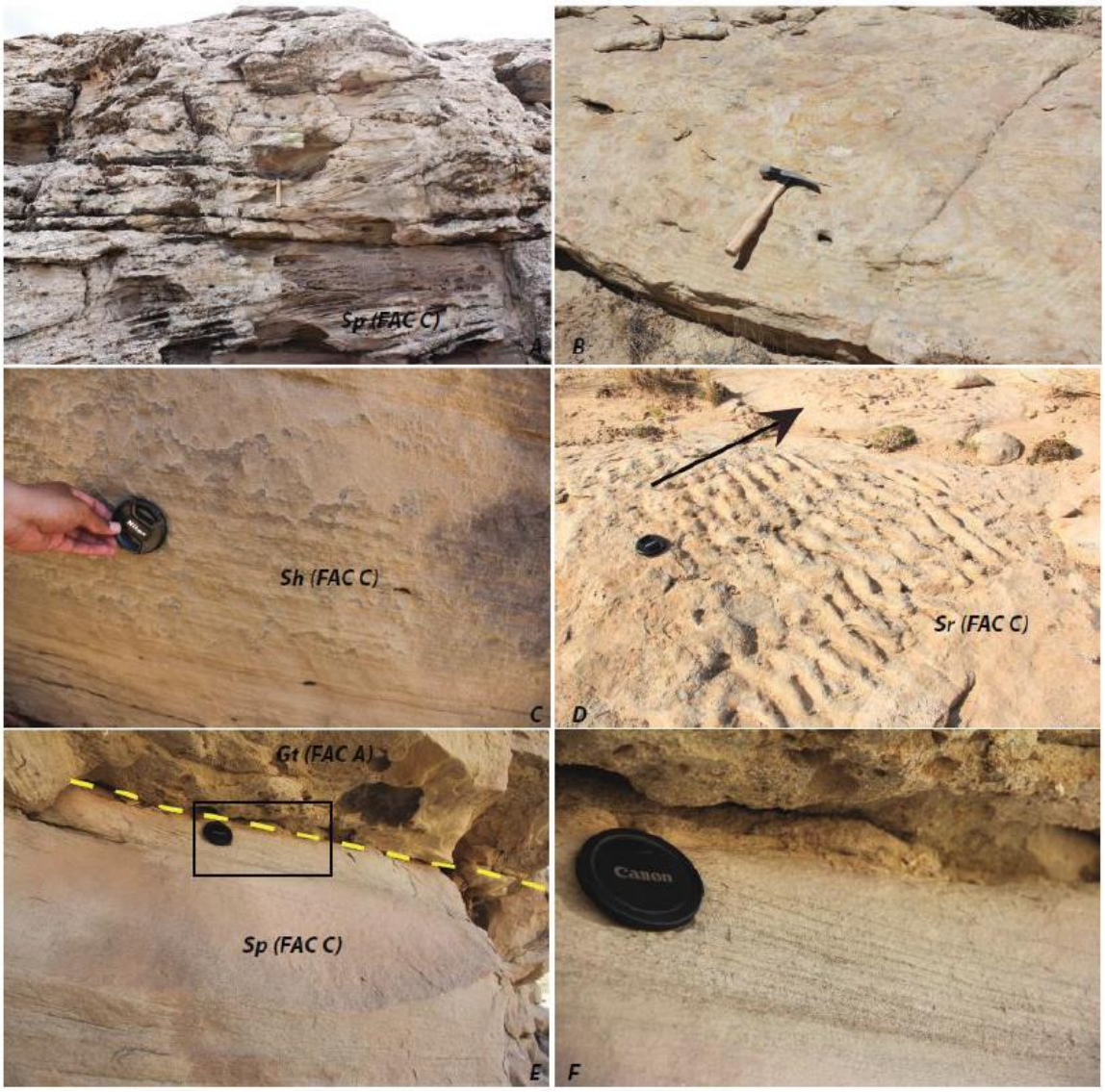

Figure 3.12 Various lithofacies in valley-filling fluvial deposits in Nielson Wash: A) Large, simple planar cross-bed set (Sp) at the bottom, overlain by high-angle small-scale cross sets. B) Very fine-to fine-grained sandstones with Liesegang banding. C) Upper plane-bed Lithofacies (Sh) with flat, parallel laminations and parting lineations on bedding planes. D) 3-D current ripples with rounded tops at the V1 surface. Arrow represents the flow direction. E) Low-angle cross-bedding (Sp) downlapping onto Sh bedding surface, indicating deposition close to the upper plane-bed condition. Double mud drapes in the foresets of dune-scale cross strata at the very top of V2 (black box). F) Double mud drapes in the foresets of dune-scale cross strata within tidal-channel deposits (area within the box in image E).

Figure 3.13 Various lithofacies in valley-filling fluvial deposits in Nielson Wash: A) Tide-influenced large, simple planar cross-bed sets (Sp) in bar deposits in V2. B) Double mud drapes in the foresets of dune-scale cross strata in V1. C) Steeply dipping, large-single foreset facies (Sf) in laterally accreting unit bar in V1. D) Single set of downstream accreting large-scale trough cross-beddings (Sf) filling a scour. E) More than 20 m long single foresets bounded by 5^{th}- order channel-basal erosional surface at the base and truncated by a 4^{th}-order macroform-basal erosional surface at the top.

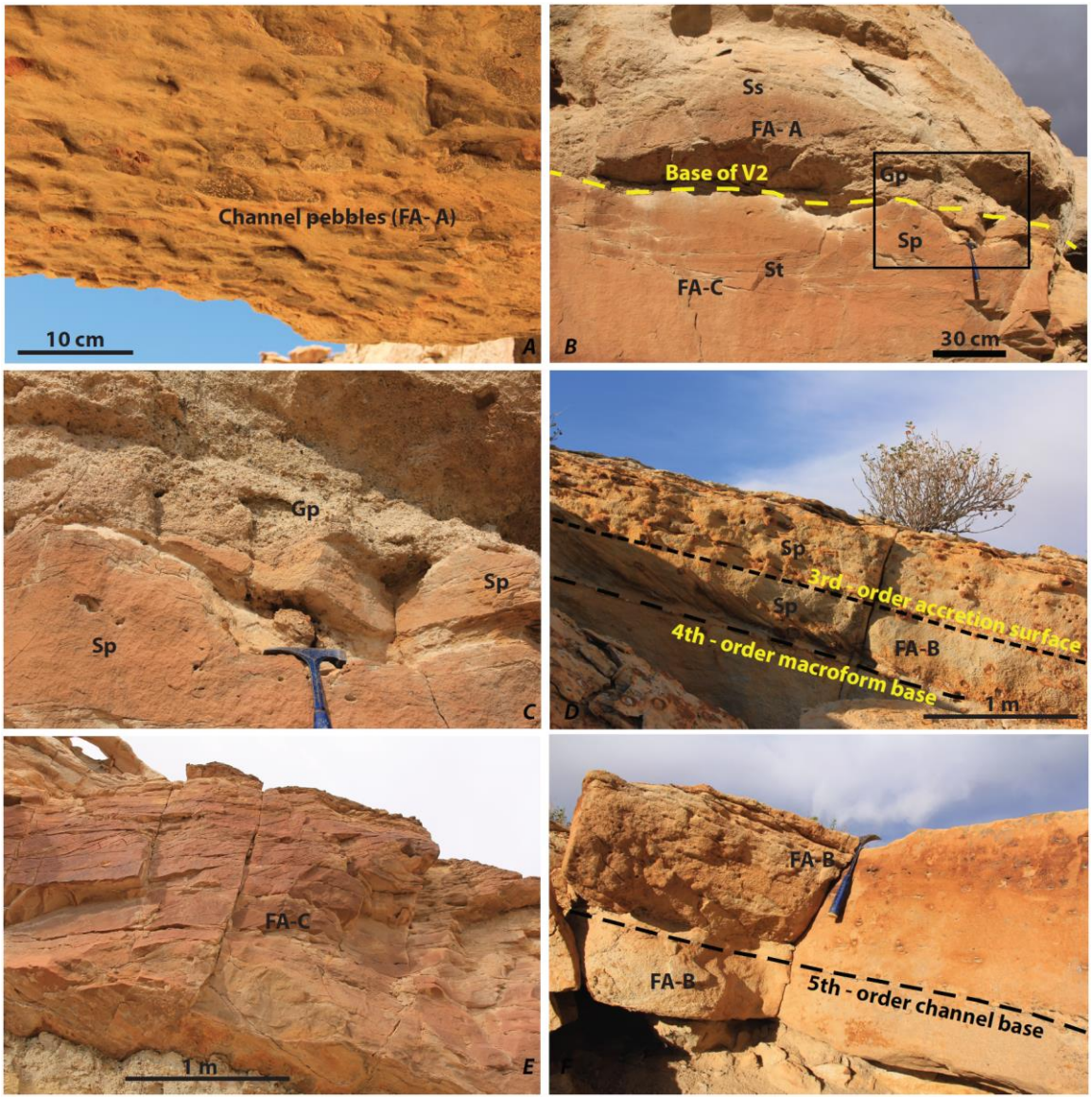

Figure 3.14 Various lithofacies in valley-filling fluvial deposits in Caineville: A) Sand matrix-filled intra-basinal pebbles/clasts in channel basal lag deposits at the base of V3. B) Erosional contact between poorly sorted planar cross-bedded lithofacies Gp at the base of V2 (top) and underlying fine to medium-grained lithofacies Sp and St in V3. C) Close up of the erosional contact between V2 and V3 (box in Fig. B). D) Coarse- to very coarse-grained bar-scale planar cross-bedded sandstone overlain by 5-10 cm thick dune-scale cross-bedding in V2. E) Laterally accreting cosets of fine- to medium-grained dune-scale planar cross-bedded sandstone in V3. The set thickness gradually decreases from the bottom to the top of the channel story. F) Multistory valley fill in V2. The fluvial sandstones in the bottom channel story comprises of decimeter-thick tabular cross sets, whereas the upper channel story has small-scale cross sets in sheet fluvial sandstone.

Except for Valley 3 in Nielson Wash, these basal deposits are significantly coarser than the fluvial sandstones at the top of the valley, as shown in Fig. 3.11 and Fig. 3.12. The valley/channel lag deposits are also distinctly coarser in the upstream part of the valley in Caineville area than those of Nielson Wash (Fig. 3.15E, 3.15F). For example, ~ 60% of the lag deposits in V3 in Caineville (Fig. 3.15F) consist of granules and pebbles, whereas the maximum grain size found in the channel lag deposits in V3 in Nielson Wash is lower coarse sand. In addition, there is a ten-fold decrease in the average grain size of the channel lag deposits from the upstream (4440 μm) to downstream parts (360 μm) of the valley (V3) (Fig. 3.15F). The lag deposits in the overlying valley (V2) in Nielson Wash (Fig. 15E) is even coarser than those in Valley 3. Unlike the deposits of Valley 3, V2 basal lag deposits in Nielson Wash show a bimodal distribution with a significant amount (~ 40%) of granules and pebbles. The lag deposits in the upstream part of the Valley 2 in the Caineville area are on average, twice as coarse as in the downstream areas and contain less than 10% sand. Compared to the basal lag deposits in Valley 2, the basal lag deposits in V1 are much finer, and are only exposed in the Nielson Wash area (Fig. 3.16).

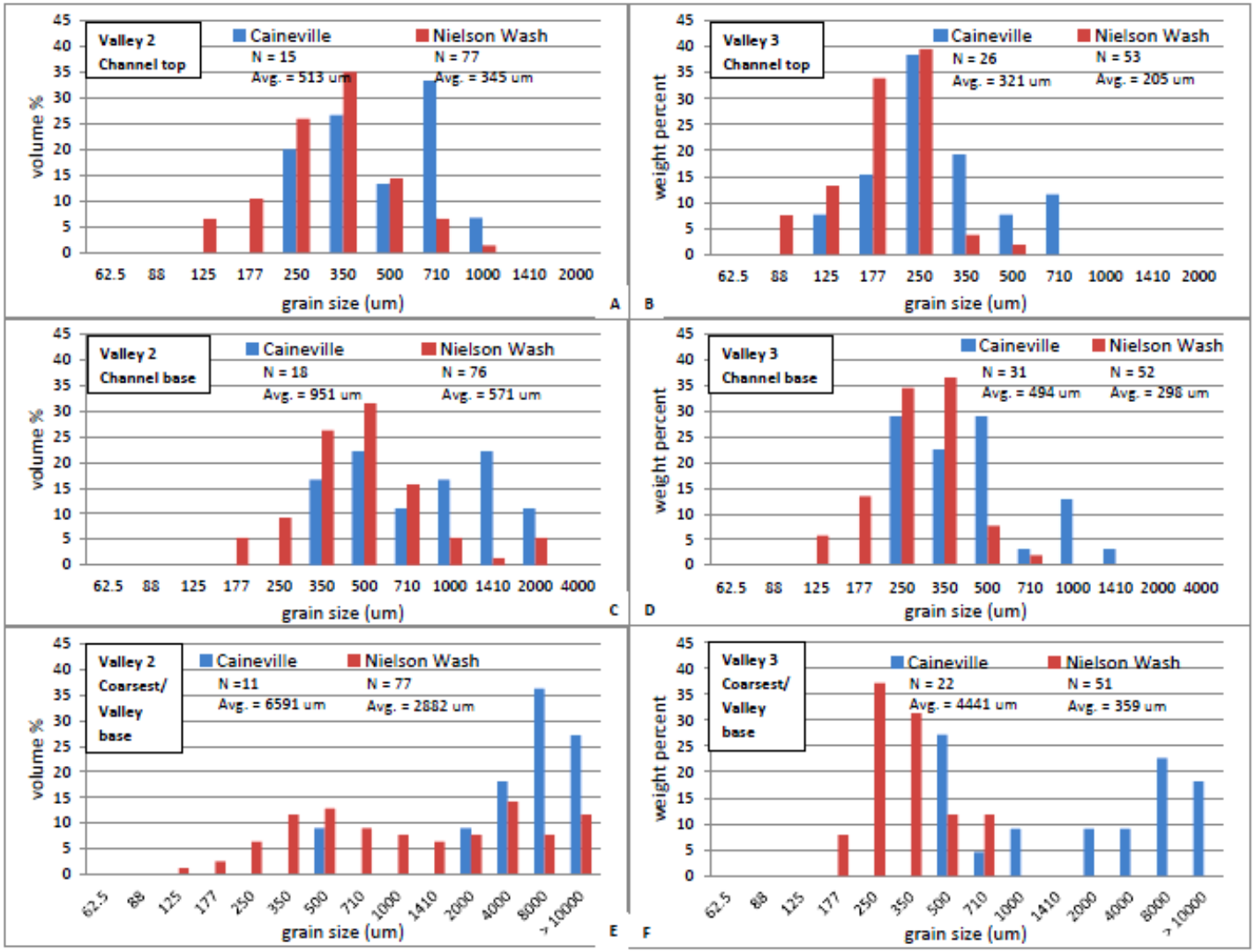

Figure 3.15 (facing page) Histogram of D50 grain sizes at the channel top, channel base, and valley base in Valley 2 and 3 in the Caineville and Nielson Wash areas.

Valley/channel basal lag deposits are interpreted as the coarsest fraction of the bedload sediments retained in the fluvial system during relative sea-level fall and early lowstand. According to Allen (1983c), cross-bedded sandy conglomerates in lag deposits form as the result of segregation of gravels from the gravel-sand mixtures in the bedload. The small-scale (< 0.5 m) cross-bed sets suggest rapid deposition of poorly sorted, coarse bedload (Miall, 1996).

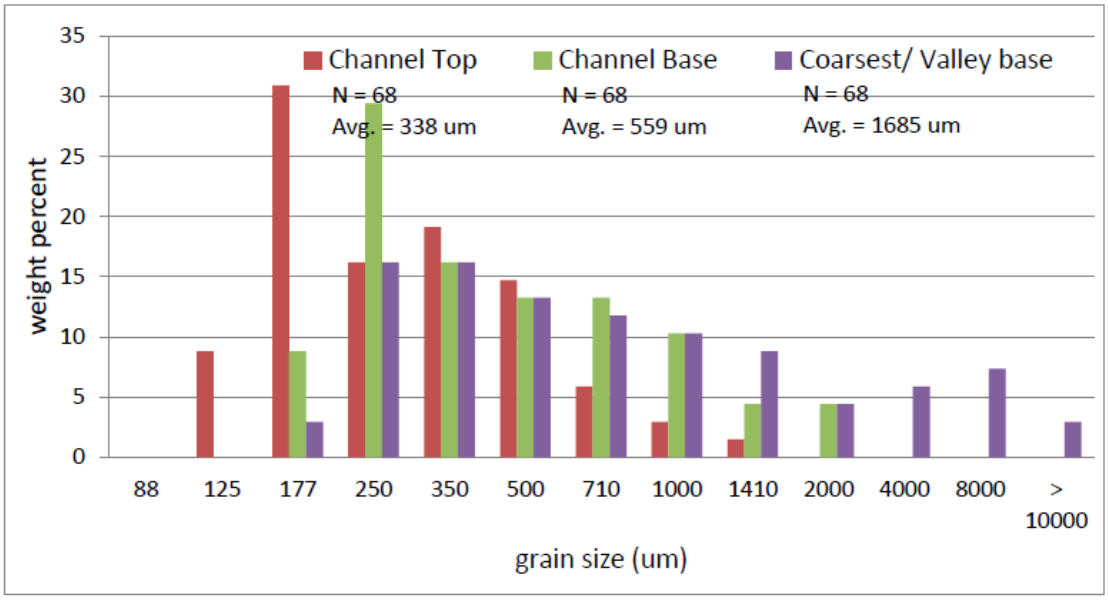

Figure 3.16 Histogram of D50 grain-sizes at the channel top, channel base, and valley base in Valley 1 in the Nielson Wash area.

Facies Association B: Coarse-grained Fluvial Sandstone

The coarse-grained sandstone facies (FA- B) comprises the most abundant channel-fill facies in both the upstream and downstream parts of Valley 2. It consists of highly amalgamated, medium- to coarse-grained sandstone with sparse, very coarse-grained sandstone with abundant petrified or coaly fossilized logs, coalified plant fragments, and almost no mudstone (Fig. 3.15C, 3.15D). The dominant sedimentary facies are dune-scale trough cross-stratified sandstones (St) and planar cross-bedded sandstones (Sp) bounded by simple, planar first-order surfaces with negligible horizontally bedded sandstones (Sh). Bar-scale, meter-long trough cross-bedded sandstones (St) and planar cross-stratified sandstones (Sp) are also seen. The coarse-grained fluvial sandstone facies association (FA-B) is common throughout Valley 3 in Caineville, but is limited to the bottom half of the valley fill in Valley 1 in Nielson Wash.

The coarse-grained fluvial sandstone facies shows significant variation in grain sizes and sedimentary structures in both the Caineville and Nielson Wash areas. The overall grain sizes in dune-scale trough-cross-bedded sandstones (St) and planar cross-bedded sandstones (Sp) in Caineville are coarser than that of the Nielson Wash area by several size classes (Fig. 3.15C, 3.15D). However, in both areas, the coarse-grained fluvial sandstone facies generally show fining upward trends, with local coarsening-upward bedsets (Fig. 3.7, 3.9). The set thickness of the dune-scale planar cross-bedded sandstones (Sp) ranges between 5 and 25 cm in Caineville; whereas the set thickness ranges up to 35 cm in Nielson Wash. The facies on top of the valley base of V1,

V2, and V3 are more amalgamated, relatively coarser grained, and more sheet-like with an absence of floodplain mudstones and overbank fines.

The coarse fluvial sandstone facies represents most of the bedload sediment retained within the channel.

Facies Association C: Fine-grained Fluvial Sandstone

The fine-grained fluvial sandstone facies association (FA-C) is characterized by very fine- to medium-grained sandstones with sparse, coarse-grained, upward fining sandstone beds that show Liesegang banding, plant root traces, and rare plant material. The typical facies in this facies association in the Caineville area are dune-scale trough-cross-bedded sandstone (St) and planar cross-bedded sandstone (Sp) with numerous small-scale cross sets, and upper flow regime, cms thick horizontally bedded sandstone (Sh). In contrast, in the Nielson Wash area, dune- and bar-scale trough-cross-bedded sandstone (St) and planar cross-bedded sandstone (Sp), upper flow regime, horizontally bedded sandstone (Sh) in lateral accretional depositional units, and current ripple cross-laminated sandstone (Sr), and climbing ripples at the very top of fully preserved channel stories are the dominant facies. Most of the cross sets in Valley 2 deposits in the Caineville area range between 5 and 15 cm thick, with an average of 11.9 cm. In the Nielson Wash area, cross sets in Valley 2 deposits are comparatively thicker, ranging from 10 and 20 cm with an average of 15.1 cm. In contrast, the V3 sandstones have thicker cross sets (~ 15.6 cm) in the Caineville area compared to those in Nielson Wash (~10.2 cm).

Compared to the coarse-grained fluvial sandstone facies association, these sandstones are finer grained and the sandstone bodies are smaller and less amalgamated. For example, the fine-grained fluvial sandstones in V3 channel top deposits in Caineville mostly consist of fine lower to medium upper sandstones (177 – 350 um) with minimal medium to coarse fractions (Fig. 3.15B). In contrast, the V3 channel top deposits in Nielson Wash are mostly very fine upper sand to fine upper sand in size (125 – 250 um) with a noticeable absence of any coarser grained fraction. Similarly, the average grain size of the V2 channel top deposits in Nielson Wash are much finer sand (~ 345 um) compared to those in Caineville (~ 513 um).

Facies Association D: Tidally Influenced Fluvial Sandstone

The tidally influenced fluvial sandstone facies (FA- D) is characterized by very fine- to fine-grained sandstones with sparse medium grained sandstones, often interbedded with thin mudstones and siltstones. Current ripple cross-laminations, climbing ripples, planar cross-bedding, flaser bedding, and dune-scale cross stratification are the most common sedimentary structures observed. All three incised valleys observed in the Nielson Wash area show an upward facies transition from coarse/fine-grained fluvial sandstones (FA- B/ FA- C) to tidally influenced sandstones (FA- D) (Fig. 3.9) that corresponds to a systematic upwards decrease in overall grain size as well as a change in fluvial channel geometry and architecture. The tidally influenced fluvial sandstone facies, however, was not observed in either of the two valleys in the Caineville area.

The proportion of tidally influenced fluvial sandstone facies increases from the middle to the upper part of both Valley 2 and Valley 1 in the Nielson Wash area, as indicated by an increasing abundance of double-mud-drapes in the cross-bedded sandstones. These double-mud-drapes, where preserved, are continuous from bottom to top of the foresets in thin-bedded sandstone (Fig. 3.12, 3.13) and often transition into ripple cross-lamination with flaser and/or wavy bedding at the top of the valley fill. In contrast, the tidally influenced fluvial sandstone facies were observed at the very basal part of Valley 3 in the Nielson Wash area, which matches the observation of Li et al. (2013) in Coalmine Wash a few km towards NE. Locally, at the base of V3, cross-strata show bi-directional paleocurrents. *Teredolites longissimus* are also found at the base of V3 in the Nielson Wash area, indicating flood-dominated tidal facies (Fig. 3.11C).

The tidally influenced fluvial sandstone facies at the upper portions of Valley 1 and Valley 2 in the Nielson Wash area are interpreted as late lowstand to transgressive deposits, as indicated by comparatively finer grained, less amalgamated sand bodies. The highstand deposits above the tidal facies at the tops of V3, V2, and V1 are not well preserved in the Nielson Wash area. However, where found, deposits at the top of V1 are more heterolithic than V2; in some cases, floodplain mudstones were present at the top of V1. Previous workers described the highstand deposits in V1 as composed of 2-5 m thick heterolithic facies association in the northern Nielson Wash area (Li et al., 2010; Hilton, 2013).

Facies Association E: Large, Steeply Dipping, Laterally Accreting Single Foresets (Sf)

This facies association (FA-E) comprises large-scale single foresets, dipping at or greater than the angle of repose, and bounded by a 5^{th} -order base of channel erosional surface at the base and truncated by a 4^{th} -order macroform-basal erosional surface at the top (Fig. 3.13). The individual foresets are between 1.5 and 4 m in height and can extend more than 20 m laterally. The foresets consist of 0.5 - 1 cm thick, alternating very fine- to medium-grained sandstone. In most cases, the large-scale foresets have concave-upward or straight inclined profiles, with some showing listric or sigmoidal profiles. Similar facies were described by Wu et al. (2015) and Ullah et al. (2015) from previous studies of the Ferron incised-valley fill in the Nielson Wash area.

Miall (1996, 2003) described these "solitary set of large-scale planar cross-bedding" in the Triassic Hawkesbury Sandstone in Australia where the maximum set thickness reaches up to 7.5 m. Despite the abnormally large size of the sets, he described this facies as a "mesoform" and assigned the feature to lithofacies Sp. Studies from the modern Brahmaputra Braided River, Bangladesh have also recorded dunes heights ranging between 1.5 and 8 m (Best et al., 2003; Bridge et al., 2006). Sambrook-Smith et al. (2006) and Parker et al. (2013) described these large foresets in modern fluvial systems as having been formed by avalanching (downstream accretion) of bedload sediments down the lee-sides of unit bars. Ullah et al. (2015) however, demonstrated that sets of steeply dipping, single large foresets can show distinct unidirectional accretion towards the channel cut bank as the river migrated laterally over the deep thalweg near the river bend filling a scour. Unlike the large-scale planar

cross-bedded (Sp) facies described by Miall (1996), the large, steeply dipping single foresets (Sf) in this study lack $2^{nd}/3^{rd}$ –order internal coset boundaries.

3.7 Estimation of Paleohydraulics and Backwater Lengths of the Valley-filling Channels

We estimated channel paleohydrologic variables such as channel width, depth, and discharge of Ferron rivers using various parameters, such as median grain size, cross-set thickness, and channel story thickness extracted from preserved channel stories. In addition, various empirically derived formulas that relate channel dimensions with preserved sandstone thickness were used (Ethridge and Schumm 1977; Bridge and Mackey 1993; Bridge, 1993b; Bridge and Tye 2000; Leclair and Bridge 2001; Bridge 2003; Bhattacharya and Tye 2004). Mean flow depths of the trunk channels in the valleys in the Caineville and Nielson Wash areas were estimated based on more than 315 measurements of cross-set thickness (see appendix). According to Bridge (1993a) and Leclair and Bridge (2001) cross-set thickness can be used to calculate the height of formative dunes, which in turn scale to the flow depth. Using the techniques by Bridge and Tye (2000) and Leclair and Bridge (2001), the estimated water depths for the V1, V2, and V3 channels in Nielson Wash were between 2.9 – 4.7 m, 3.5 - 5.8 m, and 2.4 - 4.3 respectively (Table 3.2). Formative rivers in V3 in the Caineville area have an overall greater depth (3.6 - 5.6 m) compared to the Nielson Wash area; however, rivers appear to be shallower in V2 in the Caineville area (2.8 - 4.4 m). Previous research reported flow depths of Ferron trunk channels of between 4.7–8.8 m (Bhattacharya and Tye 2004), 3.0

– 7.1 m (Li et al. 2010), and 0.8 – 9.8 m (Hilton, 2013) with an average and maximum (i.e. bankfull) flow depths of 5.1 m and 9 m respectively (Gardner et al., 2004; Garrison and Van den Bergh, 2004). Studies from plan-view outcrops on top of V1 reported channel depths of 3.5 – 4.1 m (Wu et al., 2015) and 1.38 – 1.68 m (Bhattacharyya et al., 2015) respectively.

Table 3.2 Analysis of flow depth, flow width, and paleodischarge for the formative rivers within V1, V2, and V3 in Caineville and Nielson Wash area

Valley	Location	Depth (D) m (Eq. 3.1)	Width (Wc) m (Eq. 3.2)	Area (A) (W*D) m^2	Dominant bedform	Median grain size	Velocity (U) (m/s) (Rubin, 1980)	Discharge (Q) Q= A*U (m^3/s)
V1	Nielson Wash	2.9 - 4.7	60 - 150	171 - 706	3D dune	Fine	0.8 - 1.3	137 - 918
V2	Caineville	2.8 - 4.4	56 -132	154 - 579	3D dune	Medium - Coarse	0.6 - 1.5	92 - 869
	Nielson Wash	3.5 - 5.8	87 - 216	304 - 1244	3D dune	Medium	0.7 - 1.6	213 - 1991
V3	Caineville	3.6 - 5.6	92 - 202	334 - 1121	3D dune	Fine Upper	0.8 - 1.3	267 - 1457
	Nielson Wash	2.4 - 4.3	42 - 125	100 - 532	3D dune	Fine	0.7 - 1.2	70 - 639

Table 3.3 Analysis of channel width and channel belt width for the formative rivers within V1, V2 and V3 in Caineville and Nielson Wash area

Valley #	Location	Channel width (Wc) m	Belt width (Wcb) (m) Eq. 3.2	Belt width (Wcb) (m) Eq. 3.3	Belt width/ Channel width
V1	Nielson Wash	60 - 150	396 - 978	808 - 1609	11 - 14.0
V2	Caineville	56 -132	370 - 862	768 - 1462	11 - 14.0
	Nielson Wash	87 - 216	571 - 1405	1068 - 2119	10 - 12.0
V3	Caineville	92 - 202	607 - 1314	1119 -2014	10 - 12.0
	Nielson Wash	42 - 125	282 - 817	624 - 1403	11 - 14.7

Channel width (Eq. 3.1) and channel belt width were approximated from empirical equations based on assumptions of low sinuosity (Eq. 3.2) or high sinuosity channels (Eq. 3.3) using the technique by Bridge and Mackey (1993) that used regression analysis to relate mean channel depth *(D)* with channel width *(W_c)* and channel belt width *(W_{cb})* :

$$W_c = 8.8\ D^{1.82} \quad \text{..... (3.1)}$$

$$W_{cb} = 59.9\ D^{1.8} \quad \text{..... (3.2)}$$

$$W_{cb} = 192.01\ D^{1.37} \quad \text{..... (3.3)}$$

where W_c is the channel width and W_{cb} is the channel belt width. A wide range of channel depths (D) resulted in a wide range of channel and channel belt widths in the Caineville and Nielson Wash areas. Estimated ranges of channel widths in the Caineville area were 56–132 m for Valley 2 and 92–202 m for Valley 3 channels (Table 3.3). Estimated channel widths in Nielson Wash for Valley 3 channels were 42 – 125 m, about half the width of upstream V3 channels in the Caineville area. Valley 2 channels in Nielson Wash were 87 – 216 m wide, hence are wider than their lateral counterparts in Caineville area. In Nielson Wash, there was an upward decrease in channel width in Valley 1 (60 – 150 m) compared to the channels in Valley 2. Several of the large V2 and V1 channels in Nielson Wash (~ 5 - 6 m deep, > 100 m wide) show laterally accreting point-bar deposits, suggesting high sinuosity meandering channels.

Eq. 3.3, which is more applicable for such high sinuosity channels, gives ranges of channel belt widths of 808 – 1609 m for V1, 1068 – 2119 m for V2, and 624 – 1403 m for V3 in Nielson Wash. Although the average channel belt width in V2 in the Caineville area is narrower than that at Nielson Wash, the ratio of channel belt width to channel width was actually higher in the Caineville area, probably indicating the co-existence of multiple low sinuosity channels in the channel belt. In contrast, the average width of V3 channel belts in Caineville is almost twice that of channel belts in Nielson Wash; however they show a lower range of belt width to channel width ratio than the ration at Nielson Wash. This might indicate that unlike the V2 channels, the V3 channels in the Caineville area formed from significantly larger single thread channels, which is also consistent with estimated channel widths (Table 3.3). These estimations of channel belt widths in the current study are comparable to the earlier estimations by Bhattacharya and Tye (2004), who reported a similar range of channel belt widths of 1135–1800 m with an average channel width of 250 m within the belts in the Ferron Member in Last Chance Delta.

The average bankfull flow velocities (*U*) of between 0.6 -1.6 m/sec for Ferron rivers in the study area was estimated from the bedform phase diagram of Rubin and McCulloch (1980), which requires grain size, bedform-type, and flow depth (Table 3.2). The flow velocity then can be used with cross-sectional area of the channel (*A*) (width x depth) to measure the paleo-discharge (Q):

$$Q = UA \quad (3.4)$$

Several authors (e.g., Schumm, 1977; Knighton, 1998) also showed an empirically derived relationship between discharge and cross-sectional channel dimensions. Formative rivers in V3 in Caineville have higher discharges compared to V3 rivers in Nielson Wash, since they have overall larger dimensions and approximately similar velocities. A maximum channel depth of 5.6 m and a width of 202 m would give a maximum discharge *(Q)* of ~1450 m^3/sec for the V3 channels in Caineville. Estimated paleodischarge for the channels in the Nielson Wash range between 70 – 640 m^3/s for V3, 210 – 1990 m^3/s for V2, and 140 – 920 m^3/s for V1 (Table 3.2). These results show that the formative rivers in V2 in Nielson Wash have overall higher discharge than the V2 rivers in Caineville. Therefore, the Caineville rivers can be interpreted as tributaries or possibly multi-channeled rivers. A decrease in grain size, despite this increase in discharge and flow depth, possibly indicates a change in fluvial style from Caineville to Nielson Wash.

The channel slopes (S) used in the backwater length calculations (Table 3.4), were estimated (in appendix) using the following equation (Paola and Mohrig, 1996; Holbrook and Wanas, 2014):

$$S = (RD_{50}X"\tau" *_{bf50})/H_{bf} \quad \ldots\ldots\ldots\ldots\ldots\ldots \quad (3.5)$$

where *R* is the dimensionless submerged density of quartz, the density of which is assumed to be 2.65 g/cm^3, giving a *R* of 1.65 in water of standard density. D_{50} is the median grain size recorded from the base of the channel stories. τ^*_{bf50} is the bankfull Shields number for dimensionless shear stress for the median size (D_{50}) of the mixture at the base of a channel, and is assumed to be 1.86 (after Parker,1978; Parker et al., 1998;

Dade and Friend, 1998). H_{bf} is the maximum bankfull channel depth, which is estimated by methods discussed previously. Previous studies found ancient fluvial slopes very difficult to estimate, primarily because they are low and may range over several orders of magnitude (typically 0.001 to 0.00001) (Li and Bhattacharya, 2010). Eq. 3.5 however, gives the slope directly if the median grain size and maximum bankfull channel depth are known. Li et al. (2010), estimated Ferron river slopes on the order of 0.02° - 0.006° (0.00035 - 0.0001), based on the onlap distance of coastal prisms. In a separate study, Bhattacharya et al. (in press) estimated slopes of the Ferron rivers from as steep as 0.14° to as flat as 0.043° (0.0026 - 0.00076) with an estimated valley slopes of about 0.06° (0.001). Using the technique in Eq. 3.5, the estimated valley-filling rivers slopes are on the order of 0.0009 – 0.0003 for V3, 0.003 – 0.0007 for V2, and 0.0017 – 0.0004 for V1 (Table 3.4, also see appendix).

This gives maximum backwater lengths for the V3, V2, and V1 rivers in the Nielson Wash between 6 - 16 km, 3 – 9 km, and 5 – 13 km respectively. The Caineville area, which is almost 20 km southwest of the Nielson Wash, thus almost certainly lies well beyond the vicinity of the backwater transition, even with the lowest calculated slopes above.

Table 3.4. Estimation of backwater lengths for the formative rivers within V1, V2, and V3 in Caineville and Nielson Wash area.

		Average	**Max**	**Min**
Valley 1	Channel depth (m)	2.9	4.7	1
	Slope	0.0006	0.0004	0.0017
	Backwater length (km)	**5**	**13**	**1**
Valley 2	Channel depth (m)	3.5	5.8	1.2
	Slope	0.001	0.0007	0.003
	Backwater length (km)	**3**	**9**	**0.5**
Valley 3	Channel depth (m)	2.4	4.3	0.5
	Slope	0.0004	0.0003	0.0009
	Backwater length (km)	**6**	**16**	**0.5**

3.8 Fluvial Geometry and Bedding Architecture

Figure 3.17 shows the detailed bedding architecture and paleocurrent information in V1, V2, and V3 channels along a roughly N-S elongated cliff face in the Nielson Wash area. For V1 and V2 deposits, this outcrop is oblique to paleoflow, whereas for V3 deposits, the cliff is oriented parallel to the paleoflow. A number of studies (for example, Miall, 1988; Bridge, 1993a; Bristow, 1993b; Holbrook, 2001) demonstrated that depositional-strike views (perpendicular to flow) are a prerequisite to differentiate laterally accreting unidirectional point bars from bidirectional mid-channel braid bars. Braid-bar deposits typically show bidirectional downlap in strike sections, whereas single-thread meandering rivers typically show single laterally accreting sets.

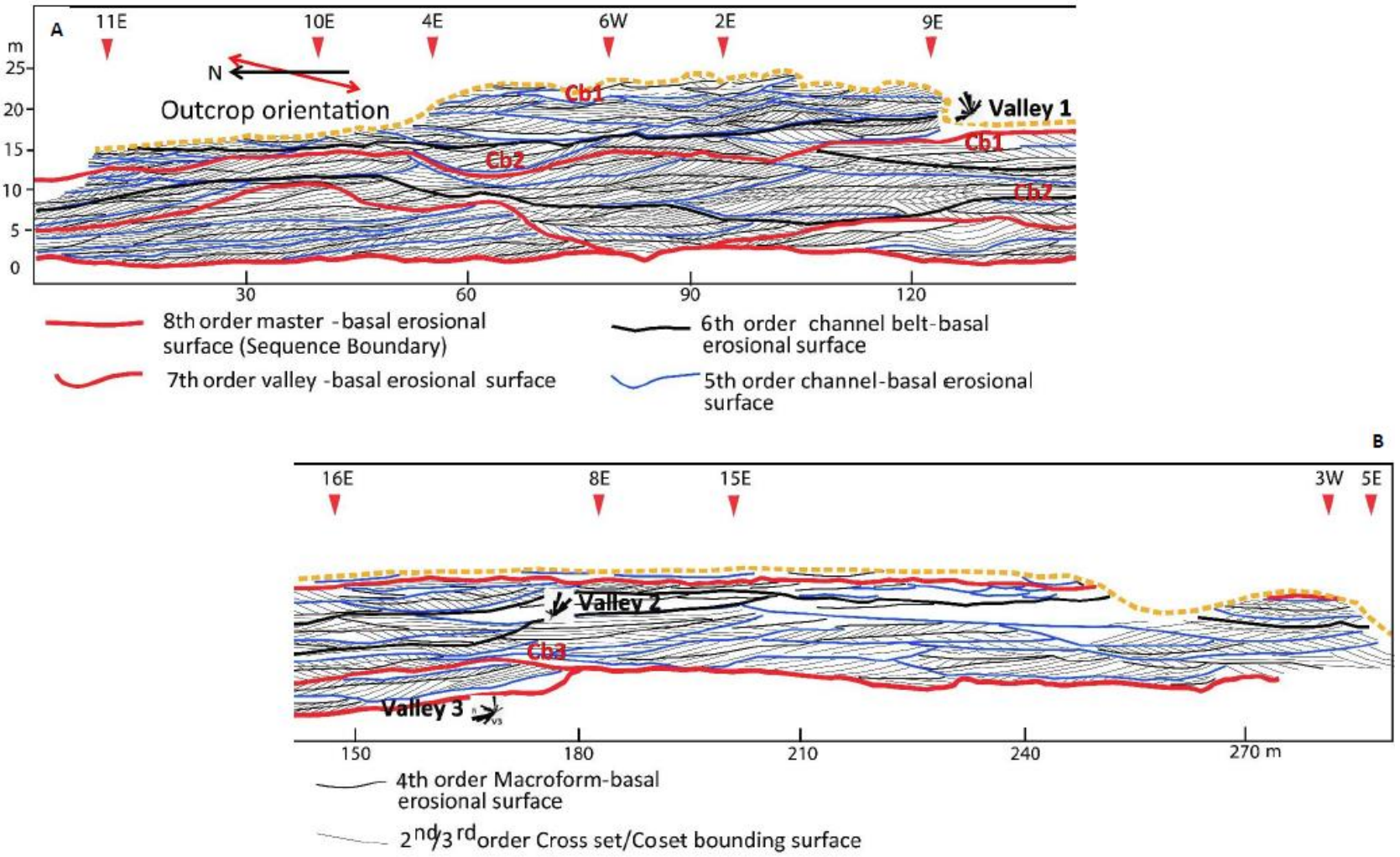
A
11E
10E
4E
6W
2E
9E
m
25
20
15
10
5
0
N
Outcrop orientation
Cb1
Cb2
Valley 1
Cb1
Cb2
30
60
90
120
8th order master -basal erosional surface (Sequence Boundary)
6th order channel belt-basal erosional surface
7th order valley -basal erosional surface
5th order channel-basal erosional surface
B
16E
8E
15E
3W
5E
Valley 2
Cb3
Valley 3
150
180
210
240
270 m
4th order Macroform-basal erosional surface
2nd/3rd order Cross set/Coset bounding surface

Figure 3.17 (previous page) Bedding diagram showing internal architecture of the channel belts and major erosional surfaces in the compound incised-valley system in Nielson Wash shown in Fig. 3.8. Surface bounding cross sets and/or co-sets and higher units are correlated and mapped in detail. Major truncation in V2 at the middle of the image is possibly caused by a confluence scour. Black arrows represent the location of the measured sections in Figure 3.9.

Figure 3.18 Large unidirectional accretion at the base of V2 in marine shoreface deposit in Nielson Wash. Valley bottom is marked by white arrows. Paleocurrents are towards east (into the photo); accretion directions are towards north (to the left of the photo).

Four channel stories were recognized in V3 deposits from the bedding diagram (Fig. 3.17) and from the correlation of the measured sections, each of which shows distinct dipping cross sets towards north-northwest. The bedding diagram shows that bars within these channel stories show distinct unidirectional downstream accretion, interpreted as downstream-accreting mid-channel bars (Fig. 18). Overlying V3 are three vertically stacked and laterally offset fluvial channel belts in V2 (Cb3, Cb2, and Cb1) that show a significant change in fluvial architecture and style (Fig. 3.17) across the basal erosional surface of V2 (Sb1b in Fig. 3.8). The dominance of unidirectional lateral accretion within channel stories exposed perpendicular to flow suggest that formative rivers in these channel belts were mostly meandering. Two vertically stacked channel belts were recognized in the V1 deposits that show similar fluvial architecture and style as observed in V2, with individual laterally accreting sets. Formative rivers in this youngest valley were thus also mostly meandering.

In the Caineville area, where paleocurrents are slightly oblique to the cliff face, bedding architecture within V3 lacks unidirectional lateral accretion and is interpreted to indicate braid bars (Fig. 3.19). The cliff is oriented NW - SE and paleoflows are towards northwest to north (into the cliff). Bedding architecture of the fluvial bodies in V2 on cliff faces normal to flow shows cross beds that dip east-southeast, parallel to the cliff face. However, accretion beds show apparent dips that are mostly west-northwest indicating upstream accretion.

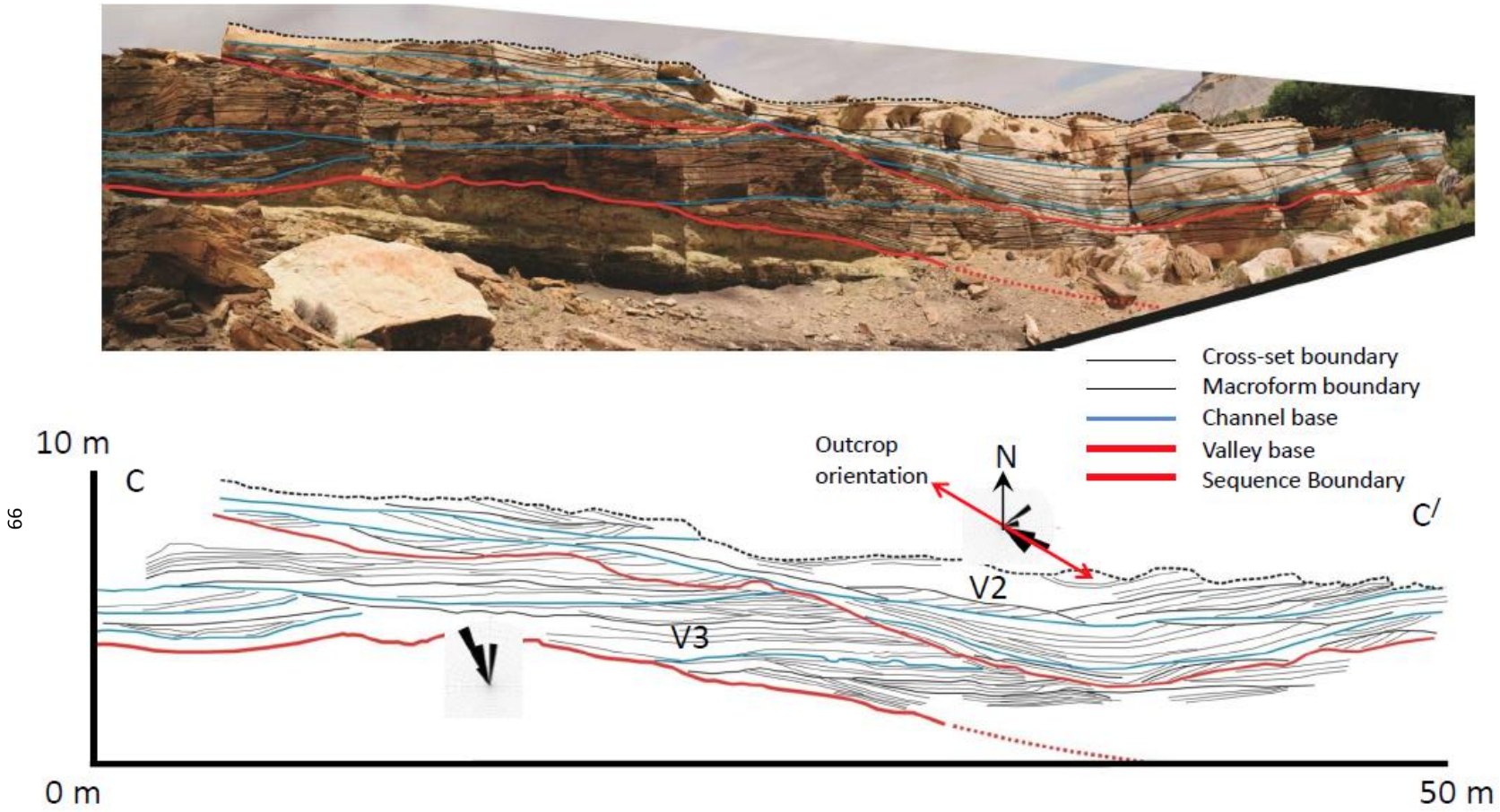

Figure 3.19 (opposite page) Photomosaic and bedding diagram showing internal architecture of the channel-belts and major erosional surfaces in the compound incised-valley system in the Caineville area.

3.9 Discussion

Control of Backwater Effect on Facies Types and Their Organization in Valleys

The controls of sea-level change on valley fills was first noticed by Fisk (1947) and Mackin (1948), who explained how a change in relative sea level led to a change in slope that controls fluvial aggradation and/or degradation. Posamentier and Vail (1988) expanded this concept and developed a conceptual model that relates fluvial deposition to change in relative sea level and slope of the fluvial system. Subsequent facies models for incised-valley fill have shown significant variability in terms of valley fill facies and their stratigraphic position within the valley (Van Wagoner et al., 1990; Dalrymple et al, 1994; Zaitlin et al., 1994; Boyd et al., 2006). Zaitlin et al. (1994), for example, proposed a predictable stratigraphic organization of a simple piedmont incised valley fill starting from back-stepping estuarine deposits in seaward reaches (outer segment) followed by drowned valley estuarine complex in the middle segment. According to Zaitlin et al. (1994), the proximal part (inner segment) of the incised valley system lies beyond the transgressive estuarine limits and is therefore characterized by fully-freshwater fluvial deposits during the entire sea-level cycle.

Willis (1997) further developed the idea of Zaitlin et al. (1994) and introduced the concept of "flood-based" vs. "flood capped" valleys based on the rate of marine transgression during the valley fill. The observations from the incised-valley system in our study area support the "flood capped" valley model of Willis (1997). Willis (1997) argued that when the relative rise of sea level is slow from the very beginning, valleys are

filled mostly by sandy fluvial facies along the whole stretch of the valley. Flooding by marine water only occurs after significant accommodation develops that capped the sandy fluvial facies with estuarine and muddy fluvial facies. The Ferron compound incised-valley system is mostly filled with sandy fluvial facies along its entire length with estuarine and muddy fluvial facies only in the upper part of Valley 1 in the Nielson Wash (Hilton, 2013) suggesting slow initial base-level rise. The upstream limit of onlap of these valley top floodplain strata onto steeper gradient valley-fill deposits were found near the Freemont River section, five kilometers southwest of the Nielson Wash area (Fig 3.3). In addition, Dinocysts were found (Akyuz et al., 2015) near the Freemont River section requiring marine influence.

The continuity of stratigraphic units (i.e., sandy fluvial facies) and occurrence of extraformational sediment (especially gravel-sized sediment) from the upstream to the downstream end of the incised valley indicate that increased runoff controlled by upstream climate or higher slope, is the primary control on sediment flux and transport capacity of the channels within the valley. A gradual upward increase in average channel discharge from Valley 3 to Valley 1 in the Nielson Wash may also support an increasing upstream control. Although the downstream persistence of fluvial sandy facies along the entire stretch of the incised valley suggests upstream climatic control, it couldn't overcome the imprint of downstream sea-level rise during the late lowstand-transgression phase when the maximum landward transgression of the shorelines caused widespread occurrence of tide-influenced fluvial facies in the upper portions of the incised-valley fills in the Nielson Wash area. The actual positions of the paleo-shorelines

during the maximum transgressive phase are hard to determine because of the lack of continuous outcrops east of Nielson Wash area. However, the transgressive limit of the paleo-shorelines can be estimated from the maximum backwater lengths of the valleys, since both of these parameters are inversely correlated to slope. Given all the valleys in the Nielson Wash area show tidal signatures, we can assume that at least those portions that show tidal signatures are well within the backwater limits. In addition, the presence of *Teredolites longissimus* at the base of V3 indicates tidal flooding during the early valley-filling phase. This suggests that the maximum landward transgression of the paleo-shoreline was much greater for the older Valley 3 because of its much gentler slope compared to the upper two valleys. This downstream decrease in bed slope is accompanied by a drastic downstream fining of median (D50) bed-loads (Fig. 3.15). Therefore, for a given rate of base-level rise, the Valley 3 channels would feel the effect of backwater further inland compared to the channels in Valley 2 and Valley 1. Due to higher slopes, the channels in Valley 2 and Valley 1 in Nielson Wash would only feel the effect of backwater later in the valley-filling phase during late lowstand- transgression period.

Valley 2 and Valley 3 in the Caineville area are located almost 20 km southwest of the Nielson Wash in an upstream direction (Fig. 3.3). These Caineville valleys are thus landward of estimated maximum backwater lengths for V1, V2, and V3 rivers. Therefore, downstream effects would not be predicted to propagate this far upstream and valley fill facies in Caineville should not show significance influence of sea-level changes. The major change in valley-fill facies, including the appearance of tidal facies in Nielson

Wash, should correspond to this backwater effect. In addition to the absence of any tidal facies (FA-D) within the valley fills in the Caineville area, there is a decrease in the median bedload grain size (D50) in the downstream direction. Moreover, the basal part of Valley 3 in Caineville is characterized by abundant granules and pebbles (FA- A), which are completely absent at the base of V3 in Nielson Wash. Recent studies on the modern Mississippi River showed that backwater hydraulics play an important role in the transport of bed material sediment in the lower reach (Wright and Parker, 2004; Parker et al., 2009; Nittrouer et al., 2011b). Nittrouer et al. (2011a) showed little downstream transfer of bedload sand during low and moderate discharge as the reduction in stress in the backwater reach reduces bed-material mobility, leading to a downstream decrease in sediment transport.

The presence of tidal facies at the top of the Valley 1 and Valley 2 in Nielson Wash suggests that the rivers entered into their backwater length at a later phase of valley filling during the late lowstand to transgressive period. A steady upward increase in backwater effect caused a gradual decrease in grain size resulting in a fining upward trend in all three valleys (Fig. 3.20). An increase in valley accommodation due to sea-level rise caused channel aggradation that might initiate channel avulsion in the upper part of the valleys. Observations from the incised valleys in the Nielson Wash area thus indicate that the backwater effect contributes to fundamental transformations in upstream controlled flow and sediment transport. Therefore, the depositional processes and facies in the backwater zone are strongly coupled not only to prevailing climatic condition but also to backwater effect.

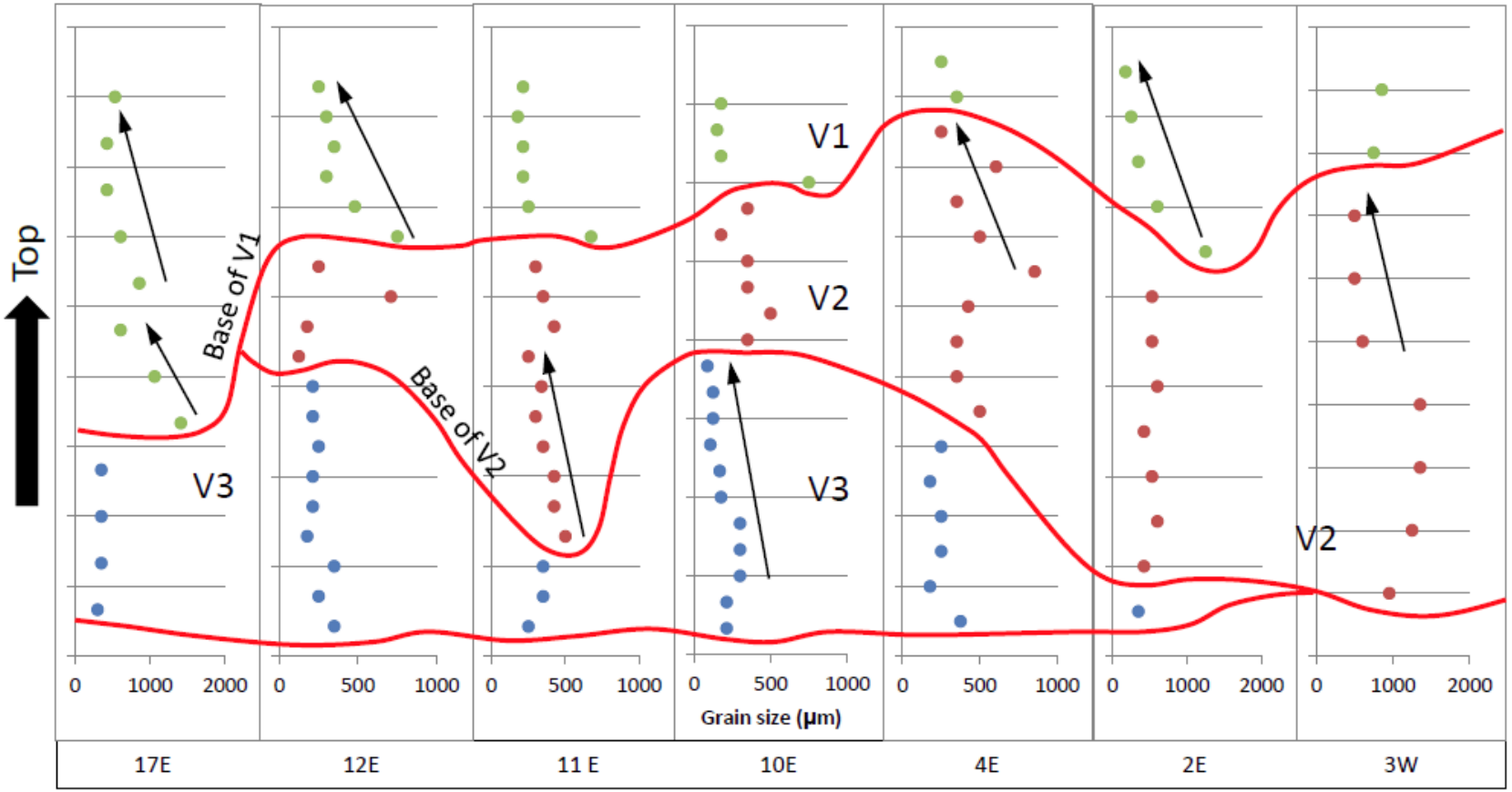

Figure 3.20 Vertical D50 grain-size profile of the fluvial sandstones in the Nielson Wash area (V3 = blue, V2 = red, V1 = green). Note that no vertical scale was used. The height of the sections range between 20 and 25 m.

Control of Backwater Effect on Fluvial Style and Architecture

According to Bristow and Best (1993), the main controls on fluvial architecture in continental strata are sediment supply, avulsion frequency, and accommodation. Traditional non-marine sequence stratigraphic models assume that local variations in sediment flux and transport capacity, which control the change in accommodation and slope, are controlled primarily by sea-level changes. This is quite evident in the sequence stratigraphic models of Shanley and McCabe (1994) and Zaitlin et al. (1994), where the sediment flux was kept constant within a cycle of changing sea level. A gradual increase in sea level with a constant sediment flux should produce a systematic change in fluvial style from low sinuosity braided at the base to meandering at the top, assuming the initial slope and water discharge are sufficient to allow braiding. Initial slope and discharge, however, are mainly controlled by upstream forces, such as, uplift or climatic change (Schumm et al., 1987; Blum, 1992), and can produce valleys that simply never have a high enough slope or discharge to allow braiding to occur. In contrast, a climatically induced increase in precipitation would increase river discharge, and this climatic effect would propagate downstream to yield higher discharge streams along the entire fluvial portion of the systems tract. Therefore, local variations in accommodation and slope during valley filling determine the fluvial style and architecture, and these are controlled by the various combinations of upstream and downstream allogenic forces at different magnitudes and time scales. Several authors (e.g., Bristow et al., 1993) attributed changes in valley slope to the change in valley accommodation within the downstream part of the incised valley. A change in accommodation in the terminal part of the valley can be

directly related to base-level changes caused by 100-kyr Milankovitch cycles (Blum and Tornqvist, 2000; Blum and Aslan, 2006) and/ or basin subsidence (Catuneanu, 2007) that control the rate of creation or filling of valley accommodation.

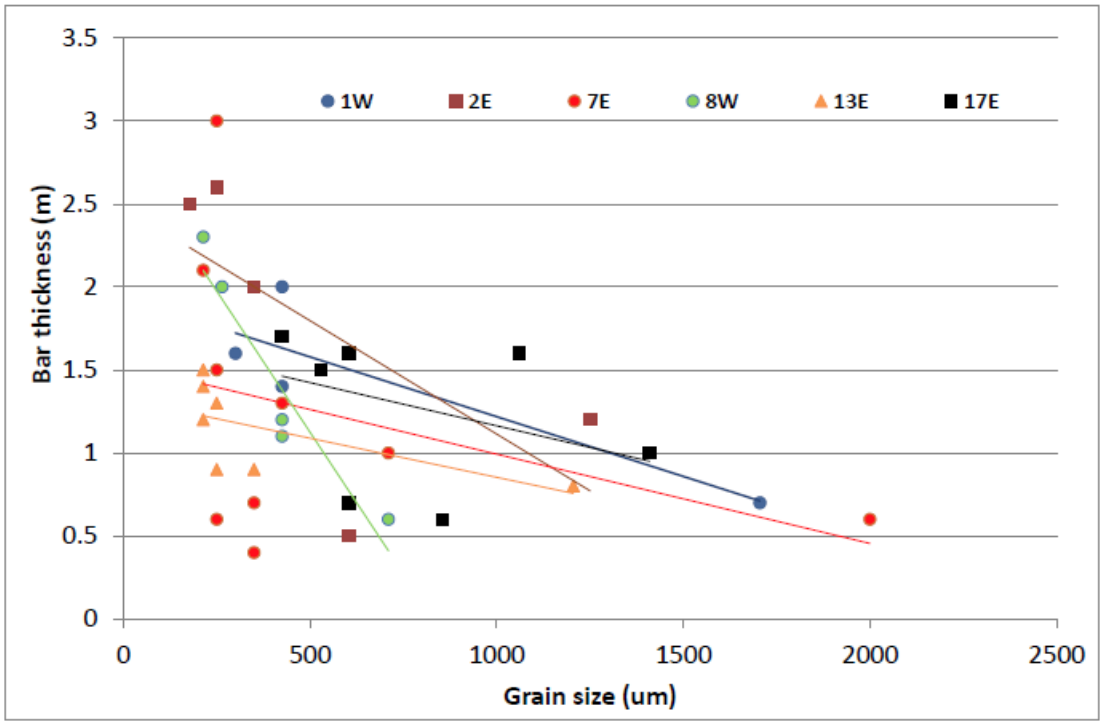

Figure 3.21 An upward decrease in grain size corresponds to an increase in bar thickness in the Nielson Wash area.

The backwater zone, where the rivers are affected by the sea level, does not necessarily limit upstream effects from propagating all the way to the coast. This transitional zone between the normal flow zone and river mouth is dynamic and is sensitive to river discharge as well as the water surface elevation at the river mouth, which is affected by sea-level change (Lamb et al. 2011, Nittrouer et al., 2012). For example, Lamb and Mohrig (2009) and Nittrouer et al. (2011b) show that during times of

high river discharge, the upstream boundary of backwater effects can be pushed toward the shoreline, creating a zone of flow acceleration and erosion of the riverbed if the sea level is lower than the normal flow depth. In contrast, during times of low flow, the backwater zone has a concave water surface profile as the water depth at the shoreline is greater than the normal-flow depth due to a fixed sea level, which creates a zone of spatial water-flow velocity deceleration and deposition (Nittrouer et al., 2012). A reduction in sediment transport capacity as the river enters the backwater influenced zone thus results in a reduction in bed material flux, causing reduced lateral migration rates and narrowing of the channel belt. This downstream narrowing induces flow acceleration and erosion that has been argued to be the potential cause of erosion in the lower Mississippi River (Parker et al., 2009; Nittrouer et al., 2012). This suggests that backwater dynamics may be far more important in shaping channel morphology through deposition and erosion, than what the current source-to-sink and stratigraphy generation models predict (Lamb et al. 2011).

Findings from this study show an downstream increase in average V2 channel depths from the Caineville to the Nielson Wash, which supports the findings by Hudson and Kesel (2000) and Nittrouer et al. (2012), that channels become deeper after entering their backwater length. Incision and deepening of the V2 channels in the lower reaches of the valley is concomitant with an upstream increase in water-flow velocity and discharge (Table 3.2). The deepening of the V2 channels in the Nielson Wash are also associated with occurrence of thick point bar deposits (Fig. 3.18, 3.21), which scale with channel depths and are thicker than point bars in Caineville V2 channel belts. An increase in

channel depths also results in an increase in both V2 channel widths and channel belt widths from Caineville to Nielson Wash (Table 3.3) according to Eq. 3.2, Eq. 3.3, and Eq. 3.4. These findings are similar to that of modern Mississippi River, where it was shown that channel top width decreases in the downstream direction between river kilometer 500 and 200 but increases in the downstream direction in the lower 200 km of the river (Lamb et al. 2012). However, when scaled by channel belt width to channel width, Caineville channel belts are comparatively wider compared to those in Nielson Wash despite their disparate scales.

There is a clear change in fluvial style in V2 from upstream braided to downstream single-thread meandering system, marked by a decrease in grain size. We interpret this as related to a drop in slope reflecting the backwater limit. The V3 channels, on the other hand, remained mostly braided up to Nielson Wash. However, Li et al. (2013) shows meandering V3 tidal channels in Coalmine Wash a few km farther downstream. A decrease in channel depth, width, discharge, and grain size in V3 channels from Caineville to Nielson Wash (Table 3.2), however, may indicate a change from trunk channels to a low sinuosity distributary system at the terminal part of the valley. These V3 distributary channels in Nielson Wash show much lower discharge compared to their trunk system in Caineville, and resulted in a deceleration of flow velocity and a drastic downstream fining of median (D50) bedload. This interpretation of the presence of low sinuosity distributary system in Valley 3 in Nielson Wash is in agreement with a number of previous studies, where it was hypothesized that backwater dynamics might be responsible for the decrease in sinuosity in the lower portions of coastal rivers (Jerolmack,

2009; Parker et al., 2009; Nittrouer et al., 2012). A decrease in width in V3 channels in Nielson Wash may also contributed to the fact that deltaic distributary channels in general tend to have very small rates of lateral migration (Jerolmack and Mohrig, 2007).

3.10 Conclusions

1. At least two cut-and-fill episodes (V3 and V2) were documented in the upstream part of the studied compound-incised valley system in the Caineville area. The erosional unconformities (Sb1a, Sb1b) that partitioned the compound valley fill in Caineville can be traced along the entire stretch of the valley fill to the downstream location at Nielson Wash. The maximum preserved valley-fill thickness is 14 m in Caineville and 25 m in Nielson Wash.
2. Five main channel-fill lithofacies associations (FA) were documented in the Caineville and Nielson Wash areas. Among them, valley/ channel basal lag deposits (FA- A) are significantly finer at the base of Valley 2 in Nielson Wash compared to Caineville. FA- A was not found at the base of Valley 3 in Nielson Wash. Moreover, coarse-grained fluvial sandstones (FA- B) and fine-grained fluvial sandstones (FA- C) are significantly coarser in proximal Caineville deposits than in more distal Nielson Wash deposits. Tidally influenced fluvial sandstone deposits (FA- D) was also not found in Valley 2 and Valley 3 in the proximal exposures at Caineville. All three incised valleys recognized in the Nielson Wash, however, show a vertical translation from fluvial to tidal facies coincident with a systematic vertical decrease in overall grain size.

3. The maximum backwater lengths calculated for the V3, V2, and V1 rivers in the Nielson Wash were between 6 - 16 km, 3 – 9 km, and 5 – 13 km respectively. The Caineville area, which is almost 20 km southwest of the Nielson Wash, thus most probably lies well beyond the vicinity of the backwater transition. The backwater transition in the valley rivers in Nielson Wash marks:
    a. a thickening of V2 channel belt deposits tied to channel deepening towards the river mouth due to scouring during high discharge;
    b. a reduction in average V3 channel belt width that may tie to reduced rate of lateral migration; and
    c. an increased proportion of finer grains in channel belt deposits tied to reduced bed material flux.

4. Although the downstream persistence of fluvial sandy facies along the entire stretch of the incised valley suggests a greater upstream control, it could not overcome the imprint of downstream sea-level rise during the late lowstand-transgression phase, when the maximum landward transgression of the shorelines caused widespread occurrence of tide-influenced fluvial facies in the middle - upper portions of the incised-valley fills in the Nielson Wash area. Steady upward increase in accommodation during the development of the late lowstand to transgressive systems tract is most probably linked with backwater length that caused an upward increase in preserved dune height and bar thickness in the Nielson Wash. Therefore, the depositional processes and facies in the backwater

zone are strongly coupled not only to prevailing climatic condition but also to backwater effect.

5. There is a clear change in fluvial style in Valley 2 from upstream braided to downstream single-thread meandering system, which is associated with a decrease in grain size and valley slope. A decrease in channel depth, width, discharge, and grain size in Valley 3 channels from Caineville to Nielson Wash, however, may indicate a change from trunk to low sinuosity distributary channel systems under the influence of backwater at the distal part of the valley.
6. Findings from this study thus support the idea that the backwater zone is a fundamental transition in coastal rivers, across which preserved sedimentary bodies display predictable and universal geometric changes.

CHAPTER 4: Paleogeographic Reconstruction and Plan-view Fluvial Macroform Architecture of an Exhumed Meander Plain: Examples from the Cretaceous Ferron Sandstone, Notom Delta, Southeastern Utah, USA.

4.1 Summary

The traditional approach of reconstructing fluvial architecture in the rock record emphasizes the use of bedding architecture from 2-D vertical cliff exposures. Depending on the evolution and flow pattern of the formative rivers, however, the growth and sedimentary architecture of the resultant macroforms can be complex, requiring detailed evaluation of planform architecture to determine the morphodynamics of formative channels. The primary aim of this study is to reconstruct the paleogeographic evolution of exhumed meander belts from plan-view outcrop exposures and to describe the plan-view depositional architecture of point bar elements located on top of a well-developed, regional-scale compound incised-valley fill in the Turonian Ferron Sandstone Member at the top of the Notom Delta, north of the Henry Mountains, southeastern Utah. Attempts were also made to reconstruct the depositional architecture and cross sectional geometries of large-scale 2-D macroforms from extensive plan-view exposures.

Based on the orientation of planform paleoflows, accretion directions, locations, and their positions in the overall stratigraphic interval, the preserved fluvial sequences in the mapped area were divided into three channel belts, from oldest to youngest

designated A, B, and C. Paleogeographic reconstructions of the bars in Channel belt A and Channel belt C indicate that the meander belts were primarily formed by successive phases of dominantly lateral expansion that caused a gradual increase in channel sinuosity with time. Channel-belt B, on the other hand, did not produce any large meander bends and was formed by mostly smaller-scale alternate bars in a relatively straight channel reach. Bars in Channel belt A and C have lower length/width ratios, as a consequence of their relatively high channel sinuosity.

Three types of architectural facies or macroforms were identified within the large-scale point bars delineated from bedding architecture analyses integrated with cross-sections and plan-views, as well from their lithofacies descriptions. Among these, Type A macroforms represent dune and bar-scale cross sets that form amalgamated compound bars. Type B macroforms were interpreted as unit bars, which consist of moderately to steeply dipping single large foresets. Type C macroforms represent the large, steeply dipping upper flow regime (UFR) planar strata. The concurrence of UFR planar beds along cut banks upstream of the interpreted point bars, indicates that the large UFR planar bed facies in the study area form due to lateral accretion over the deep channel thalweg upstream of a bend apex. Incorporating established models for determining geometry and paleohydraulics of point-bar deposits into the reconstructed plan-view architecture of the macroforms, we infer that with progressively increasing sinuosity, Type B and Type C macroforms become thicker and steeper in a 2-D vertical section, due to the greater variations in point bar geometry.

4.2 Introduction

Three-dimensional (3-D) fluvial architectural analysis in modern rivers typically requires trenching, coring, or the use of ground penetrating radar (GPR) (e.g., Bridge et al., 1995, 1998; Best et al., 2003; Lunt et al., 2004a, b). The traditional approach of reconstructing fluvial architecture the in rock record emphasizes the use of bedding architecture from 2-D vertical cliff exposures (e.g., Miall, 1985; Galloway and Hobday, 1996; Holbrook, 2001; Adams and Bhattacharya, 2005; Bridge, 1993B, 2006; Li et al., 2010; Ullah et al. 2015), mainly due to the scarcity of truly 3-D exposures at the channel belt scale (Willis, 1989), although there have been a few studies that integrate 3-D GPR, cores, and vertical cliff sections in outcrops (e.g., Best, 2003; Corbeanu et al., 2004). Also, there are studies based on 3-D seismic geomorphology that reconstruct the planform architecture of ancient meander belts (Reijenstein et al. 2011; Fustic et al., 2012; Musial et al., 2012). Advances in GPR techniques over the past two decades has significantly improved our understanding of the 3-D architecture of fluvial macroforms (Bridge 2009).

A number of studies (e.g., Willis, 1989, 1993; Chen & Duan, 2006; Smith et al., 2009) suggest that different channel-bend transformations, which ultimately control channel flow pattern, are a function of channel dimensions, discharge, and slope, which in turn affect sinuosity and other morphological constraints. Depending on the evolution and flow pattern of the formative rivers, the growth and sedimentary architecture of the resultant macroforms can be complex (Bridge, 1977; Jin and Schumm, 1986; Smith, 1998; Sambrook-Smith et al., 2006), requiring detailed evaluation of planform architecture to determine the morphodynamics of channels (Deb et al., 2012; Wu, 2015b). Several

theoretical models (e.g., Bridge 1976, 1977, 1982; Willis, 1989, 1993b, 2010) and flume studies (e.g., Ashworth et al., 1999; Peakall et al., 2007; Van Dijk et al., 2012) demonstrated wide variations in fluvial sand body geometry, corresponding to variations in channel migration patterns and the channel belts that they form. However, models based on flume tests and numerical simulation require further testing using outcrop examples. Planform architecture has been routinely studied in modern meander plains (e.g., Cant and Walker 1978; Best et al. 2003; Sambrook-Smith et al. 2006, 2009). Numerous studies have been done describing the morphology and geometries of various macroforms in ancient 2-D fluvial outcrops (e.g., Allen 1974, 1983; Rust 1984; Miall 1996; Martinius et al. 2002). However, depicting various fluvial macroforms from plan-view data in ancient outcrops has rarely been attempted in the past. Nevertheless, a number of recent studies (Wang, 2013; Ielpi and Ghinassi, 2014; Wu et al., 2015a, b) on ancient meander belts have attempted to reconstruct the planform architecture of fluvial deposits from direct observation of plan-view exposures.

The primary aim of this study is to reconstruct the paleogeographic evolution of exhumed meander belts and to describe the plan-view depositional architecture of various macroforms located on top of a well-developed regional-scale compound incised-valley fill in the Turonian Ferron Sandstone Member at the top of the Notom Delta wedge, north of the Henry Mountains, southeastern Utah. Attempts were also made to reconstruct the depositional architecture and cross-sectional geometries of large-scale 2-D macroforms from extensive plan-view exposures. In addition to the plan-view exposures, the meander belts are also exposed in adjoining cliffs, which also allows us to link the cross-sectional

facies architecture to the plan-view expression. Reconstruction of the 2-D cross sectional macroform architecture provides valuable information about the scale and geometry of different fluvio-morphological units, information, which is essential to construct models for reservoir fluid flow.

4.3 Study area and field methods

Field data from the plan-view and cliff exposures of exhumed meander belts were acquired through ground mapping, photomosaic interpretation, and measured sections from a 2 km by 1 km area located east of Nielson Wash canyon near Factory Butte, Utah, north of Highway 24 (Fig. 4.1). Extensive erosion and lack of vegetation enabled us to image and link both planform and 2-D vertical facies architecture at the same location. Extensively exposed bedding surfaces are suitable for ground mapping to constrain the plan-view geometry of the channel and bar deposits.

In recent studies, Wang (2013), Wu et al. (2015), and Bhattacharyya et al. (2015) demonstrated the migration pattern and paleohydraulics of a single meander belt using plan-view data. Wu et al. (2015) described the architecture of unit bars, which have been shown to be a fundamental element in the formation of larger-scale point bars and braid bars (Sambrook-Smith et al., 2006; Bridge 2006), but are not widely recognized in ancient fluvial systems. This study attempts to reconstruct the channel patterns of an ancient alluvial plain, containing a number of amalgamated meander belts, over a larger area than the previous studies, rather than a single meander belt. This allows us to address the degree of preservation and amalgamation of a meander belt complex, which is not

commonly incorporated in theoretical or numerical alluvial stratigraphic models (e.g., Willis and Tang, 2010).

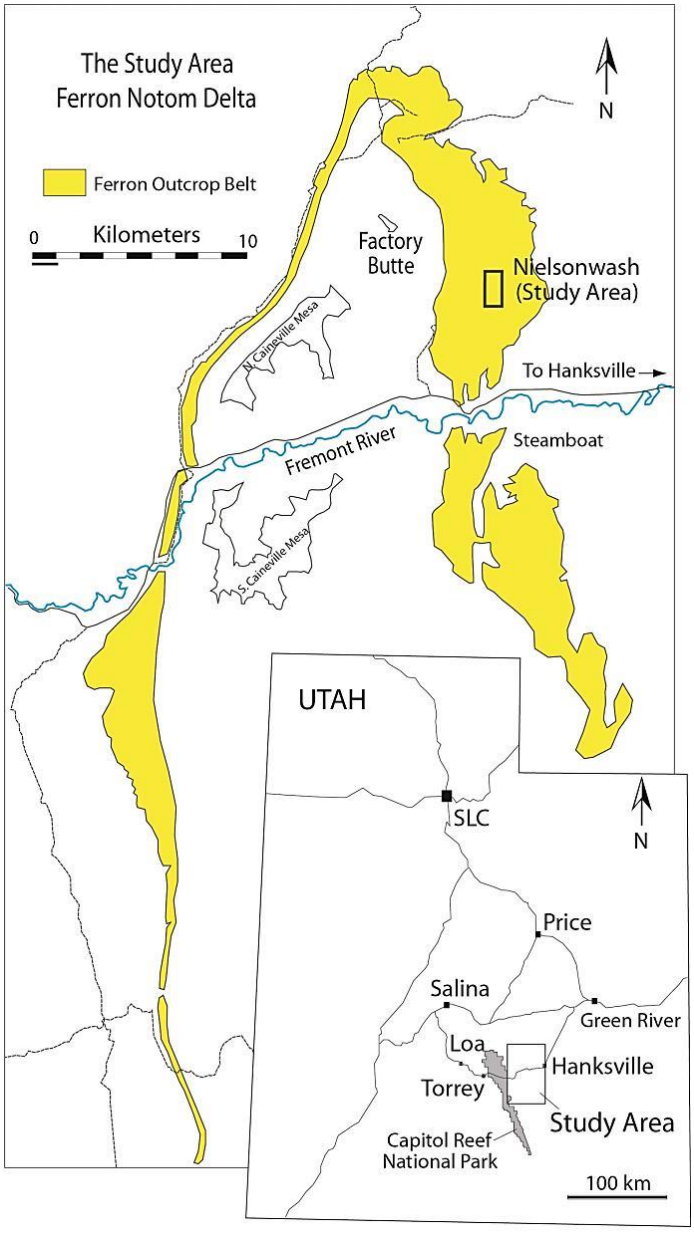

Figure 4.1 Shown in yellow is the outcrop of the Ferron Notom delta between Hanksville and Caineville, Southeast Utah. The black box outlines Nielson Wash East (study area) (Shown in Fig. 4.3).

Sediment transport and mean flow directions were estimated exclusively from dip direction of rib-and-furrow structures of trough cross-beds exposed in plan-view using a compass (Fig. 4.2A). Although the direction of sediment transport could deviate from mean flow direction (Wu et al., in review), a number of studies (e.g., Rubin, 1987) showed that measurements of rib-and-furrows associated with large-scale trough cross-stratification is a good general paleoflow indicator. A large number of paleocurrent measurements (~1880) were collected from each of the meander bends to average out local topographical effect. Fields of paleocurrents were plotted in plan-view using ArcMap® and are interpreted to represent the locally averaged direction of steepest topographic gradient (Paola and Mohrig, 1996).

A total of 549 measurements of larger-scale macroform accretion beds were made (Fig. 4.2B). The accretion surfaces were distinguished from dune-scale foresets or unit bar foresets by the 2nd or 3rd order bar accretion surfaces, which show an oblique relationship with the orientations of the foresets. Grain sizes from the trough cross beds were also measured in the field using a hand lens and a standard grain size card in 1/2 phi increments. The length and thickness of cross sets and the width and dip angle of rib-and-furrow structures were also recorded. Based on thickness, these are classified as small-, medium-, and large-scale sets and were designated to match the vertical thicknesses to that of their formative bedforms, i.e. dune-scale vs. bar-scale (Bridge, 2009). Internal bedding and facies architecture of stacked bar and channel deposits were documented based on the correlation of bounding surfaces of different scales (zero to eighth order) as defined by Miall (1985).

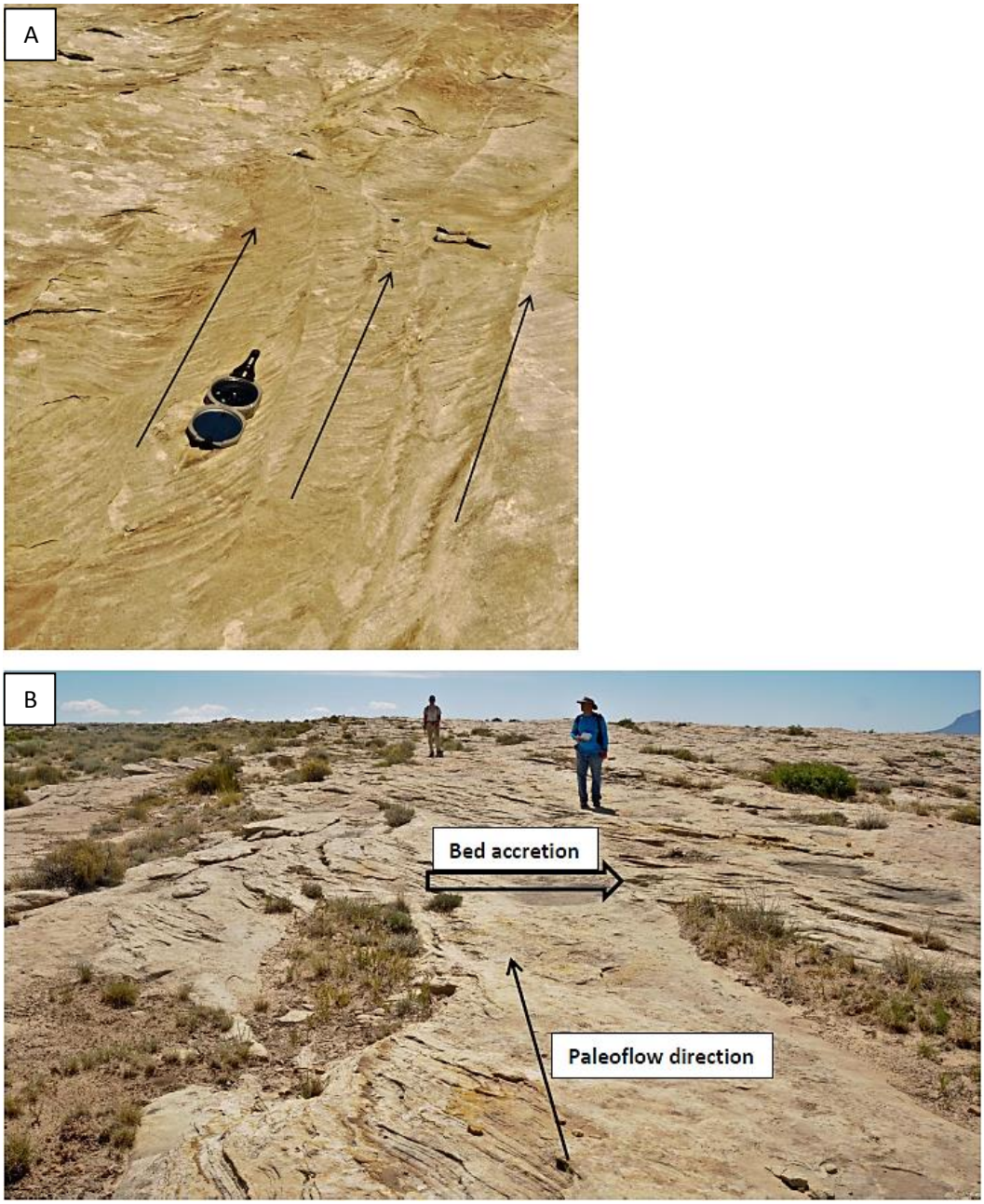

Figure 4.2 A) Rib and furrow structures: trough cross-bedding seen in plan-view. Flow is interpreted as being away from the camera. **B)** Bed accretion directions were estimated from direct observations of the accretion surfaces.

Channel style is interpreted using the methods of Miall (1994). Paleohydraulic parameters of the channels were calculated using the empirical equations of Ethridge and Schumm (1977), Bridge and Mackey (1993), Bridge and Tye (2000), Leclair and Bridge (2001), Bhattacharya and Tye (2004), and Pranter (2007).

A high-resolution Digital Elevation Model (DEM) (10 cm ground resolution) created from airborne LiDAR collected in 2012 by QSL Research Group at the University of Houston enabled us to conduct detailed ground mapping at a sub-meter scale (Fig. 4.3). Prior to DEM creation, the LiDAR point cloud was cleaned to remove artifacts and anomalous points without generalizing the data. The average structural trend in the studied meander belts has a 1.4 degree apparent dip to the west, and 0.4 degree apparent dip to the north, as estimated from the elevations of the bentonite layers stratigraphically below the meander belts that are assumed to have been approximately horizontal at the time of deposition (Hilton, 2013). Therefore, the elevation model was corrected in order to eliminate the effect of the regional structural trend. Field measurements were then plotted onto the corrected DEM using GPS coordinates of the points (Fig. 4.3). The elevations for individual paleocurrent measurement locations were extracted from the DEM and classified using 4 m elevation contour intervals. Individual channel stories are about 4 m thick as estimated by the previous studies. In addition, a shaded relief image of the area was created. This was used to differentiate plan-view bar morphologies from the pervasive NW-SE-oriented fractures that can obscured original depositional features (Fig. 4.4).

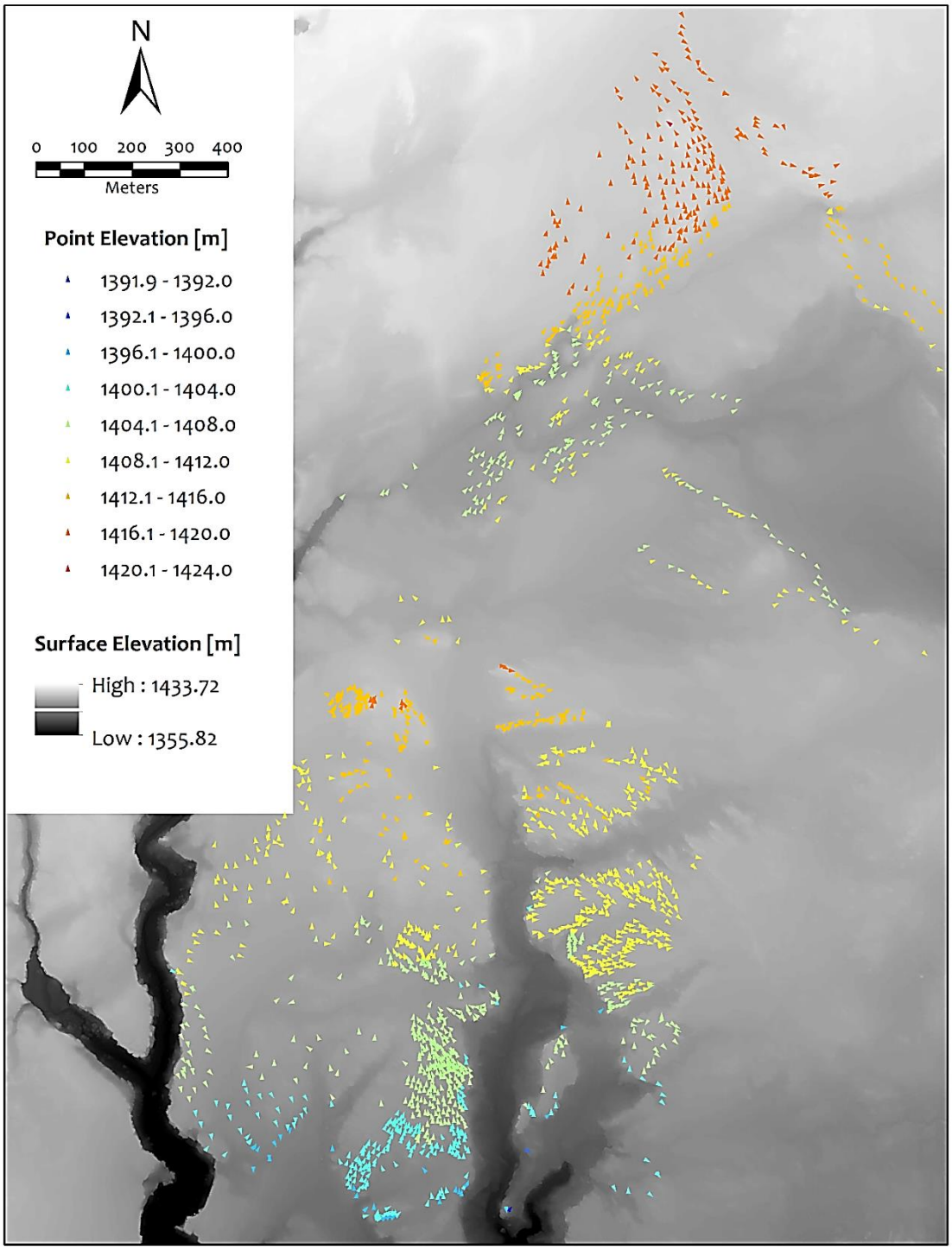

Figure 4.3 Projection of paleocurrent directions (colored arrows) on DEM. Surface elevations of the paleocurrent points indicate that there are >30 m of fluvial deposits preserved in several channel belts.

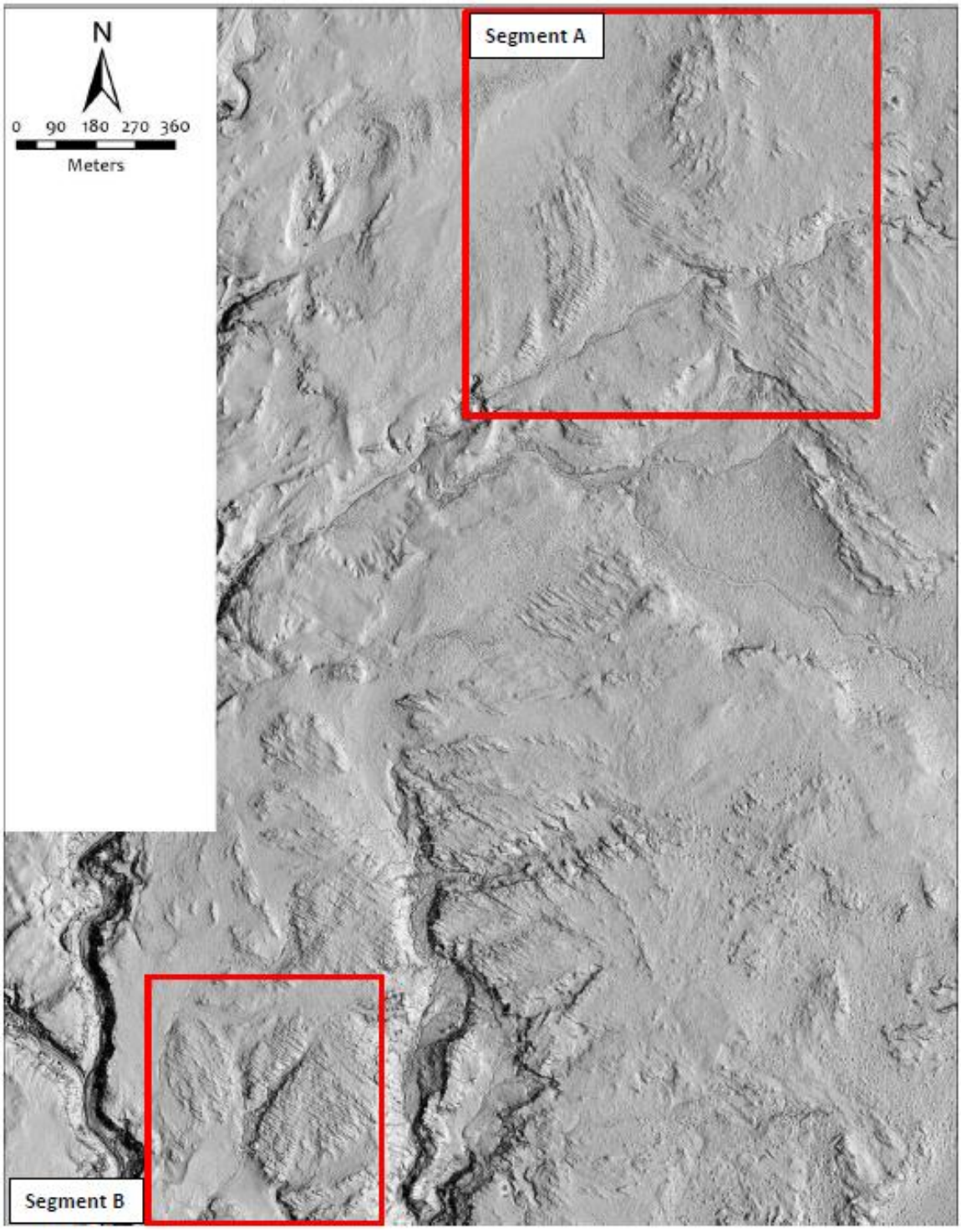

Figure 4.4 Hill-shade image of the plan-view fluvial geometry showing scroll bars (ridges and swales). The areas in red box shown in detail in Figure 4.7A and 4.7B.

Plan-view sedimentary facies were described from the meander belt deposits based on lithology, sedimentary structures, and their plan-view architecture. Internal bedding and facies architecture of the plan-view outcrops were compared with the adjacent vertical cliffs, where possible, based on the correlation of bounding surfaces of different scales.

4.4 Interpretation of bars, channels and channel belts in plan-view

Bars, channels, and channel belts were identified from the surface topography observed from hill-shade image in combination with the orientation of paleoflows relative to their associated bed accretion/sediment transport directions. Although aerial photography is a common technique to map planform exposure of exhumed fluvial systems (Edwards et al., 1983; Smith, 1987; Ielpi and Ghinassi, 2014) and to study the evolution of modern river-bed topography (Stojic et al., 1998; Lane et al., 2001, 2003), hill-shade images interpolated from LiDAR is a relatively new but effective approach to studying ancient fluvial topography (Wu et al., 2015, submitted; Bhattacharyya et al., 2015). The surface elevation of the paleocurrent measurement points from Digital Elevation Model (DEM) from LiDAR (Fig. 4.3) ranges between 1392 and 1424 m. The large elevation difference (~ 32 m after correcting for structural tilt) between the lowest and highest measurement points indicates an aggregate valley thickness that is larger than previous estimates (Li et al., 2010; Hilton, 2013; Ullah et al., in progress).
Post-depositional erosion over the last few million years has also contributed to shaping the modern landscape and modifying the local topography. Additionally, numerous sets of

regional NW-SE-oriented fractures also obscure much of the original depositional topography created by the paleo-channel bends (Fig. 4.4).

Point Bars

The hill-shade images show a distinctive array of linear arcuate ridges and swales, especially well-developed in the northern and southern parts of the study area (Fig. 4.5A, 4.5B). These are interpreted as scroll bars formed inside a meander loop, (Allen, 1965; Hickin, 1974; Jackson, 1976; Nanson, 1980). Individual unit bars, such as accrete onto the upstream parts of point bars as bar-head lobes or onto the downstream parts as bar-tail scrolls (Lunt and Bridge, 2004) are not identifiable in the hill-shade image (Fig. 4.4). Systematic rotation of the unidirectional paleocurrents, moreover, parallels with the well-developed ridge-and-swales visible on the hill-shade image (Fig. 4.6). The sandstone ridges are quite prominent on the hill-shade images, as they are more resistant than the adjacent low-lying swales in which shales were deposited either on floodplains and inter-ridge swales or in abandoned channels. Some swales could also be chute channels filled with fine-grained sediment. Although commonly done with aerial photos (Edwards et al., 1983; Smith, 1987; Brookes, 2003; Foix et al., 2012), only a few previous studies have describe similar ridges and swales in sinuous channel deposits using LiDAR images (Wang, 2013; Bhattacharyya et al., 2015; Wu et al., 2015a). These studies also interpreted the ridges and swales as scroll bars in a meander belt.

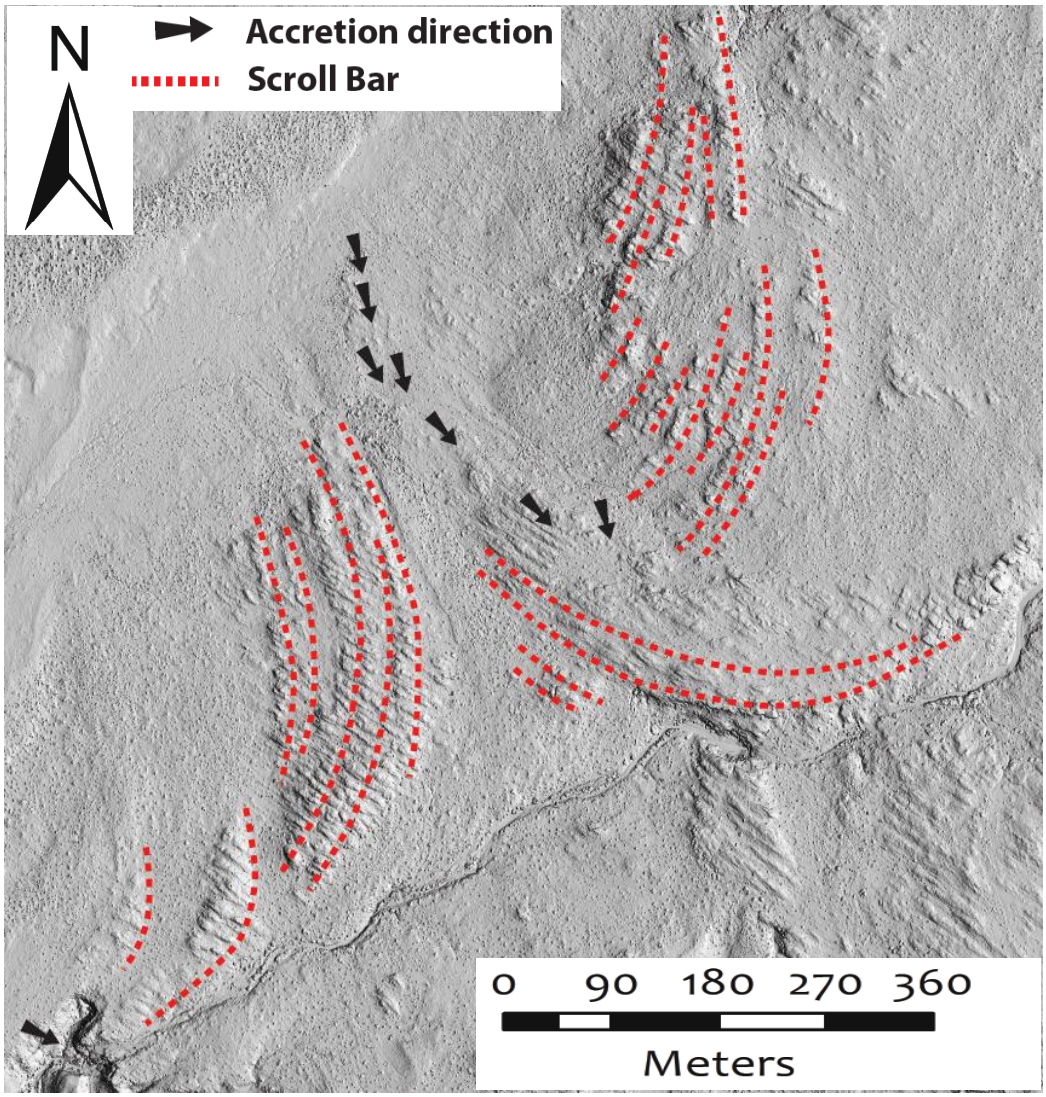

Figure 4.5A Interpreted scroll bars from the segment A in the hill-shade image in Fig. 4.4

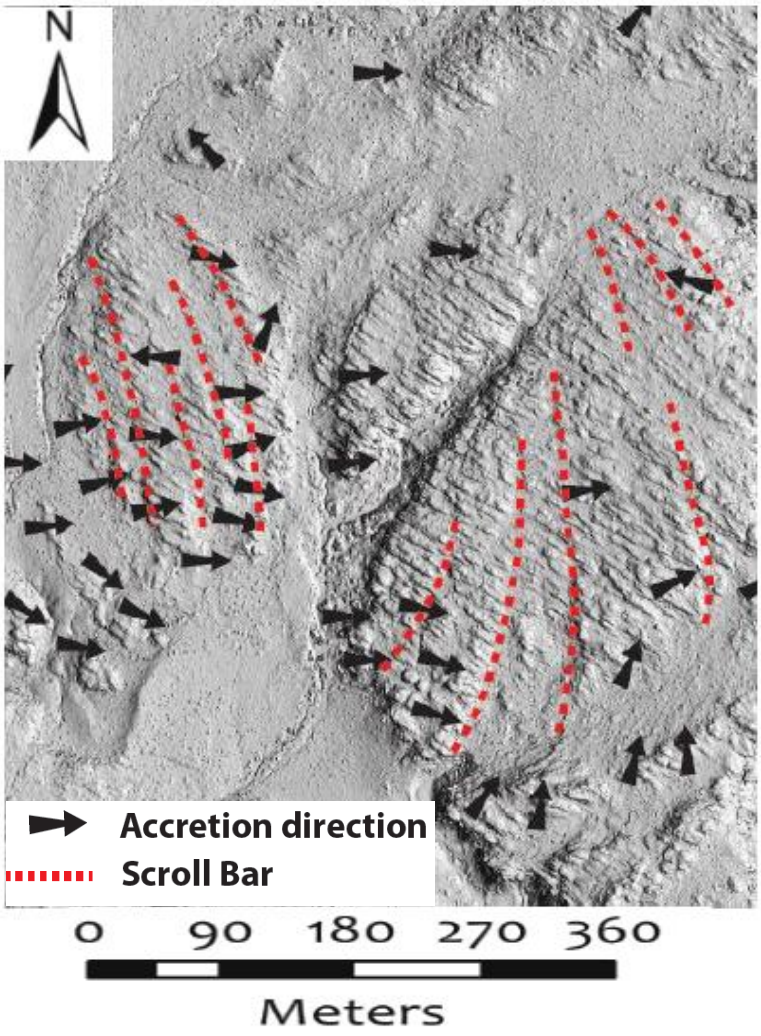

Figure 4.5B Interpreted scroll bars from the segment B in the hill-shade image in Fig. 4.4

In areas where the ridge-and-swale topography was not obvious, interpretation of Ferron point bars was made from the high angle of paleoflow to the strike of laterally accreting bar surfaces, assuming the central part of the bar is located near the point of maximum flow curvature (Fig. 4.6). The paleocurrent measurements and accretion directions show little variation within a single macroform or bar but vary systematically from bar to bar along channels. This systematic variation of paleocurrents and accretion

directions along the channel lengths was used to infer channel and bar migration patterns (as mapped in Figs. 4.6 and 4.7). The upstream and downstream segments of the bars were inferred mainly on the basis of paleo-flow measurements, and the direction of downstream translation of meander scrolls. Point bars account for more than 75% of the plan-view exposures in the studied meander belts because of their high preservation potential compared to overbank fine-grained deposits. In plan-view exposures, they are represented by large curved fluvial bodies resulting from amalgamation of crescent-shaped scroll bars.

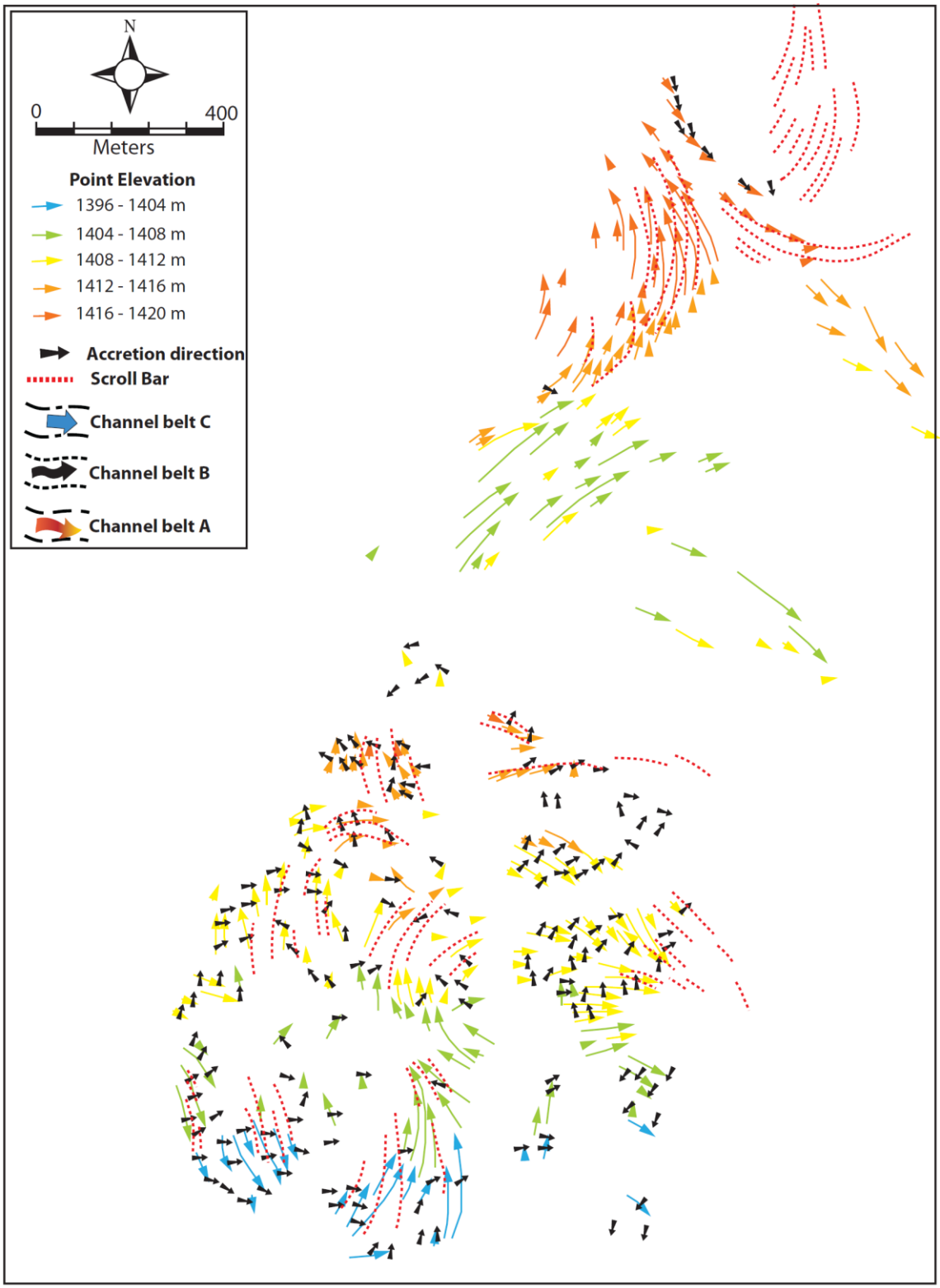

Figure 4.6 The orientations of the scroll bars obtained from the hill-shade images projected on the paleoflow paths (interpolated from Fig. 4.3).

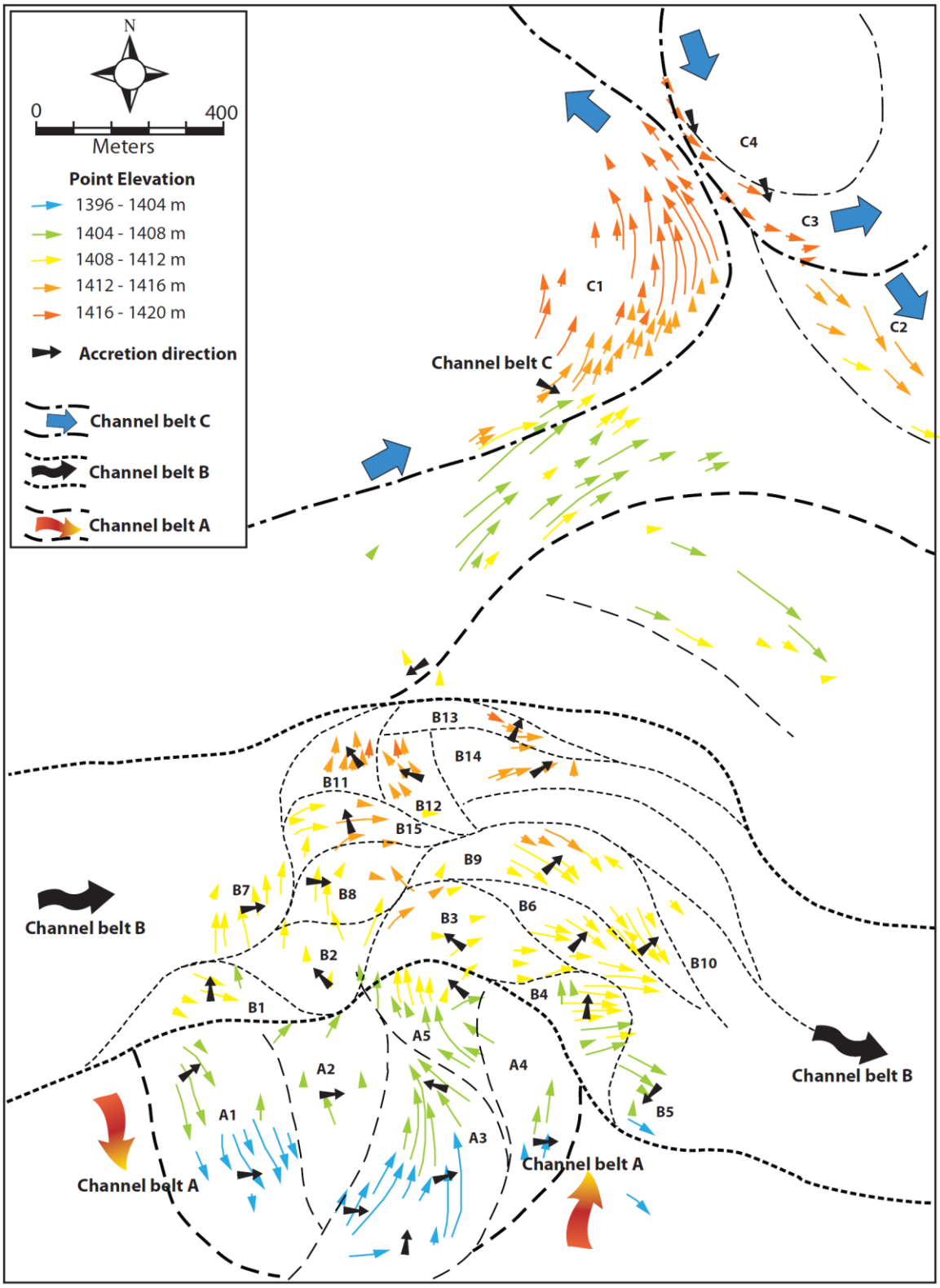
N
0
400
Meters
Point Elevation
1396 - 1404 m
1404 - 1408 m
1408 - 1412 m
1412 - 1416 m
1416 - 1420 m
Accretion direction
Channel belt C
Channel belt B
Channel belt A
C4
C3
C2
C1
Channel belt C
B13
B14
B11
B12
B15
B9
B7
B8
B6
B3
B2
B10
B1
B4
A5
A4
A2
A1
A3
B5
Channel belt B
Channel belt B
Channel belt A
Channel belt A

Channels and Channel belts

The channels were interpreted from the paleo-current directions and are mostly parallel to the curved sandstone ridges on the hill-shade images. Individual ridges in a scroll bar commonly show similar paleoflow orientations and are interpreted as the downstream portion of the meander loop. In addition to the interpreted ridges and paleocurrents, bed accretion directions were collected to supplement reconstructions of the paleochannel paths (Fig. 4.6). The colored arrows in Fig. 4.6 represent both interpreted paleoflows and their elevations. The channels are assumed to be located at the outer edge of the point bar deposit, unless removed by erosion.

Previous studies (e.g., Bhattacharya and Tye, 2004; Bhattacharya and MacEachern, 2009; Li et al., 2010) determined that the Cretaceous rivers in the Ferron delta generally had a depth of less than 7 meters. Recent studies of adjacent areas showed plan-view and 2-D vertical outcrops with reported channel depths of 3.5 – 4.1 m (Wu, 2015), 1.38 – 1.68 m (Bhattacharyya, 2015) and 2.9 – 4.7 m (this study, see appendix). Considering this, there should be at least several stacked channel stories within the 32 m of valley-fill stratigraphy, built by channels that flowed mostly towards the north-northeast to east (Fig. 4.3). Relatively smaller (second-order) cross-bar channels were not interpreted from the paleocurrent maps or hill-shade image for the sake of

Figure 4.7 (opposite page): Interpretations of channel belts and channel bars from the paleocurrents, accretion directions, and the orientation of the ridges obtained from the hill-shade image. Channel-belt A and channel bars 1 (in each of the channel belts) has the lowest surface elevations and represent the stratigraphically oldest deposits from the cross-cutting relationships. Channel-belt A and C shows flow roughly towards north-northeast, whereas channel belt B was more west-east oriented.

simplicity.

Individual channel belts were delineated on the basis of the extent of consistently oriented paleoflows, common elevations, and from the cross-cutting relationships. The projected paleocurrents show locally consistent orientations and systematic rotations in both the southern and northern parts of the mapped area; however channel orientations in the central area appear less coherent (Fig. 4.3). The trunk channels at the northern part of the area (red and orange) are topographically higher than the channels in the southern part (blue and green); hence, assuming the absence of terraces, they represent the younger, stratigraphically higher fluvial deposits. The channels in the central part of the image (yellow and orange) lie at an intermediate elevation, hence are inferred to be of intermediate age. Each of these three groups of channels, at different locations and elevations, have similar paleoflow orientations in the same stratigraphic range, but vary according to their stratigraphic level. Based on the orientation of plan-form paleoflows, accretion directions, and locations within the overall stratigraphic interval, the preserved fluvial sequence in the mapped area was divided into three channel belts (Fig. 4.7). These channel belts were named, (from oldest to youngest), Channel-belt A, B, and C.

In order to better visualize the reconstructed time-lapse stratigraphic sequences of the channels-belts, each of them was analyzed separately for paleoflow, bed accretion direction, and finally paleogeography.

4.5 Paleogeographic reconstructions of the channel belts: Evolution of an ancient meander plain

Channel-Belt A

Description: The oldest Channel-belt A, has up to 16 m (1392 – 1408 m) of relative relief and is the thickest among the three channel belts assuming the lowest outcrop represents the basal part. Paleoflow direction of Channel-belt A is from SSW – NNE. Channel-belt A deposits were mostly eroded and/or overlain by the deposits of Channel-belt B in the central portion of the study area and by Channel-belt C in the northern region (Fig. 4.7).

Paleogeographic reconstructions of Channel-belt A show that it was formed by several phases of bar growth with migration of the channel belt towards the east (Fig. 4.7). At least five phases of fluvial deposits or macroforms (A1 – A5) were interpreted in the southern portion of the Channel Belt A, the largest two of which showed the development of scrolls (A1 and A3). Among these macroforms, A1 represents the most upstream portion of Channel-belt A where the paleoflows show rotation from S to S-SE. The beds accreted from west to east, which is perpendicular to the mean paleoflow (Fig. 4.6). From A1 – A3, the channel belt deposits show a sharp counter clock-wise rotation of paleoflow from E to NE and finally towards the N-NW. The bed accretion directions are oblique to the paleoflow and show a slight rotation from E-SE to E-NE. A set of paleoflow and associated accretion directions at the southernmost portion of A3, however, show similar orientations, exhibiting variations from the overall paleoflow and accretion trends (Fig.

4.8A). Paleoflow and accretion directions in A4 show similar trends to those observed in A3. Paleoflow directions in A5, however, show a clear rotation from NW to N and finally NE with an accretion direction towards the northwest, oblique to paleoflow.

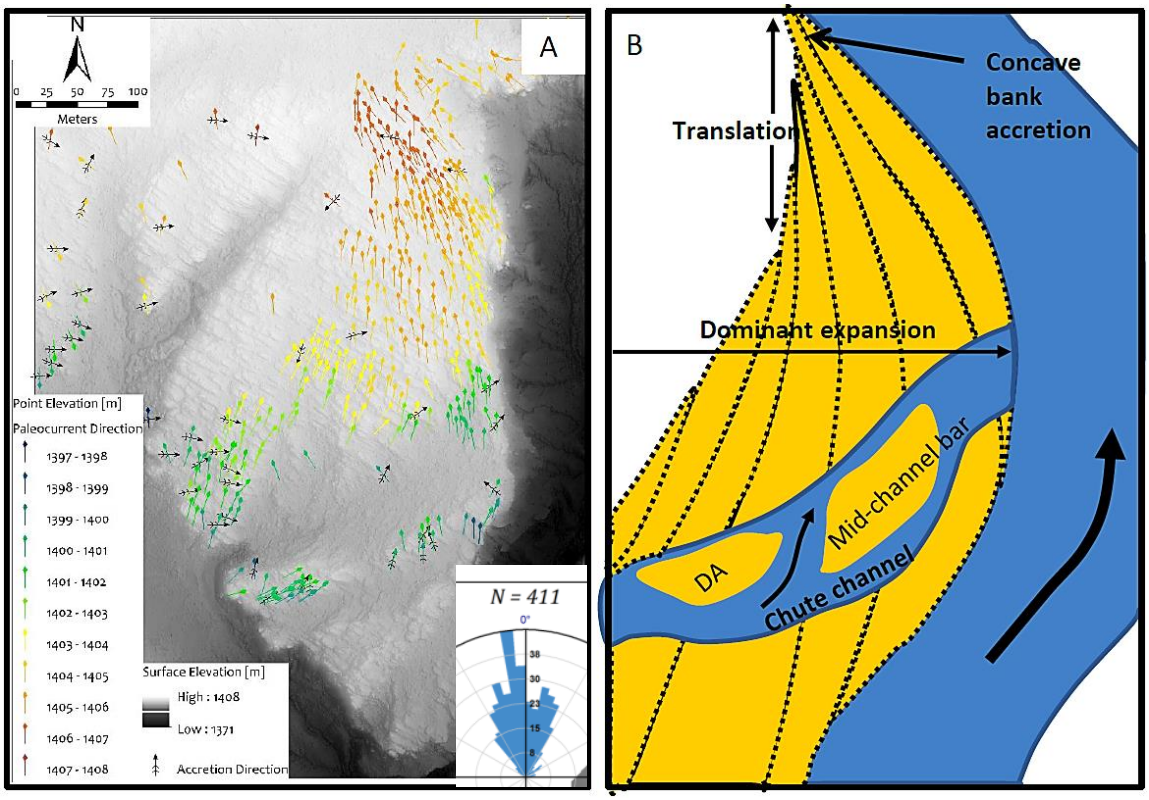

Figure 4.8 Paleoflows and bed accretion directions (A) and paleogeographic reconstructions (B) of point bar A3 in Channel-belt A. Note that separate elevation range and color legends were used in Fig. 4.8 specific for bar A3.

Interpretation: The fluvial macroforms (A1-A5) that compose Channel-belt A are interpreted as laterally accreting point bars deposited on a tight meander bend that gradually migrated east, as indicated by the predominant eastward bed accretion directions. Additionally, there is generally a high angle between paleoflow and bed accretion directions in all of the macroforms implying lateral migration. In contrast, the paleoflows and accretion directions at the lower part of the point bar A3 are similar,

hence are interpreted as a downstream accreting mid-channel bar within a chute channel that dissected the point bar during a later high flow stage (Fig. 4.8B).

In bar A1, the channel appears to have migrated towards the E-SE by expansion (Fig. 4.7). The presence of sandstone ridges may indicate that the preserved fluvial deposits in A1 represent the downstream scroll bar segment of a larger point bar complex, the upstream part of which was either eroded or covered by the overlying Channel-belt B deposits. Point bar A3 shows a complex pattern of migration that began with lateral expansion towards the east, which resulted in an increase in sinuosity and the deposition of point bar A4. This dominant expansion phase was followed by a period of downstream translation, which deposited the scroll bars in A3. The youngest point bar (A5), which does not show any ridge development, shows concave bank accretion near the crossover point. The downstream portion of A5 was eroded by the overlying Channel-belt B deposits.

Point bars A1- A5 most probably represent deposition within a large meander cutoff. The increased sinuosity of the channel towards the east might cause an avulsion after the deposition of A5 that caused the channel to flow in a relatively straight path from SW to NE. In that case, the paleoflows in between Channel-belt B and Channel-belt C may represent the youngest bars deposited following that avulsion. If not, paleoflows in between Channel-belt B and Channel-belt C were just deposits of a different channel belt, which was not interpreted in Fig. 4.7.

Channel-Belt B

Description: Channel-belt B, which is stratigraphically located between the older Channel-belt A and the youngest Channel-belt C, has at least 8 m (1408 – 1416 m) of preserved fluvial deposits. Unlike Channel-belt A, Channel-belt B did not produce a large meander bend and followed a relatively straight flow path from east to west. The individual channels within Channel-belt B, however, demonstrate a wide range of sinuosity that produced macroforms of various geometries. Cross-cutting relationship with Channel-belt A indicates that Channel-belt B is younger and eroded many of the Channel-belt A deposits in the central region.

Paleocurrents in Channel-belt B do not show the systematic rotation across a large meander bend as in Channel-belt A. Instead, paleoflows vary among different channels (dashed lines) in different parts of the channel belt (Fig. 4.7). Detailed observation of these localized paleoflow trends, in combination with their accretion directions and orientation of the sand ridges (Fig. 4.6), reveals the presence of at least fifteen macroform elements (B1-B15) (Fig. 4.7). Among these, B1, which is in the upstream end of the exposed channel belt, flowed east-southeast. Accretion directions, however, are dominantly to the northeast, perpendicular to paleoflow. From B2 to B6, along the inner part of the channel belt, paleoflow show a rotation from north-to-northeast (B2, B3) and finally east-southeast (B4 – B6). The bed accretion directions are oblique to perpendicular to the paleoflow in all of these macroforms, and show a similar rotation in orientation from northwest (B2, B3) to northeast (B4, B5). Gradual northward migration of Channel-belt B resulted in a second string of bar deposits (B7 – B10) from east to west

that filled the old channels and eroded some of the previously deposited bars. The channels that deposited these bars show paleocurrent rotation from north-northeast (B7, B8) to east-southeast (B9, B10), parallel to the old channels. Beds accreted perpendicular to the paleoflow directions in these bars and show a rotation from east (B7, B8) to northeast (B9, B10). Further lateral migration of Channel-belt B towards the north resulted in the deposition of the third string of bars (B11 – B14) along the outer bend. Channels that were associated with the deposition of these bars show a change in paleoflow from east (B11) to north-northwest (B12, B13) and finally east. The bed accretion directions were either perpendicular (B11, B14) or oblique (B12, B13, B15) to the paleoflow in these bars.

Interpretation: Paleogeographic reconstruction of Channel-belt B indicates that the entire channel-belt complex was formed by three successive phases of bar deposition as it gradually migrated north (Fig. 7). The fluvial macroforms in the innermost Channel-belt B (B1 – B6) are interpreted as laterally accreting point bars or alternate bars. At least two of these bars (B2 and B3) show some sort of scroll development. As the channel belt gradually increased its sinuosity during its northward migration, these bars were abandoned and eroded by new channels that deposited another string of point bars (B7 – B10) along the channel-belt axis. Among these, B9 has both its upstream and downstream areas preserved and shows the development of bar tail scrolls. The youngest point bars (B11 – B15) were deposited along the outer bend of Channel-belt B and show higher relief compared to the point bars deposited previously. The upstream part of these point

bars were poorly preserved as the succeeding younger bars were superimposed over the older ones. However, the downstream portion of these point bars are well preserved, as is indicated by the presence of bar-tail-scrolls. This may indicate a period of lateral channel migration driven by expansion, which increased the sinuosity and subsequently was followed by downstream translation.

Channel-Belt C

Description: Channel-belt C represents the youngest fluvial sequence located in the northern part of the study area. Almost 12 meters of fluvial deposits (1412 – 1424 m) are preserved in four different fluvial macroforms (C1 – C4). Extensive study of these deposits were presented by Wang (2013) and Wu et al. (2015) in both plan-view and vertical outcrops.

Compared to the older Channel-belts A and B, the channels in the Channel-belt C seem to have higher sinuosity and much larger meander loops (Fig. 4.7). Paleocurrent directions in the most distal end of C1 show a systematic change from E-NE to N-NE along the outer bend of the channel. The bed accretes roughly E-SE, almost perpendicular to the paleoflow directions. From the upstream to downstream end of the C1, the paleoflows show a systematic rotation from N-NE to N-NW, which are parallel to the strike of the ridges seen in the hill-shade LiDAR images. Paleocurrents in successive bars (C2 – C4), however, show a complete reversal of paleoflow. Cross-cutting relations with other bars reveal that C2 was deposited first, where paleocurrents rotate in the opposite direction than that of the earlier C1. As the channel belt gradually migrated N-NW after

the deposition of C2, the channel that caused the deposition of C3 and C4 became gradually more sinuous and produced tight meander bends. The paleoflow directions in C3 change from E-SE to E-NE as bars accreted S-SE. In C4, the channel sharply rotated from E-SE to NE-N. In both of these bars, paleoflow is again parallel to the sandstone ridges.

Interpretation: The paleogeographic reconstructions of the bars in C1 indicate that the entire point bar complex was mostly formed by several phases of lateral migration towards the east causing an increase in channel sinuosity towards the outer bend. Wu et al. (2015) identified at least four stages of lateral migration, during which the point bar complex was formed at the inner bank of the channel bend with component alternate bar, compound bars, and unit bars. From the overall geometry of the sandy facies and from the similar accretion directions, Wu et al. (2015) interpreted that point bar C1 was deposited through the migration of a single-thread channel. The crossover area of the channel bend is most probably located near the upstream end of the bar, which explains the formation of scroll bars in the downstream by translation. Due to the oblique relationships between the paleoflow and accretion directions, the fluvial deposits in C2, C3, and C4 are also interpreted as a laterally accreting point bar complex. Sinuosity of the channel that deposited these point bars gradually increased as the entire point bar complex dominantly migrated primarily by lateral accretion and expansion.

4.6 Dimension of Channels and Channel belts

Various paleohydraulic parameters of meander belts were interpreted from the paleogeographic reconstructions of the channel belts (Fig. 4.7) and from the interpreted hill-shade images. Using the radius of curvature *(R_c)* estimated from Fig. 4.7, bankfull width *(W_b),* bankfull depth *(D_b),* and discharge *(Q)* of each meander loop were calculated using the following equations,

$$W_b = 0.71 * R_c^{0.89} \quad \ldots\ldots\ldots\ldots\ldots\ldots\ldots\ldots\ldots\ldots\ldots\ldots\ldots\ldots (4.1)$$

$$D_b = 0.082 * R_c^{0.66} \quad \ldots\ldots\ldots\ldots\ldots\ldots\ldots\ldots\ldots\ldots\ldots\ldots\ldots\ldots (4.2)$$

$$Q = U*A \quad \ldots\ldots\ldots\ldots\ldots\ldots\ldots\ldots\ldots\ldots\ldots\ldots\ldots\ldots\ldots\ldots (4.3)$$

where, U is the flow velocity estimated from bed phase diagram and A is the cross sectional area of the channel (D_b* W_b) (Williams, 1986; Brookes, 2003 and Bhattacharya and Tye, 2004).

Table 4.1. Analysis of flow depth, flow width, and paleodischarge for the formative rivers in Channel-belts A and C

Channel belt	Point bar	R_c (m)	Width (W) m	Depth (D) m	Area (W*D) m^2	Discharge Q = A*U (m^3/s)
A	SB A1	290 - 375	110 - 139	3.5 - 4.1	380 - 570	305 - 740
	SB A2	285 - 490	109 - 176	3.4 - 4.9	370 - 860	300 - 1120
C	SB C1	270 - 370	104 - 137	3.3 - 4.1	340 - 560	275 - 725
	SB C3	240 - 330	93 - 124	3.1 - 3.8	285 - 465	230 - 605
	SB C4	200 - 230	79 - 90	2.7 -3.0	215 - 270	170 - 345

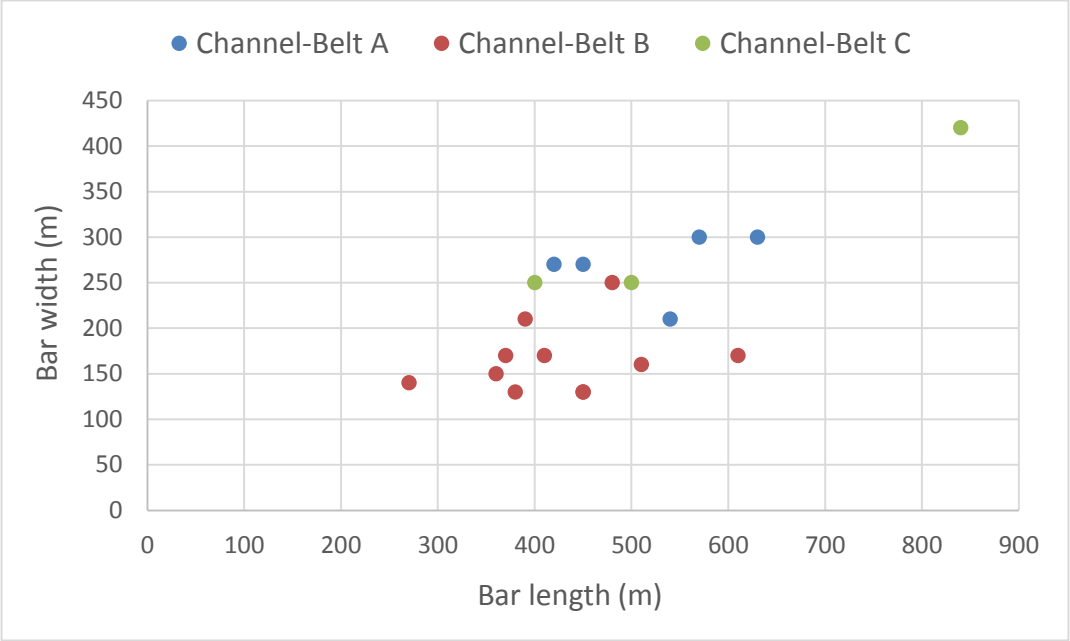

Figure 4.9 The comparison between the dimensions of the bars in Channel belt A, B, and C. Figure shows that the point bars in Channel belt A are overall larger than that of B and C.

The large compound point bars that occur on the inner banks of channel bends in Channel-belt A are between 420 and 630 m long and between 210 m and 300 m wide (Fig. 4.9). The average length/width ratio of these point bars is 2.0. Bars in Channel-belt B are smaller and have lengths between 270 and 610 m and widths between 130 and 250 m. They shows alternate growth across the channel-belt axis. Channel Belt B bars show larger length/width ratio (2.7) compared to Channel-belt A, and may indicate greater influence of downstream translation. Bars in Channel-belt C are dominated by lateral expansion, as indicated by the lowest length/width ratio and highest channel sinuosity. Among these bars, C1 is the largest in all three channel belts with a length and width of 840 m and 420 m respectively. Grain-size distribution map (Fig. 4.10) shows that C1

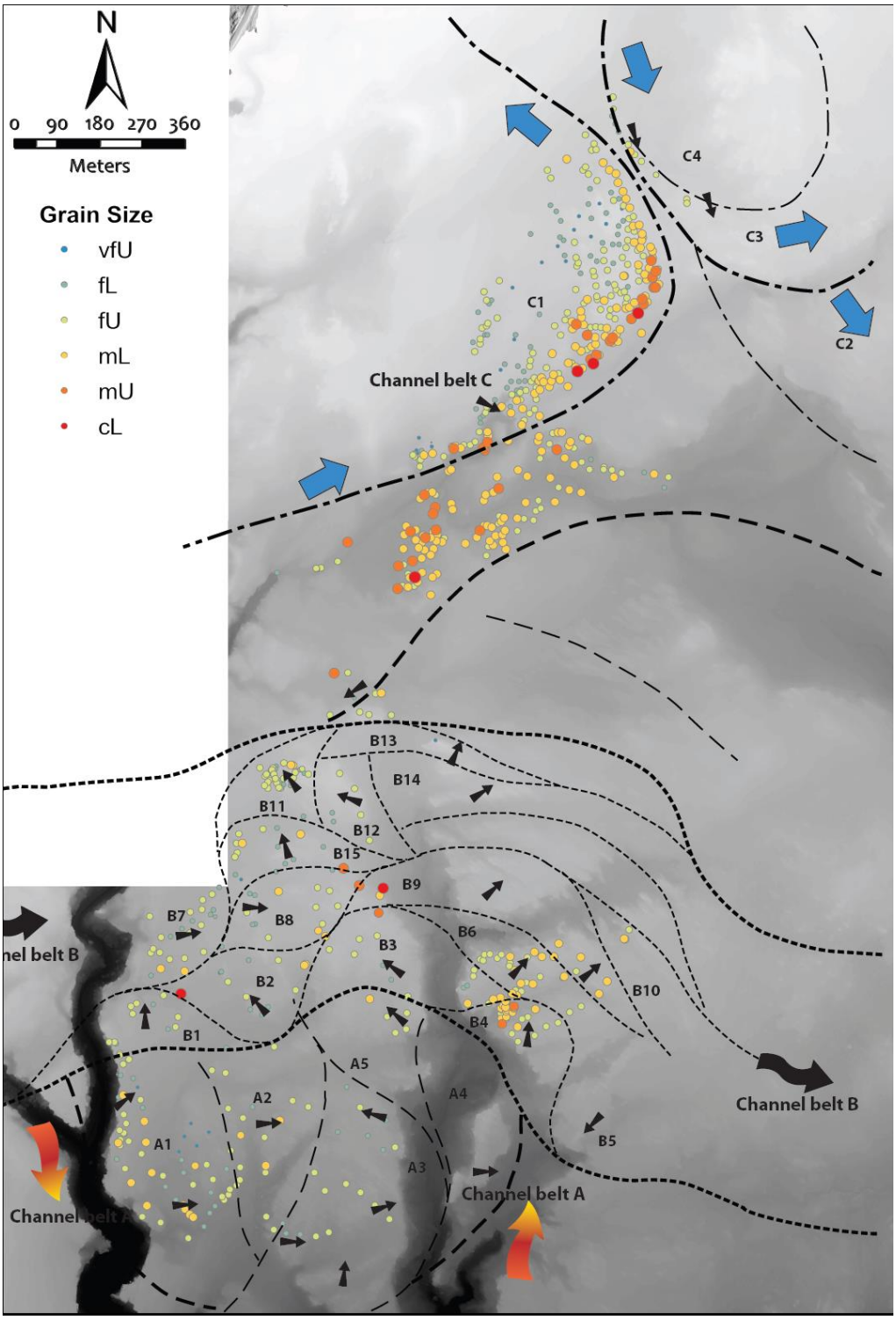

Figure 4.10 The distribution of grain sizes among each bar in a single channel belt and also between the different channel belts. Note that size of the circles correlates with the relative grain size.

is also the coarsest among all point bar deposits in the three channel belts.

4.7 Plan-view Facies Architecture of Point Bars

Detailed observations of the exhumed channel belts in this study reveal a great deal of variation in the depositional architecture (e.g., bed geometry, accretion dip of the bed-sets, and relief) across the large-scale laterally accreting macroforms. These various depositional architectural elements were studied in both plan-view and adjacent 2-D vertical outcrops, and grouped into three genetically linked architectural facies. The following section will describe these three architectural facies identified within the large-scale point bars delineated from the bedding architecture analysis integrating cross-sections and plan-views as well lithofacies description.

Architectural Facies A (Type A Macroform)

Bedding Architecture: On a vertical section oriented parallel to the channel-belt axis, Architectural Facies A consists of mostly dune or bar-scale thin to thick cross-strata and/or lower flow regime parallel planar strata. Internally they have first-, second-, and third-order bounding surfaces and a fourth-order macroform basal erosional surface (Fig. 4.11). The first- and second-order surfaces bound the sets and cosets of planar and trough cross-stratifications.

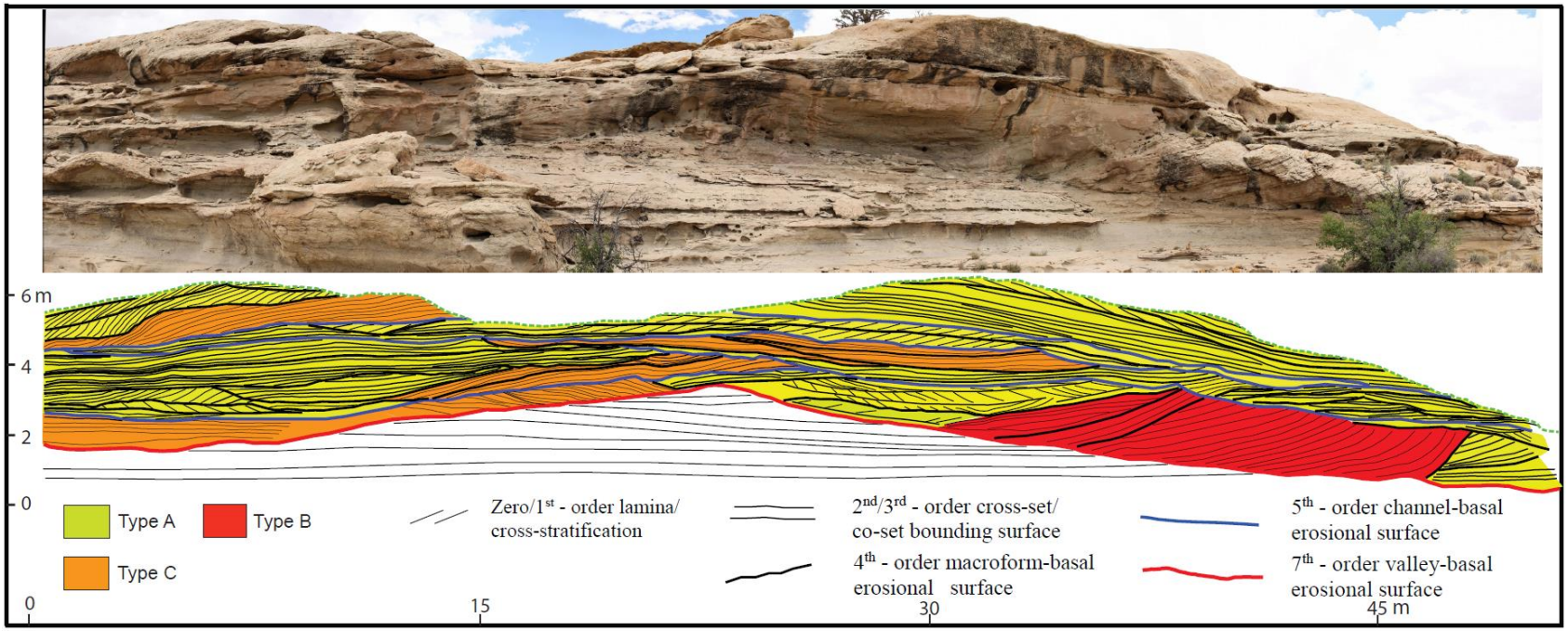

Figure 4.11 Bedding diagram depicting the architecture of Type A, Type B, and Type C macroforms.

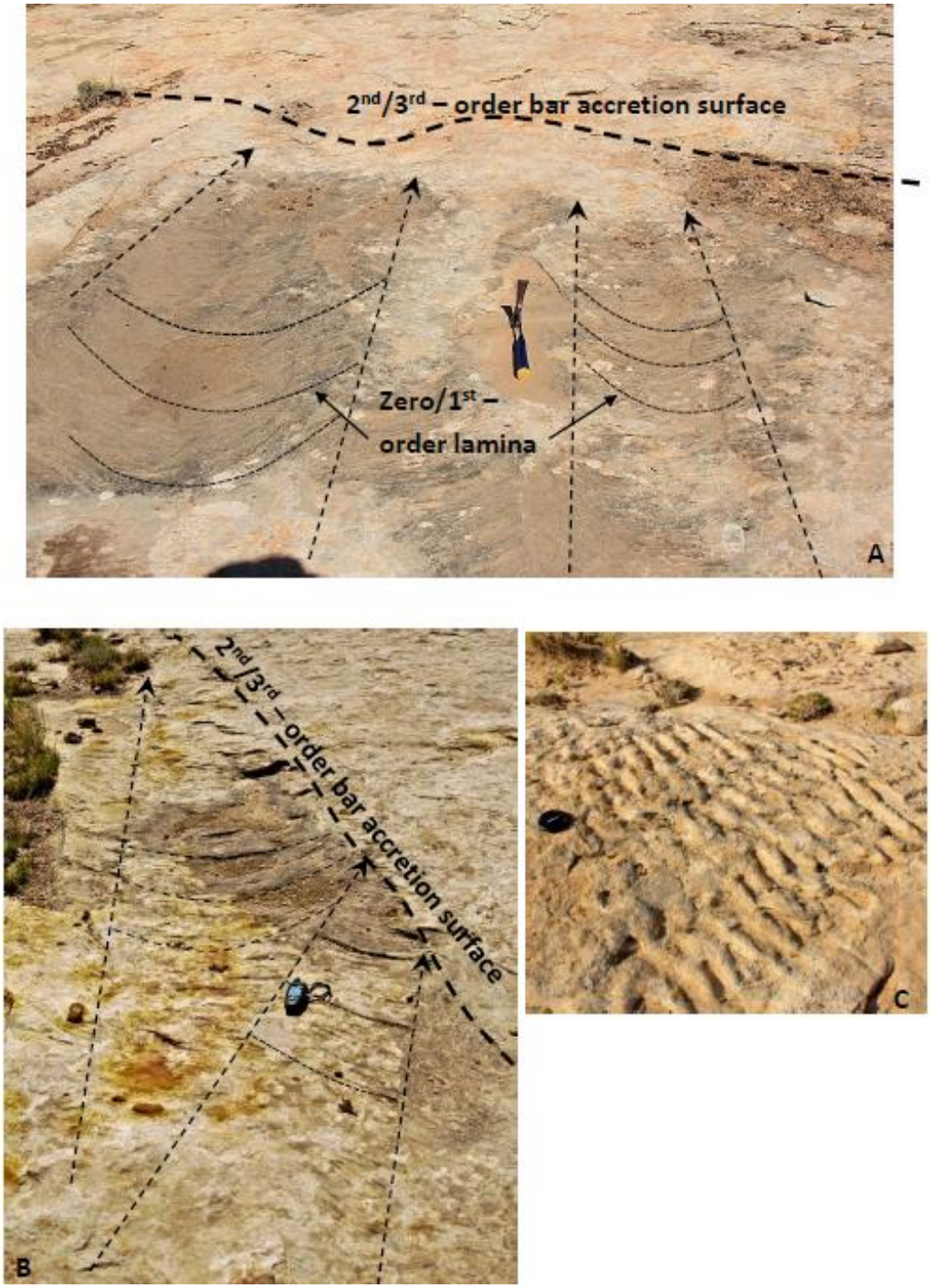

Figure 4.12 Plan-view facies architecture of the Type A macroform.

In plan-view, Macroform A appears as sets of decimeter to meter-thick amalgamated, gently inclined (< 5°) bedsets (Fig. 4.12). The first-order bedding surfaces are represented by the crescent-shaped individual ribs, which formed by downstream migration of dune-scale planar or trough foresets. The boundaries that separate the overlapping ribs represent the second-order surface that bound the cosets of cross-beds. The third-order surface represents the base of the cosets that accrete obliquely or perpendicular to the cross-bed set/coset migration direction. On smooth plan-view exposures, these third-order bar accretion surfaces are usually not visible. Within this macroform, the accretion surfaces at the base of cross-bed sets and cosets have a relatively gentle dip of between 2° and 4° towards the outer bank. These compound macroforms are typically less than 3 meters thick on the adjacent vertical outcrops.

The width of the ribs (i.e., furrows) were recorded from the plan-view exposures in Channel-belt C and were compared to a similar sets of furrow widths collected from a different meander belt (Martin and Bhattacharya, 2015) at a similar stratigraphic level located a km north of the study area (Fig. 4.13). The furrow widths in Channel-belt C range from 15 - 230 cm, with an average of 104 cm. The furrow widths collected from the adjacent meander belt range from 17 - 403 cm, with an average of 75 cm. In both cases, the furrow width histograms show a unimodal distribution with a peak at 41 – 60 cm (Martin and Bhattacharya, 2015) and 81 – 100 cm (this study). It indicates that 90% the typical furrow widths in the Type A macroforms range between 20 and 160 cm. Among them, furrow widths more than 1 m most probably represents the bar-scale cross sets.

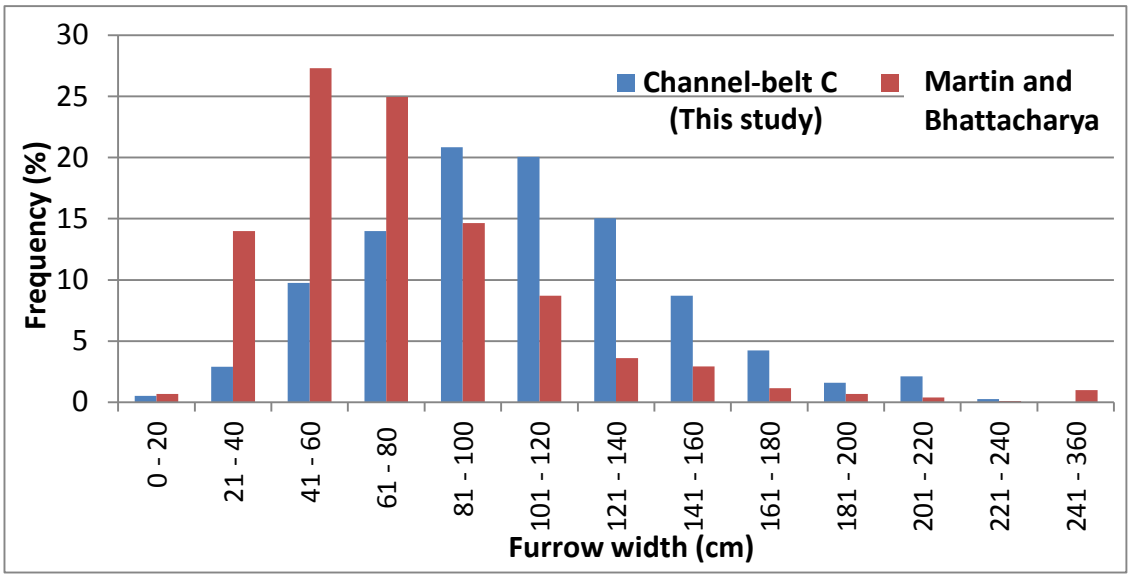

Figure 4.13 Histogram of furrow widths collected from the Channel-belt C compared with the furrow widths in an adjacent meander belt just north of the study area.

Lithofacies Description*:* Lithofacies dominantly consist of fine to medium-grained trough (St) or planar (Sp) cross-stratified sandstone. In some cases, the cross-bedded sandstones are capped by very fine-grained sandstone with ripple cross-laminations (Sr), and show an overall fining-upward trend that may represent the upper parts of channel fills (Fig. 4.12C). The top of Macroform A often developed siderite nodules and iron oxide bands. In most cases the ripple cross laminations at the top are truncated by adjacent sandy facies Sf or St of another overlapping bar. The cross sets can be as thin as 3 cm but never exceed 25 cm in the adjacent vertical outcrops. Gravel-sized mudstone intraclasts, petrified wood logs, and pebbles are sometimes present at the base of the macroform ($4^{th}/5^{th}$ order bounding surface), which is interpreted as the bar migration in the channel thalweg.

Interpretation: The planar and trough cross-stratified beds in vertical exposures or rib-and-furrows in plan-view exposures were described in many studies of modern and ancient fluvial outcrops as progradation of planar and trough dunes towards the bar core (Sambrook-Smith et al., 2006; Bridge, 2006, Adams and Bhattacharya, 2005; Ielpi, 2014). Together, the bar- and dune-scale cross sets form amalgamated compound bars, which build the laterally accreting macroforms. Studies from modern and ancient river deposits have shown that compound bars are formed by amalgamated bar-scale cross-beds with dunes on top. Large-scale compound fluvial macroforms, such as bank-attached point bars or mid-channel braided bars are formed by amalgamation of many successive small-scale macroforms (Sambrook-Smith et al., 2003; Bridge, 2006). The coalescence of dune- and bar-scale Type A macroforms is characterized in plan-view by the ridge and swale topography, as seen in the hill-shade LiDAR images.

Architectural Facies B (Type B Macroform)

Bedding Architecture*:* Type B macroforms consist of a moderately to steeply dipping single large foresets, greater than 1 m thick, which lack internal second- and third-order bounding surfaces and have a fourth- or a fifth-order channel-basal erosional surface in vertical sections (Fig. 4.11). Individual foresets in the macroform are continuous from top to bottom and do not terminate against each other. In dip view, most foresets have a concave-upward or listric profile (Fig. 4.11). The lack of smaller-scale internal cross sets and co-sets indicates they are not compound in nature, as are the type A macroforms. The single, oversize foreset deposits are often capped by a secondary fourth-order macroform

erosional surface overlain by a compound-bar deposit (i.e., Type A Macroform). The maximum preserved thickness of Type B macroforms found on 2-D vertical sections in the study area, is 3 m. Miall (1996) described this facies as large-scale planar cross-bedded (Sp) facies comprising solitary sets that may be traced for tens of meters parallel to bedding. Because of the continual channel shifting and associated scours, complete foresets are rarely preserved in most fluvial systems (Miall, 1996).

The large scale of the Type B macroform is reflected in the large lateral extent of bar sets relative to smaller bedforms (i.e., dunes in Type A). In plan-view, the single set of large foresets are represented by ribs, wider than 2 m (Fig. 4.14, 4.15A). Figure 4.13 shows that Type B macroforms constitute < 5% of all furrow widths recorded from the Channel belt C. Data from plan-view exposures of the adjacent meander belt (Martin, 2015) also shows a similar range. The maximum furrow width of the Type B macroforms recorded in all three meander belts exposures is 6 m.

Figure 4.14 An example of a downstream accreting unit bar (Type B) consisting of ~ 4 m wide furrows.

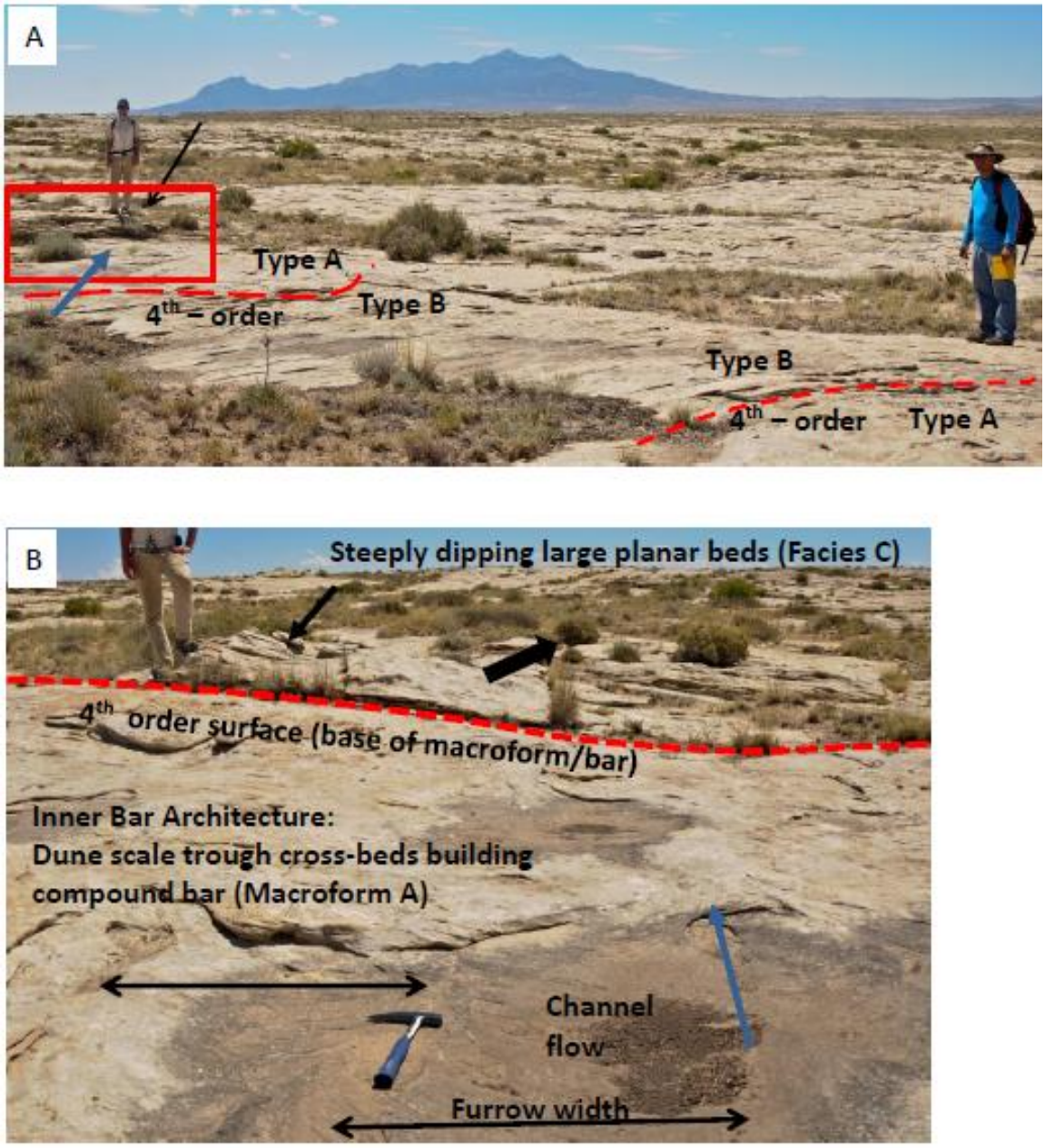

Figure 4.15 Lateral change in macroform geometries as a channel migrated laterally towards its outer bend: (A) A 15 m long and 3 meter wide Type B macroform accreting from right to left, (B) Abrupt increase in bed dip up to 30 ^{o} as the channel laterally accreted over its deep scour at bend apex/cut bank with large laterally extensive UFR planar beds (blue arrows for paleoflows; black arrows for bed accretions).

Figure 4.15 shows the lateral change in macroform geometries as a channel migrated laterally towards its outer bend. Figure 4.15A shows a plan-form example of a 15 m long and 3 meter wide Type B macroform accreting from right to left. Field measurements show that the upstream end of the bar overlies a gently accreting dune-scale trough-cross-bedded (3^o - 4^o) Type A macroform with a fourth-order macroform basal erosional surface (red dashed line) in between them. The downstream end of the bar (red box in figure 4.15A), on the other hand, is overlain by a Type A macroform (Fig 4.15B) that has furrows less than a meter-wide dipping at an angle less than that of Type B. The boundary between Type A and Type B at the downstream end is also represented by a fourth-order bar base. The dip of the Type B macroform accretion surfaces gradually increased from 3~4^o to 6^o from upstream to downstream. This relatively steeply dipping Type B macroform in between Type A macroforms might indicate the initial filling of a channel depth that is larger than the typical smaller Type A bars fill. The Type A macroform on top of the Type B (Fig. 4.15B) might represent the filling of the additional accommodation and scale to average channel depth.

Lithofacies Description*:* The steeply dipping large single foresets consist of fine to medium- grained sandstones. The foresets are usually between 2 – 4 cm thick and show normal grading. The contact between the foresets are usually sharp in both dip and strike view. In strike view, foreset boundaries are often distinguished by an abrupt increase in grain size from fine-medium to granule. The length of the individual foresets in Type B macroforms ranges between 1 m and10 m in the vertical outcrops.

Interpretation: The moderately to steeply dipping single set of large foresets in Type B macroforms are interpreted as unit bars. Reesink and Bridge (2007) described the unit bars as large-scale solitary depositional units that formed by some sort of unsteady flow, and are fundamentally different from large-scale compound bars (i.e., Type A macroforms in this study). The possible geometric and architectural variations caused by a range of fluvial plan forms and flow depths can result in a great deal of variation in relative abundance and composition of unit bars in braided and meandering rivers (Bridge, 2009; Lunt et al., 2004; Sambrook-Smith et al., 2006; Reesink and Bridge, 2007). Lunt et al. (2004), Sambrook-Smith et al. (2006), and Reesink and Bridge (2007) described unit bars as lobate bedforms found in both braided and meandering rivers, with lengths that are proportional to the flow width and heights that can approach bankfull depth (Bridge 2003). According to Bridge (2006), bar heads and bar tails of large compound bars in meandering rivers are formed by downstream accretion of unit bars. In the braided riverbed on the other hand, a unit bar is often associated with the infilling of excess local accommodation created by confluence scours when bars migrate across the scour (Bridge, 2006; Ullah et al., 2015). Large-scale foresets in unit bars were also reported to be formed near the thalweg of the river (Lunt and Bridge 2004).

The steeply dipping single set of large foresets are formed by avalanching of bed-load sediments down the leeside of unit bars as the scour is filled by vertically accreting and laterally migrating thick foreset deposits. Similar structures have been described by Bridge (2006), Sambrook-Smith et al. (2006) and Parker et al. (2013) in

modern fluvial system, and interpreted by Boersma et al. (1968) and Hartkamp-Bakker and Donselaar (1993) in ancient deposits.

Architectural Facies C (Type C Macroform)

Bedding Architecture: Type C macroforms consist of vertically and laterally stacked inclined planar laminations and/or beds dipping at 15° to 35° towards the channel pool in the upstream portion of bend apex (Fig. 4.16A). These large steeply dipping planar beds are slightly wavy in some cases, and are bound by forth-order macroform or a fifth-order channel-basal erosional surface in vertical sections (Fig. 4.11). At the top they are commonly overlain by small- to medium-scale cross bedding (Type A) with a fourth-order erosional surface in between them.

The large lateral extent of these planar beds form sheet-like sandstones, the width of which in the studied outcrops can be up to 100 m along the channel margin (Fig. 4.16 B, C). Internally, Facies C, shows large laterally extensive bedsets formed by smaller bedforms (i.e., dune-scale cross sets and bar-scale cross sets) as described in Type A and Type B macroforms in the previous sections.

Lithofacies Description: UFR planar strata are a few mm to a few cm thick and are commonly internally graded or have gradational boundaries. These laterally continuous beds consist of alternating very fine- and coarse-grained sandstones- both inverse and normal grading. In vertical outcrops, the gradational planar laminations are slightly wavy.

Figure 4.16: Steep large upper flow regime planar bed accretions at bend apex in a tight meander cut bank: A) 3-D outcrop, B, C) plan-view exposure.

Internal bounding surfaces were not seen within the thick packages. However, parting lineations perpendicular to bedset dip were seen in some cases.

Interpretation: Architectural Facies C (Type C Macroform) mainly consists of laterally accreting upper flow regime (UFR) planar strata that form either from migration of low amplitude bedforms or burst and sweep cycles (Bridge and Best, 1988; Paola et al., 1989). UFR sedimentary structures in general, are rarely preserved in fluvial sequences. However, high depositional rate from suspended sediment concentrations increase aggradation that facilitate their preservation potential (Allen and Leeder, 1980; Bridge and Best, 1988, 1997; Paola et al., 1989; Cheel, 1990). UFR structures are therefore, common in modern highly seasonal river systems, such as those in monsoonal and subtropical climates (Plink-Bjorklund, 2015).

According to previous studies (Paola et al., 1989; Cheel, 1990; Bridge and Best, 1997; Fielding, 2006), planar laminations formed at low depositional rates are typically thinner (few mm) and have more distinct laminations with parting lineations than planar laminations formed during high depositional rates, which are commonly internally graded or have gradational boundaries (Plink-Bjorklund, 2015). Preservation of cm-scale internally graded UFR planar strata studied in outcrops indicates that the UFR sedimentary structures were deposited at high depositional rates. Previous studies (Paola et al., 1989; Cheel, 1990; Bridge and Best, 1997) described these thicker laminations as the product of the migration of thicker low-angle bedforms.

Figure 4.15 shows an example of the progression of macroform architecture as the large-scale, compound bar migrated laterally over a deep scour near the bend apex (red dashed line in Fig. 4.15B). The dune-scale trough-cross-bedded Type A macroforms in the inner bar were overlain by a Type C macroform, which consists of extensive laterally accreting upper flow regime (UFR) planar beds. The UFR planar beds dip more steeply (~ 30^{o}) compared to the accretion surfaces in underlying Type A macroforms (< 5^{o}), and dip at an angle greater than the angle of repose. The change from gently dipping small-scale trough cross-beds (Type A) to steeply dipping single large planar bedsets (type B) occurred without any apparent change in flow and bed accretion directions. The boundary between these two different macroforms is represented by an erosional fourth-order macroform basal surface. These steeply dipping, laterally extensive UFR planar beds (Type C macroforms) are a fairly common feature on the exposed channel belts in the study area, and their GPS locations were noted wherever found. Interestingly, the locations of these Type C macroforms always coincides along the cut bank in the upstream portion of the interpreted point bars (Fig. 4.17). This may indicate that Type C macroforms form due to lateral accretion over the deep channel thalweg along the cut bank upstream of the bend apex.

In many case, the UFR planar beds can be easily mistaken for large inclined foresets in unit-bar deposits described from braided rivers, which show a somewhat similar internal geometry and architecture. However, these two facies formed from fundamentally different hydrodynamic processes on the river bed and need to be distinguished clearly for correct morphodynamics interpretations.

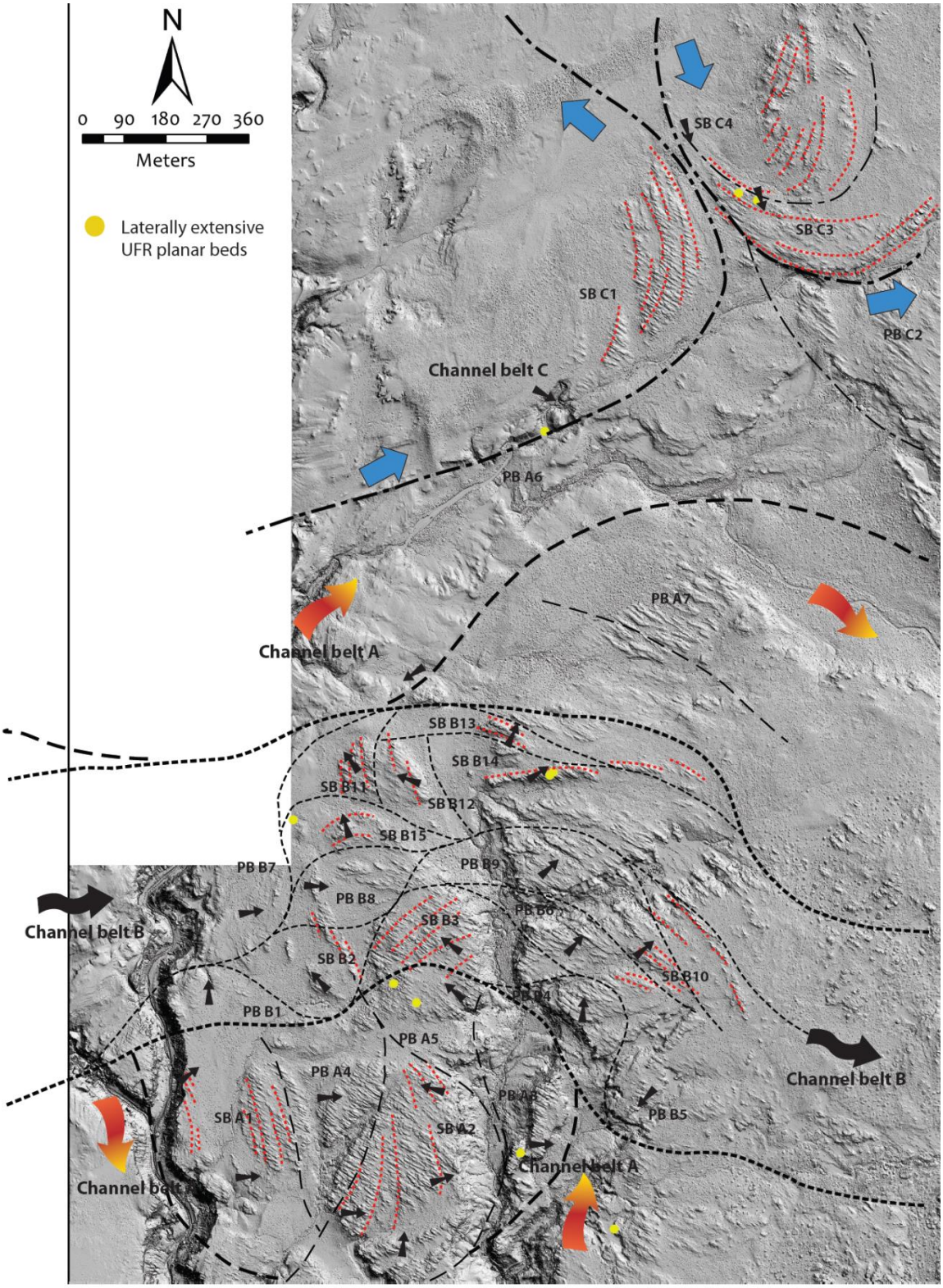
N
0 90 180 270 360
Meters
Laterally extensive UFR planar beds
SB C4
SB C3
SB C1
PB C2
Channel belt C
PB A6
PB A7
Channel belt A
SB B13
SB B14
SB B11
SB B12
SB B15
PB B7
PB B9
PB B8
PB B6
Channel belt B
SB B3
SB B2
SB B10
PB B4
PB B1
PB A5
PB A4
PB A3
PB B5
SB A1
SB A2
Channel belt A
Channel belt B

4.8 Distinguishing Upper Flow Regime Structures and Dune/Bar-scale Cross-strata

Steeply dipping upper flow regime (UFR) sedimentary structures are relatively uncommon in existing fluvial facies models and are often overlooked or commonly misinterpreted as lower flow regime (LFR) dune-scale cross strata or wave-dominated hummocky and swaley cross strata. Because many of the UFR structures produce different types of cross stratification, they are easy to confuse with cross strata produced by dune migration. Transition between UFR sedimentary structures, however, is abrupt compared to lower flow regime (LFR) structures as small variations in Froude number can completely modify the previous structure to a new one. For example, UFR humpback or sigmoidal cross-strata form during the transition phase between LFR dune and UFR plane bed deposition (Bridge, 1981; Bridge and Best, 1988; Fielding, 2006) at Froude numbers just below the Froude numbers required for UFR plane beds (Plink-Bjorklund, 2015). Experimental studies by Bridge and Best (1988) produced humpback or sigmoidal cross strata at Froude number 0.81 and UFR planar laminations at Froude numbers 0.91 and 0.98. Therefore, UFR sedimentary structures are highly variable and transition both vertically and laterally into other UFR sedimentary structures (Plink-Bjorklund, 2015). In a vertical section, the UFR structures can transition from low-angle cross strata to a scour and fill or convex-up laminae in a flow parallel-view. Recognition of UFR structures is thus critical for correct morphodynamic interpretations.

Figure 4.17 (opposite page) Shows the location of the large inclined UFR planar beds with respect the geometry of the point bars. In most cases, the large UFR planar beds (Type C macroforms) form in the upstream portions of point bars.

Unlike the LFR sedimentary structures, the UFR sedimentary structures are formed from suspended sediments rather than bedload deposition (Allen and Leeder, 1980; Plink-Bjorklund, 2015). High deposition rates create aggradational thicker laminae which are often gradational and have indistinct boundaries. UFR sedimentary structures therefore, commonly occur in much thicker sets than dune-scale cross strata.

In vertical sections, the laterally continuous sets of LFR dune-scale cross strata have planar laminae or scour-and-fill features in a strike (flow-perpendicular) view. In contrast, the UFR structures may look like scours or hummocky-like mounds from both strike and dip (flow –parallel) view. Most importantly, UFR planar beds have parting lineations perpendicular to bedset dip, which is not common in the foresets of 0cross-stratifications.

4.9 Reconstruction of 2-D Architectural Elements

This chapter attempts to reconstruct the 2-D vertical architectural elements of the macroforms based on plan-view data described in the previous sections. Reconstructing 2-D macroform architecture using plan-view data involves three stages – 1) analysis of paleoflows with respect to bed accretion, 2) reconstruction of plan-view architectural elements and 3) reconstruction of 2-D vertical architectural elements using previously proposed hypotheses/models (Fig. 18). Previous sections discussed the reconstruction of plan-view architectural elements of various macroforms from plan-view data. This section incorporates available hypotheses/models on geometries and paleohydraulics of

point-bar deposits with the interpreted plan-view architecture of the macroforms to reconstruct their 2-D/3-D vertical architecture.

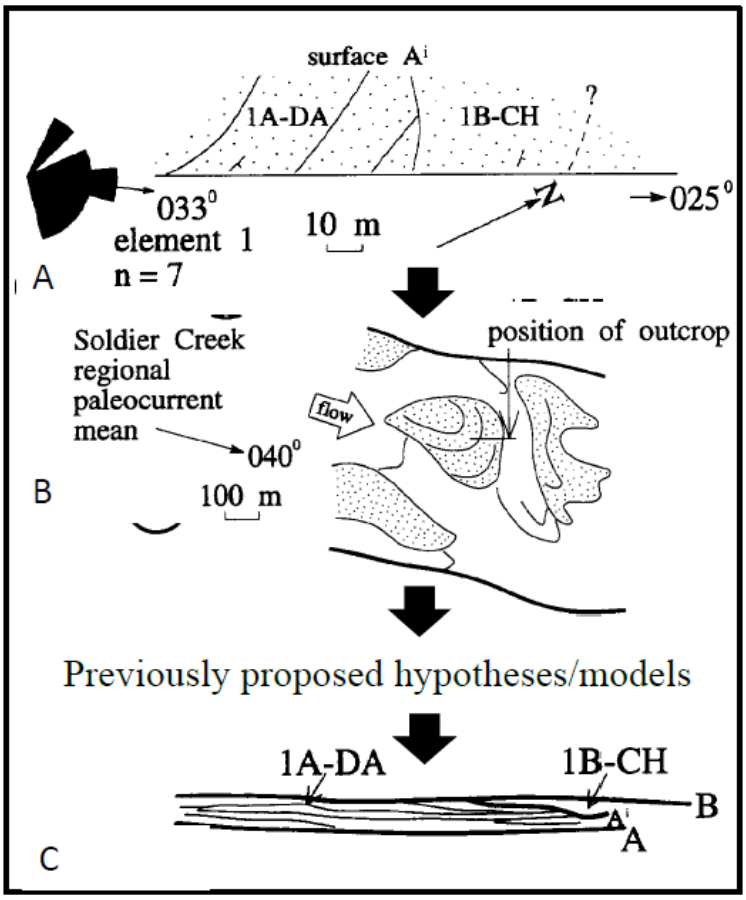

Figure 4.18 Reconstructing 2D macroform architecture using plan-view data: (A) Step 1 - Paleoflow and bed accretion analysis; (B) Step 2 - Reconstruction of plan-view architectural elements; (C) Step 3 - Reconstruction of 2-D vertical architectural elements using previously proposed hypotheses/models (modified from Miall, 1994).

A number of models predicted the flow strength, topography, geometry, and sediment size distribution of accretionary beds formed around meander bends across a channel (Bridge 1976, 1977, 1982; Willis 1989, 1993a, b, 2010). Some of these models (e.g., Willis, 1989,1993a) have been widely used to interpret the bedding geometries and paleohydraulics of point-bar deposits in ancient river deposits exposed in 2-D vertical

outcrops; whereas others (e.g., Bridge, 1982; Bridge and Jarvis 1982; Bridge 1992) predicted variations in bed topography and spatial variations in sediment texture along modern river bends. However, all of these models show a deviation of flow and sediment transport direction around the point bar from the mean downstream direction, which is produced by the interaction of channel geometry, channel migration pattern, stages of the flow (rising, falling, and equilibrium) and varying bedform orientation relative to the channel centerline (Bridge, 1977; Bridge and Jarvis, 1982; Bridge, 1985). This deviation of channel flow from the mean downstream direction produces helical flow that causes an increase and decrease in shear stress along the outer and inner bank respectively. This results in erosion and cutbank retreat along the outer channel bend and aggradation of that sediment on the inner point bar during individual flood events (Dietrich et al., 1979; Dietrich and Smith, 1983; Frothingham and Rhoads, 2003) causing channel migration. Brice (1974) recognized several modes of meander migration, including translation (movement of a meander bend downstream), expansion (increase in meander-bend sinuosity), rotation (development of meander-bend plan-view asymmetry), and combination of all these. Model results by Willis (1989) show that when a channel migrates by expansion, sinuosity increases; whereas both meander wavelength and amplitude increase with expansion and downstream translation of the channel bend.

Theoretical models by Willis (1989, 2010) (Fig. 4.19) show how the point bar geometry and topography is primarily controlled by channel flow stage and sinuosity. As the channel segment increases in sinuosity, its thalweg successively incises deeper along the bend apex and builds up bars that thicken away from the channel-belt axis along the

insides of bends. Because the channel both cuts deeper along the outside of a higher sinuosity meander bend and builds up a bar higher along the inside of that meander bend, preserved beds successively dip more steeply outward as the deposit thickens. Bed topography and slope become highest at the bend apex, and dip down more gradually into the adjacent channel in both upstream and downstream edges of point bar. Therefore, effects of varying discharge on bar shape are greater for higher sinuosity channel bends, since greater areas of more steeply dipping beds in a high-sinuosity channel become emergent during lower flow conditions. Lower sinuosity bends, in contrast, show much less variation in topography and bar slope across the point bar. Therefore, lateral variation of point-bar thickness with progressively increasing sinuosity is assumed to be greater than variations produced by simple translation of a point bar with consistent geometry. According to Willis (2010), scours near the apex of a higher sinuosity meander bend can be more than twice as deep as the mean channel depth in a straight channel segment carrying the same discharge.

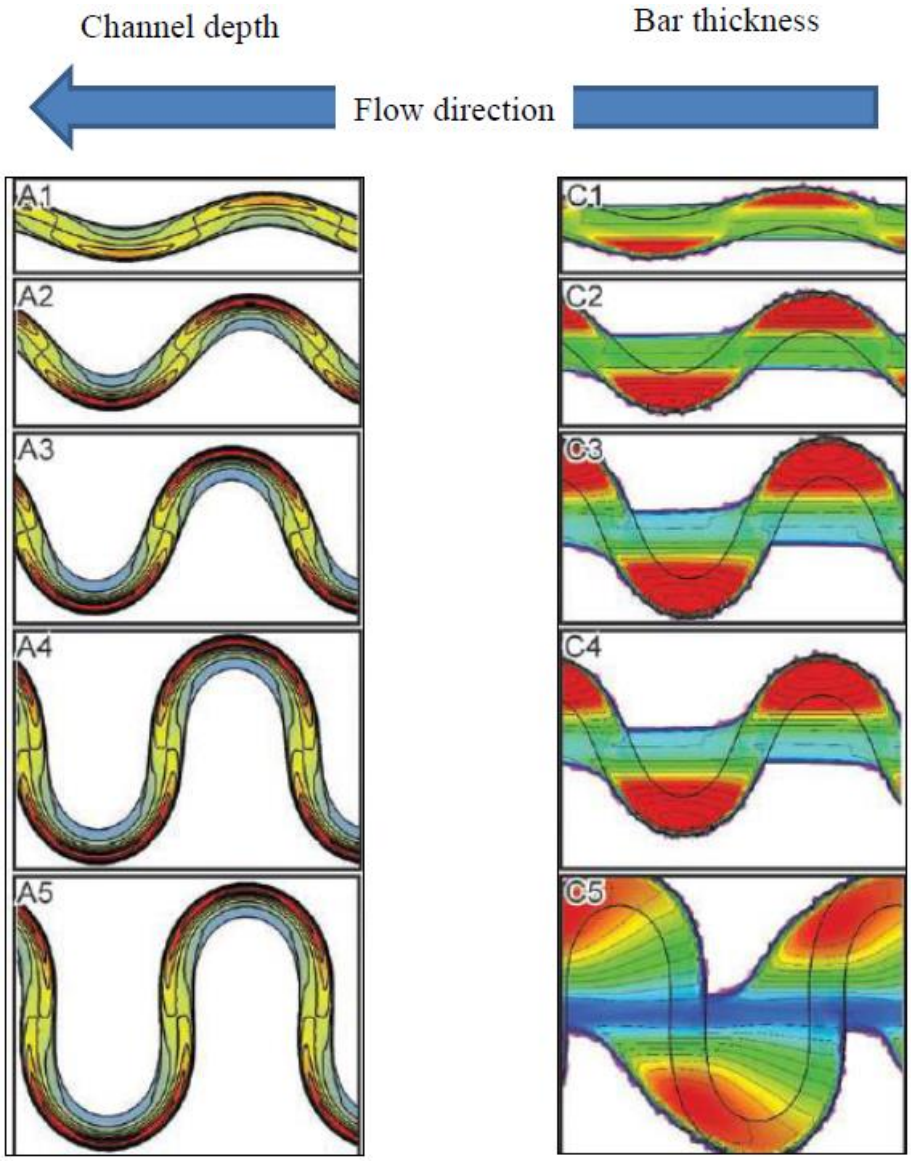

Figure 4.19 Model results shows the gradual change in point bar geometry and bed topography as sinuosity increases with no translation (hotter color): (A) increase in channel thalweg depth at the bend apex; (B) increase in point bar thickness and relief (Willis, 2010).

Paleogeographic reconstructions of a number of channel bends in different segments of the study area (Figs. 4.7, 4.8) indicates that the majority of channels had moderate to high sinuosity with meander bends of various scales. Almost all of the

locations where we found steeply dipping large planar beds, coincide with upstream portion of meander bends. From theoretical modelling, Willis (1989, 2010) (Fig. 4.20) showed that for a tight meander bend during high flow stage, bed accretion in the inner bend is much steeper compared to channels in low flow stage. Therefore, based on the models proposed by Willis (1989, 2010), we interpret these steeply dipping large planar beds as lateral accretion over deep scour upstream of bend apex or channel cutbank.

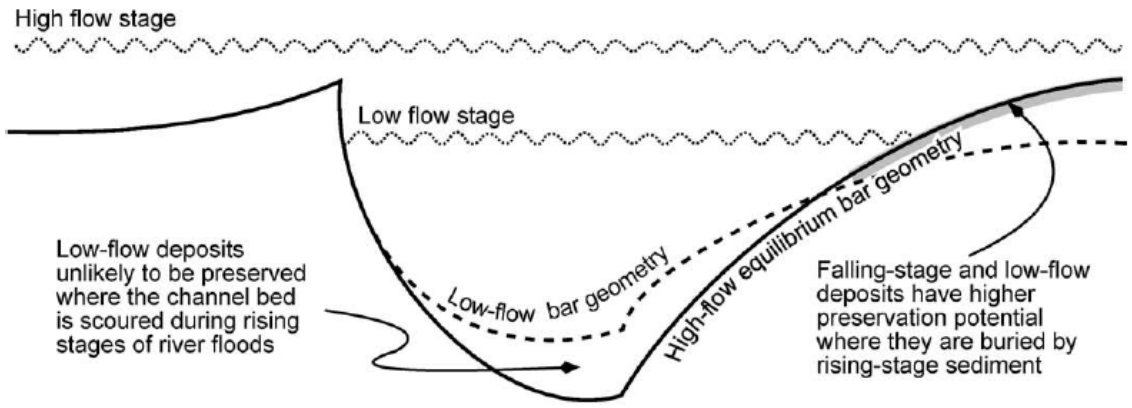

Figure 4.20 Schematic diagram showing the control of flow stages on sediment transport direction, which ultimately shape the bar geometry and architecture. Formation of deep scour by channel thalweg at tight meander bend during rising stages of flood is later filled by steeply dipping large single planner beds during lateral channel migration over the scour in the falling stage.

4.10 Conclusions

1. The large elevation difference between the lowest and highest paleocurrent measurement points from DEM indicates a maximum valley thickness (~ 32 m) larger than the previous estimations from the measured sections. Based on the orientation of planform paleoflows, accretion directions, locations, crosscutting relationships and their positions in the overall stratigraphic interval, the preserved fluvial sequences in the mapped area were divided into three channel

belts. These channel belts were named, stratigraphically from oldest to youngest, Channel-belt A, B, and C.

2. Channel-belt A is the thickest (~16 m) among the three channel belts, flowed towards the N-NE, and was formed by five successive phases of lateral point bar accretion during its migration towards the east. Channel-belt B (~8 m thick), did not produce a large meander bend and had relatively low sinuosity from west to east. Paleogeographic reconstruction of Channel-belt B indicates that it was formed by 15 point and/or alternate bars in three successive phases as it gradually migrated north. Channel-belt C (~ 12 m thick) is subdivided into four different fluvial macroforms. Compared to the Channel-belts A and B, the channels in the Channel-belt C show higher sinuosity with the development of tight meander bends. The paleogeographic reconstructions of the bars in Channel-belt C indicate that the entire point bar complex was primarily formed by several phases of dominantly lateral expansion that caused a gradual increase in channel sinuosity with time.
3. The compound point-bars in Channel belt A are between 420 and 630 m long and between 210 m and 300 m wide. Bars in Channel belt B are relatively smaller with lengths between 270 and 610 m and widths between 130 and 250 m. Bars in Channel-belt C have the lowest length/width ratio, as would be expected with their relatively high channel sinuosity.

4. Three types of architectural facies or macroforms were identified within the large-scale point bars. Type A macroforms, the most common in the study area, formed by progradation of mostly dune-and bar-scale cross sets that form amalgamated compound bars. Type B macroforms were interpreted as unit bars, which consist of moderately to steeply dipping single sets of large foresets. In the study area, unit bars are associated with the infilling of excess local accommodation created by either confluence scours or deep channel thalweg in some cases. Type C macroforms mainly consist of large, steeply-dipping upper flow regime (UFR) planar strata. Preservation of cm-scale internally graded UFR planar beds in the studied outcrops indicates that the UFR sedimentary structures were deposited at high depositional rate. The concurrence of UFR planar beds along the cut bank in the upstream portion of the interpreted point bars indicate that the large UFR planar bed facies in the study area form due to lateral accretion over the deep channel thalweg upstream of the bend apex.
5. By incorporating previously established models for predicting the geometry and paleohydraulics of point-bar deposits into the reconstructed plan-view architecture of the macroforms, we infer that with progressively increasing sinuosity, Type B and Type C macroforms become thicker and steeper in a 2-D vertical section due to the greater variations in point bar geometry.

CHAPTER 5: Summary and Conclusions

This study documents the facies architecture of large valley-scale to intermediate bar- and smallest bed - scale fluvial elements in a compound incised-valley fill in the Cretaceous Ferron Notom Delta in southeastern Utah, U.S.A. Examples of autogenic modification of allogenically formed incised valleys in this paper indicate that both allogenic forcing and autogenic feedback can act simultaneously in fluvial systems. This demands attention to more balanced approach in terms of defining allogenic vs. autogenic mechanisms in ancient and modern fluvial outcrops. Observations of cross-sectional geometries from confluence scour fills also demonstrate that autogenic processes can produce unique patterns that are similar across a large range of spatial and temporal scales.

This study also demonstrates that the backwater effect could be an important control on the valley filling facies in the ancient rock records. This backwater transition in the valley rivers in the Nielson Wash area is marked by a thickening of channel belt deposits tied to channel deepening towards the river mouth, a reduction in average channel belt width that may be related to a reduced rate of lateral migration, an increased proportion of finer grains in channel belt deposits tied to reduced bed material flux, a change in fluvial style from upstream braided to downstream single-thread meandering system, and a vertical upward translation from fluvial to tidal facies in the valley fills. This study shows that the morphological and sedimentological changes, within the

backwater zone can induce a downstream transition of fluvial style from braided to meandering, as suggested by the traditional non-marine sequence stratigraphic models. Therefore, the sinuosity and planform fluvial style can also be affected by the backwater effect independent of base-level change.

This study also reconstructed the paleogeographic evolution of a number of meander belts from extensive plan-view exposures in which their plan-view macroform architectures were preserved. Reconstructions of plan-view architecture reveals that these channel-belts were formed by successive phases of dominantly lateral expansion that caused a gradual increase in channel sinuosity with time. This study also demonstrate that plan-view bedding architectural analysis, can be a useful method to identify various fluvial macroforms. Using plan-view data integrating with cliff exposures, this study classified the architectural facies or macroforms in a large-scale compound bar into three groups. Among them Type C macroforms, which consist of large, steeply-dipping upper flow regime (UFR) planar beds were only found along the cut bank in the upstream portion of the interpreted point bars. This might indicate that the large UFR planar bed facies in the study formed due to lateral accretion over the deep channel thalweg upstream of the bend apex. Incorporating established models, we also infer that with progressively increasing sinuosity, Type B, and Type C macroforms become thicker and steeper in a 2-D vertical section due to the greater variations in point bar geometry.

References

Adams, M.M., and Bhattacharya, J.P., 2005, No change in fluvial style across a sequence boundary, Cretaceous Blackhawk and Castlegate Formations of central Utah, U.S.A.: Journal of Sedimentary Research, v. 75, p. 1038–1051.

Akyuz, I., Warny, S., Famubode, O., and Bhattacharya, J.P., (submitted) Palynology of the Upper Cretaceous (Turonian) Ferron Sandstone Member, Utah, USA: identification of marine flooding surfaces and Milankovitch cycles in subtropical, ever-wet, paralic to non-marine paleoenvironments: Palynology.

Allen, J.R.L., 1965, A review of the origin and characteristics of recent alluvial sediments: Sedimentology, v. 5, 91 p.

Allen, J.R.L., 1974, Sedimentology of the Old Red Sandstone (Siluro-Devonian) in the Clee Hills area, Shropshire, England. Sedimentary Geology, v. 12, p. 73-167.

Allen, J.R.L., 1983, Studies in fluviatile sedimentation: bars, bar-complexes and sandstone sheets (low-sinuosity braided streams) in the Brownstones (L. Devonian), Welsh Borders: Sedimentary Geology, v. 33, p. 237-293.

Allen, J.R.L., 1984. Sedimentary Structures; Their Character and Physical Basis: Amsterdam, Elsevier, 1256 p.

Allen, J. R. L., and Leeder, M. R., 1980, Criteria for the instability of upper‐stage plane beds: Sedimentology, v. 27, p. 209-217.

Allison, M.A., Demas. C.R., Ebersple, B.A., Kleiss, B.A., Little, C.D., Meselhe, E.A., Powell, N.J., Pratt, T.C., Vosburg, B.M., 2012, A water and sediment budget for the Lower Mississippi – Atchafalaya River in flood years 2008 -2010: Implications for

sediment discharge to the oceans and coastal restoration in Louisiana: Journal of Hydrology, v. 432-433, p. 84-97.

Armstrong, R.L., 1968, Sevier orogenic belt in Nevada and Utah: Geological Society of America, Bulletin, v. 79, p. 429–458.

Ashmore, P., and Parker, G., 1983, Confluence scour in coarse braided streams: Water Resources Research, v. 19, p. 392–402.

Ashmore, P.E., Ferguson, R.I., Prestegaard, K., Ashworth, P., and Paola, C., 1992, Secondary flow in coarse grained braided river confluences: Earth Surface Processes and Landforms, v. 17, p. 299-312.

Ashworth, P. J., Best, J. L., Peakall, J., and Lorsong, J. A., 1999, The influence of aggradation rate on braided alluvial architecture: field study and physical scale-modelling of the Ashburton River gravels, Canterbury Plains, New Zealand, *in* Smith, N.D., and Rogers, J., eds, Fluvial Sedimentology VI, International Association of Sedimentologists Special Publication, v. 28, p. 333-346.

Ashworth, P.J., Best, J.L., Roden, J.E., Bristow, C.S., and Klaassen, G.J., 2000, Morphological evolution and dynamics of a large, sand braid-bar, Jamuna River, Bangladesh: Sedimentology, v. 47, p. 533–555.

Ashworth, P.J., Ferguson, R.I., Ashmore, P.E., Paola, C., Powell, D.M., and Prestegaard, K.L., 1992, Measurements in a braided river chute and lobe 2 Sorting of bed load during entrainment, transport and deposition: Water Resources Research, v. 28, p. 1887-1896.

Barton, M.D., Tyler, N., and Angle, E.S., 2004, Facies architecture and permeability structure of valley-fill sandstone bodies, Cretaceous Ferron Sandstone, Utah, *in* Chidsey, T.C., Adams, R.D., and Morris, T.H., eds., Regional to Wellbore Analog for Fluvial–Deltaic Reservoir Modeling, The Ferron of Utah: American Association of Petroleum Geologists, Studies in Geology, v. 50, p. 383–403.

Best, J.L., 1985, Flow dynamics and sediment transport at river channel confluence: Ph.D. Dissertation, Birbeck College, University of London, 393 p.

Best, J.L., 1986, The morphology of river channel confluences: Progress in Physical Geography, v. 10, p. 157–174.

Best, J.L., 1987, Flow dynamics at river confluences: implications for sediment transport and bed morphology, *in* Ethridge, F.G., Flores, R.M., eds., Recent and Ancient Nonmarine Depositional Environments: SEPM, Special Publication 31, p. 27-35.

Best, J.L., 1988, Sediment transport and bed morphology at river channel confluences: Sedimentology, v. 35, p. 481-498.

Best, J.L., Ashworth, P.J., 1997, Scour in large braided rivers and the recognition of sequence stratigraphic boundaries: Nature, v. 387, p. 275-277.

Best, J. L., Ashworth, P.J, Bristow, C.S., Roden, J, 2003, Three-dimensional sedimentary architecture of a large, mid-channel sand braid bar, Jamuna River, Bangladesh: Journal of Sedimentary Research, v. 73, p. 516–530.

Best, J.L., Ashworth, P.J., Sarker, M.H., and Roden, J.E., 2007, The Brahmaputra-Jamuna River, Bangladesh, *in* Gupta, A., ed., Large Rivers: Geomorphology and Management: London, John Wiley & Sons, Ltd., 414 p.

Best, J.L., and Roy, A.G., 1991, Mixing-layer distortion at the confluence of channels of different depth: Nature, v. 350, p. 411-413.

Bhattacharya, J.P., and MacEachern, J.A., 2009, Hyperpycnal rivers and prodeltaic shelves in the Cretaceous Seaway of North America: Journal of Sedimentary Research, v. 79, p. 184-209.

Bhattacharya, J.P., and Tye, R.S., 2004, Searching for modern Ferron analogs and application to subsurface interpretation, *in* Chidsey, T.C., Jr., Adams, R.D., and Morris, T.H., eds., Regional to Wellbore Analog for Fluvial–Deltaic Reservoir Modeling, The Ferron Sandstone of Utah: American Association of Petroleum Geologists, Studies in Geology 50, p. 39–57.

Bhattacharya, J.P., Lawton, T., Copeland, P., Holbrook, J., in press, Chapter 8. Estimation of source area, river paleoslope, paleo- discharge, and sediment budgets of linked deep time depositional systems and implications for hydrocarbon potential and reservoir analogs, *in* Walsh, J.P. et al., Earth Surface Process Connections from Mountains to Margins, Source to Sink, invited paper submitted to Special Issue of Earth-Science Reviews.

Bhattacharyya, P., Bhattacharya, J. P., and Khan, S. D., 2015, Paleo-channel reconstruction and grain size variability in fluvial deposits, Ferron Sandstone, Notom Delta, Hanksville, Utah: Sedimentary Geology, v. 325, p. 17-25.

Biron, P., Roy, A.G., Best, J.L., and Boyer, C.J., 1993, Bed morphology and sedimentology at the confluence of unequal depth channels: Geomorphology, v. 8, p. 115–129.

Blum, M.D., 1992, Climatic and eustatic controls on Gulf coastal plain sedimentation: An example from the late Quaternary of the Colorado River, *in* Armentrout, J. M., and Perkins, R.F., eds., Sequence Stratigraphy as an Exploration Tool: Concepts and Practices in the Gulf Coast, Eleventh Annual Research Conference: Houston, Gulf Coast Section, Society of Economic Paleontologists and Mineralogists Foundation, p. 71-84.

Blum, M.D., Martin, J., Milliken, K., Garvin, M., 2013, Paleovalley systems: Insights from Quaternary analogs and experiments: Earth-Science Reviews, v. 116, p. 128 – 169.

Blum, M.D., and Törnqvist, T.E., 2000, Fluvial responses to climate and sea-level change: A review and a look forward: Sedimentology, v. 47, p. 2–48.

Blum, M.D., and Aslan, A., 2006, Signatures of climate vs. sea-level change within incised valley-fill successions: Quaternary examples from the Texas Gulf Coast: Sedimentary Geology, v. 190, p. 177–211.

Boersma, J.R., Van De Meene, E.A., and Tjalsma, R.C., 1968, Intricated cross-stratification due to interaction of a mega ripple with its lee-side system of backflow ripples (upper-point bar deposits, Lower Rhine): Sedimentology, v. 11, p. 147-162.

Boyd, R., Dalrymple, R.W., and Zaitlin, B.A., 2006, Estuarine and incised valley facies models, *in* Walker, R.G., and Posamentier, H., eds., Facies Models Revisited: SEPM, Special Publication, v. 84, p. 171–235.

Brice, J. C., 1974, Evolution of meander loops: GSA Bulletin, v. 85, p. 581-586.

Bridge, J. S., 1976, Mathematical model and FORTRAN IV program to predict flow, bed topography and grain size in open-channel bends. Computers & Geosciences, v. 2(4), p. 407-416.

Bridge, J.S., 1977, Flow, bed topography, grain size and sedimentary structure in open channel bends: A three-dimensional model: Earth Surface Processes, v. 2, p. 401-416.

Bridge, J.S., 1993a, Description and interpretation of fluvial deposits: a critical perspective: Sedimentology, v. 40, p. 801–810.

Bridge, J.S., 1993b, The interaction between channel geometry, water flow, sediment transport and deposition in braided rivers, *in* Best, J.L., and Bristow, C.S., eds., Braided Rivers: Geological Society of London, Special Publication, v. 75, p. 13–71.

Bridge, J.S., 2003, Rivers and Floodplains: Oxford, U.K.: Blackwell Science, 491 p.

Bridge, J.S., 2006, Fluvial facies models: recent developments, *in* Posamentier, H.W., and Walker, R.G., eds., Facies Models Revisited, Society of Economic Petrology and Mineralogy, Special Publication, v. 84, p. 83-168.

Bridge, J. S., 2009, Rivers and Floodplains: Forms, Processes, and Sedimentary Record: John Wiley & Sons, 504 p.

Bridge, J. S., Alexander, J. A. N., Collier, R. E. L., Gawthorpe, R. L., and Jarvis, J., 1995, Ground-penetrating radar and coring used to study the large-scale structure of point-bar deposits in three dimensions: Sedimentology, 42(6), 839-852.

Bridge, J., and Best, J.L., 1997, Preservation of planar laminae due to migration of low-relief bed waves over aggrading upper-stage plane beds: comparison of experimental data with theory: Sedimentology, v. 44, p. 253-262.

Bridge, J. S., and Best, J. L., 1988, Flow, sediment transport and bedform dynamics over the transition from dunes to upper-stage plane beds: implications for the formation of planar laminae. Sedimentology, v. 35, p. 753-763.

Bridge, J., Collier, R., and Alexander, J. A. N., 1998, Large-scale structure of Calamus River deposits (Nebraska, USA) revealed using ground-penetrating radar: Sedimentology, 45(6), 977-986.

Bridge, J.S., and Demicco, R.V., 2008, Earth Surface Processes, Landforms and Sediment Deposits: Cambridge, UK, Cambridge University Press, 392 p.

Bridge, J. S., and Jarvis, J., 1982, The dynamics of a river bend: a study in flow and sedimentary processes: Sedimentology, 29(4), 499-541.

Bridge, J.S., and Lunt, I.A., 2006, Depositional models of braided rivers, *in* Sambrook-Smith, G.H., Best, J.L., Bristow, C.S., and Petts, G.E., eds., Braided Rivers: Process, Deposits, Ecology and Management: International Association of Sedimentologists, Special Publication 36, p. 11–50.

Bridge, J.S., and Mackey, S.D., 1993, A theoretical study of fluvial sandstone body dimensions, *in* S.S., Flint and I.D., Bryant, eds., Geological Modeling of Hydrocarbon Reservoirs: International Association of Sedimentologists Special Publication, v. 15, p. 213–236.

Bridge, J.S., and Tye, R.S., 2000, Interpreting the dimensions of ancient fluvial channel

bars, channels, and channel belts from wireline-logs and cores: American Association of Petroleum Geologists, Bulletin, v. 84, p. 1205–1228.

Bristow, C. S., 1993a, Sedimentary structures exposed in bar tops in the Brahmaputra River, Bangladesh: Geological Society, London, Special Publications, v.75.

Bristow, C.S., 1993b, Sedimentology of the Rough Rock: a Carboniferous braided river sheet sandstone in northern England, *in* Best, J.L., and Bristow, C.S., eds., Braided Rivers: Geological Society of London, Special Publication 75, p. 291–304.

Bristow, C.S., and Best, J.L., 1993, Braided rivers: Perspectives and problems, *in* Best, J.L., and Bristow, C.S., eds., Braided Rivers: Geological Society of London, Special Publication, v. 75, p. 1–11.

Bristow, C. S., J. L. Best, and A. G. Roy, 1993, Morphology and facies models of channel confluences, *in* Marzo, M., Puigdefèbregas (eds.), Alluvial Sedimentation, Special Publication of the International Association of Sedimentologists, v. 17, p. 91-100.

Brookes, I.A., 2003. Palaeofluvial estimates from exhumed meander scrolls, Taref Formation (Turonian), Dakhla Region, Western Desert, Egypt. Cretaceous Research, v. 24, p. 97–104.

Cant, D.J. and Walker, R.G., 1976, Development of a braided-fluvial facies model for the Devonian Battery Point Formation, Quebec: Canadian Journal of Earth Science, v. 13, p. 102–119.

Catuneanu, O., 2007, 9(b). Sequence stratigraphic context of microbial mat features: http://www.indiana.edu/~sepm04/PDF/Catuneau-Chapter9b.pdf

Cheel, R.J., 1990, Horizontal lamination and the sequence of bed phases and stratification under upper-flow-regime conditions: Sedimentology, v. 37, p. 517–529.

Chen, D., and Duan, J. G., 2006, Modeling width adjustment in meandering channels: Journal of Hydrology, v. 321, p. 59-76.

Corbeanu, R.M., Wizevich, M.C., Bhattacharya, J.P., Zeng, X., and McMechan, G.A., 2004, Three-dimensional architecture of ancient lower delta-plain point bars using ground penetrating-radar, Cretaceous Ferron Sandstone, Utah, *in* Chidsey, T.C., Adams, R.D., and Morris, T.H., eds, The Fluvial-deltaic Ferron Sandstone: Regional-to-Wellbore-scale Outcrop Analog Studies and Applications to Reservoir Modeling, AAPG Studies in Geology 50, p. 427-449.

Dade, W. B., and Friend, P. F., 1998, Grain size, sediment transport regime, and channel slope in alluvial rivers: Journal of Geology, v. 106, p. 661 – 675.

Dalrymple, R.W., Boyd, R., and Zaitlin, B.A., 1994, Incised-Valley Systems: Origin and Sedimentary Sequences: SEPM, Special Publication, v. 51, 381 p.

Deb, M., Das, D. and Uddin, M., 2012, Evaluation of meandering characteristics using RS and GIS of Manu River: Journal of Water Resource and Protection, v. 4, p. 163–171.

DeCelles, Peter G., 2004, Late Jurassic to Eocene evolution of the Cordilleran thrust belt and foreland basin system, western USA: American Journal of Science, v. 304, p.105-168.

De Serres, B., Roy, A.G, Biron, P.M., and Best, J.L., 1999, Three-dimensional structure of flow at a confluence of river channels with discordant beds: Geomorphology, v. 26, p. 313–335.

Dickinson, William R., 2004, Evolution of the North American cordillera: Annual Review Earth Planet Science, v. 32, p. 13-45.

Dietrich, W.E., Smith, J.D., and Dunne, T., 1979, Flow and sediment transport in a sand bedded meander: The Journal of Geology, v. 78, p.305-315.

Dietrich, W.E., and Smith, J.D., 1983, Influence of the point bar on flow through curved channels: Water Resources Research, v. 19, p. 1173-1192.

Edwards, M. B., Eriksson, K. A., and Kier, R. S.,1983, Paleochannel geometry and flow patterns determined from exhumed Permian point bars in north-central Texas. Journal of Sedimentary Research, v. 53, p. 1261-1270.

Eilertsen, R.S., and Hansen, L., 2008, Morphology of river bed scours on a delta plain revealed by interferometric sonar: Geomorphology, v. 94, p. 58–68.

Ethridge, F. G., & Schumm, S. A.,1977, Reconstructing paleochannel morphologic and flow characteristics: methodology, limitations, and assessment, *in* Miall, A.D., ed, Fluvial Sedimentology, p. 703-721.

Famubode, O., and Bhattacharya, J.P, (in review), Sequence stratigraphic analysis of the youngest non-marine sequence in the Cretaceous Ferron-Notom Delta, south central Utah, USA: Journal of Sedimentary Research.

Feldman, H.R., Franseen, E.K., Joeckel, R.M., and Heckel, P.H., 2005, Impact of longer-term modest climate shifts on architecture of high-frequency sequences

(cyclothems), Pennsylvanian of mid-continent U.S.A.: Journal of Sedimentary Research, v. 75, p. 350–368.

Fielding, C.R., 2006, Upper flow regime sheets, lenses and scour fills: extending the range of architectural elements for fluvial sediment bodies: Sedimentary Geology, v. 190, p. 227-240.

Fielding, C.R., 2007, Sedimentology and stratigraphy of large river deposits: recognition in the ancient record, and distinction from incised valley fills, *in* Gupta, A., ed., Large Rivers: Geomorphology and Management: John Wiley & Sons, Ltd, Chichester, p. 97–114.

Fielding, C.R., 2010, Planform and facies variability in asymmetric deltas: facies analysis and depositional architecture of the Turonian Ferron Sandstone in the western Henry Mountains, south-central Utah, U.S.A.: Journal of Sedimentary Research, v. 80, p. 455–479.

Fielding, Christopher R., 2015, Anatomy of falling-stage deltas in the Turonian Ferron Sandstone of the western Henry Mountains Syncline, Utah: Growth faults, slope failures and mass transport complexes: Sedimentology, v. 62, p. 1-26.

Fisk, H.N., 1947, Fine Grained Alluvial Deposits and Their Effects on Mississippi River Activity: Mississippi River Commission, Vicksburg, MS, v. 1 and 2.

Flood Action Plan 24, Delft Hydraulics and DHI, 1996a, FAP24 River Survey Project: Final Report, Annex 5: Morphological Characteristics (prepared for FPCO), Dhaka, Bangladesh.

Flood Action Plan 24, Delft Hydraulics, DHI and Leeds University, 1996b, FAP24 River Survey Project: Special Report 9, Bedform and bar dynamics in the main rivers of Bangladesh (prepared for FPCO), Dhaka, Bangladesh, 107 p.

Foix, N., Allard, J.O., Paredes, J.M., Giacosa, R.E., 2012. Fluvial styles, palaeohydrology and modern analogues of an exhumed, Cretaceous fluvial system: Cerro Barcino Formation, Cañadón Asfalto Basin, Argentina. Cretaceous Research 34, 298–307.

Frothingham, K.M., and Rhoads, B.L., 2003, Three-dimensional flow structure and channel change in an asymmetrical compound meander loop, Embarras River, Illinois: Earth Surface Processes and Landforms, v. 28, p. 625-644.

Fustic, M., Hubbard, S.M., Spencer, R., Smith, D.G., Leckie, D.A., Bennett, B., Larter, S., 2012. Recognition of down-valley translation in tidally influenced meandering fluvial deposits, Athabasca Oil Sands (Cretaceous), Alberta, Canda. Marine and Petroleum Geology, v. 29, p. 219-232

Galloway, W.E., and Hobday, D.K., 1996, Terrigenous Clastic Depositional Systems: Berlin, Springer, 489 p.

Gardner, Michael, H., Timothy A. Cross, and Mark Levorsen, 2004, Stacking Patterns, Sediment Volume Partitioning, and Facies Differentiation in Shallow-Marine and Coastal-Plain Strata of the Cretaceous Ferron Sandstone, Utah, *in* Regional to Wellbore Analog for Fluvial-Deltaic Reservoir Modeling: The Ferron Sandstone of Utah : American Association of Petroleum Geologists Studies in Geology, v. 50, p. 94-124.

Garrison Jr., James, R., and Van den Bergh, T. C. V., 2004, High-resolution depositional sequence stratigraphy of the upper Ferron Sandstone Last Chance Delta: an application of coal-zone stratigraphy, *in* Regional to Wellbore Analog for Fluvial-Deltaic Reservoir Modeling: The Ferron Sandstone of Utah: American Association of Petroleum Geologists Studies in Geology, v. 50, p. 125-192.

Hartkamp-Bakker, C.A., and Donselaar, M.E., 1993, Permeability patterns in point bar deposits: Tertiary Loranca Basin, central Spain, *in* Flint, S.S., and Bryant, I.D., eds., The Geological Modelling of Hydrocarbon Reservoirs and Outcrop Analogs: International Association of Sedimentologists Special Publication 15, 157 – 168.

Hickin, E. J., 1974, The development of meanders in natural river-channels. American Journal of Science, 274(4), 414-442.

Hilton, B.D., 2013, 3D Allostratigraphic Mapping and Facies Heterogeneity of a Compound, Tributary Incised Valley System, Turonian Ferron Sandstone, Notom Delta, South-Central Utah, Master's Thesis: University of Houston, 136 p.

Hirst, J.P.P., Blackstock, C.R. and Tyson,T., 1993, Stochastic modelling of fluvial sandstone bodies, *in* Bryant, I.D., and Flint, S.S., eds., The Geological Modelling of Hydrocarbon Reservoirs and Outcrop Analogues: International Association of Sedimentologists, Special Publication 15, p. 237–252.

Holbrook, J.M., 2001, Origin, genetic interrelationships, and stratigraphy over the continuum of fluvial channel-form bounding surfaces: an illustration from middle Cretaceous strata, southeastern Colorado: Sedimentary Geology, v. 124, p. 202–246.

Holbrook, J., Scott, R.W., and Oboh-Ikuenobe, F.E., 2006, Base-level buffers and buttresses: A model for upstream versus downstream control on fluvial geometry and architecture within sequences: Journal of Sedimentary Research, v. 76, p. 162–174.

Holbrook, J., Wanas, H., 2014, A fulcrum approach to assessing source-to-sink mass balance using channel paleohydrologic paramaters derivable from common fluvial data sets with an example from the Cretaceous of Egypt: Journal of Sedimentary Research, v. 84, p. 349-372.

Hudson, P.F., Kesel, R.H., 2000, Channel migration and meander-bend curvature in the lower Mississippi River prior to major human modification: Geology, v. 28, p. 531 – 534.

Ielpi, A., and Ghinassi, M., 2014, Planform architecture, stratigraphic signature and morphodynamics of an exhumed Jurassic meander plain (Scalby Formation, Yorkshire, UK): Sedimentology, v. 61, p. 1923-1960.

Jackson, R.G., 1976, Depositional model of point bars in the lower Wabash River: Journal of Sedimentary Petrology, v. 46, p. 579–594.

Jerolmack, D.J., 2009, Conceptual framework for assessing the response of delta channel networks to Holocene sea level rise: Quaternary Science Reviews, v. 28, p. 1786–1800,

Jerolmack, D. J., and D. Mohrig, 2007, Conditions for branching in depositional rivers: Geology, v. 35, p. 463–466.

Jin, D., and Schumm, S.A., 1987, A new technique for modeling river morphology, *in* Gardiner, V., ed., International Geomorphology, Part I: Chichester, U.K., John Wiley and Sons, p. 681–690.

Klaassen, G.J., and Vermeer, K., 1988, Confluence scour in a large braided river with fine bed material: Proceedings of the International Conference on Fluvial Hydraulics, Budapest, Hungary, International Association of Hudraulic Research, Budapest, p. 395–408.

Klaassen, G.J., Vermeer, K., and Uddin, N., 1988, Sedimentological processes in the Jamuna (Lower Brahmaputra) river, Bangladesh: Proceedings of the International Conference on Fluvial Hydraulics, Budapest, Hungary, p. 381–394.

Knighton, D., 1998, Fluvial Forms and Processes: A New Perspective: London: Hodder Arnold, p. 167.

Korus, J.T., Kvale, E.P., Eriksson, K.A., and Joeckel, R.M., 2008, Compound paleovalley fills in the Lower Pennsylvanian New River Formation, West Virginia, USA: Sedimentary Geology, v. 208, p. 15–26.

Lamb, M. P., and D. Mohrig, 2009, Do hyperpycnal-flow deposits record river-flood dynamics?: Geology, v. 37, p. 1067–1070.

Lamb, M. P., J. A. Nittrouer, D. Mohrig, and J. Shaw, 2012, Backwater and river-plume controls on scour upstream of river mouths: Implications for fluvio-deltaic morphodynamics: Journal of Geophysical Research: Earth Surface, v. 117.

Lane, S. N., James, T. D., Pritchard, H., and Saunders, M., 2003, Photogrammetric and laser altimetric reconstruction of water levels for extreme flood event analysis: The Photogrammetric Record, v. 18104, p. 293-307.

Lane, S. N., Chandler, J. H., and Porfiri, K., 2001, Monitoring river channel and flume surfaces with digital photogrammetry: Journal of Hydraulic Engineering, v. 127, p. 871-877.

Leclair, S. F., and Bridge, J. S., 2001, Quantitative interpretation of sedimentary structures formed by river dunes. Journal of Sedimentary Research, v .71, p. 713-716.

Li, W., Bhattacharya, J.P., and Campbell, C., 2010, Temporal evolution of fluvial style in a compound incised-valley fill, Ferron "Notom Delta," Henry Mountains region, Utah (USA): Journal of Sedimentary Research, v. 80, p. 529-549.

Li, W., Bhattacharya, J.P., Zhu, Y., 2011, Architecture of a forced regressive systems tract in the Turonian Ferron “Notom Delta”, southern Utah, U.S.A.: Marine and Petroleum Geology, v. 28, p. 1517 – 1529.

Li, W., Bhattacharya, J.P., Zhu, Y., Garza, D., and Blankenship, E., 2011, Evaluating delta asymmetry using three-dimensional facies architecture and ichnological analysis, Ferron ‘Notom Delta’, Capital Reef, Utah, USA: Sedimentology, v. 58, p. 478-507.

Li, Y., and Bhattacharya, J.P., 2013, Facies-architecture study of a stepped, forced regressive compound incised valley in the Ferron Notom Delta, Southern Central Utah, USA: Journal of Sedimentary Research, v. 83, p. 206-225.

Lunt, I.A., and Bridge, J.S., 2004, Evolution and deposits of a gravelly braid bar, Sagavanirktok River, Alaska: Sedimentology, v. 51, p. 415-432.

Lunt, I. A., Bridge, J. S., and Tye, R. S., 2004, A quantitative, three-dimensional depositional model of gravelly braided rivers: Sedimentology, v. 51, p. 377-414.

Mackin, J. H., 1948, Concept of the graded river: Geological Society of America Bulletin, v. 59, p. 463–512.

Martin, H.K., and Bhattacharya, J.P., 2015, Scaling relationships of rib-and-furrow structures in modern and ancient dunes and bars in rivers: AAPG Datapages/Search and Discovery Article #90216.

Martinius, A. W., Geel, C. R., and Arribas, J., 2002, Lithofacies characterization of fluvial sandstones from outcrop gamma-ray logs (Loranca Basin, Spain): The influence of provenance. Petroleum Geoscience, v. 8, p. 51-62.

Martinsen, O.J., 1994, Evolution of an incised-valley fill, the Pine Ridge Sandstone of southeastern Wyoming, USA: Systematic sedimentary response to relative sea-level change, *in* Dalrymple, R.W., Boyd, R., and Zaitlin, B.A., eds., Incised-Valley Systems, Origin and Sedimentary Sequences: SEPM Special Publication v. 51, p. 107 - 126.

McGowen, J.H., and Garner, L.E., 1970, Physiographic features and stratification types of coarse-grained pointbars: Modern and ancient examples 1: Sedimentology, v. 14, p. 77-111.

Miall, A.D., 1985, Architectural-element analysis: A new method of facies analysis applied to fluvial deposits: Earth-Science Reviews, v. 22, p. 261-308.

Miall, A.D., 1988, Reservoir heterogeneities in fluvial sandstone: lessons from outcrop studies: American Association of Petroleum Geologists, Bulletin, v. 72, p. 682–687.

Miall, A. D., 1994, Reconstructing fluvial macroform architecture from two-dimensional outcrops: Examples from the Castlegate Sandstone, Book Cliffs, Utah. Journal of Sedimentary Research, v. 64, p. 146-158.

Miall, A. D., 1996, The Geology of Fluvial Deposits: Berlín: Springer Verlag, 582 p.

Miall, A.D., and Jones, B.G., 2003, Fluvial architecture of the Hawkesbury Sandstone (Triassic), near Sydney, Australia: Journal of Sedimentary Research, v. 73, p. 531–545.

Mosley, M.P., 1976, An experimental study of channel confluences: Journal of Geology, v. 84, p. 535–562.

Musial, G., Reynaud, J., Gingras, M.K., Fenies, H., 2011. Subsurface and outcrop characterization of large tidally influenced point bars of the Cetaceous McMurray Formation (Alberta, Canada). Sedimentary Geology, v. 17, 17 p.

Nanson, G.C., 1980. Point bar and floodplain formation of the meandering Beatton River, northeastern British Columbia, Canada. Sedimentology v. 27, p. 3–29.

Nittrouer, J.A., Mohrig, D., and Allison, M.A., 2011a, Punctuated transport of bed materials in the lowermost Mississippi River: Journal of Geophysical Research: Earth Surface (2003-2012), v. 116.

Nittrouer, J.A., Mohrig, D., and Allison, M.A., 2011b, The lowermost Mississippi River: A mixed bedrock-alluvial channel: Sedimentology, v. 58, p. 1914-1934.

Nittrouer, J.A., Shaw, J., Lamb, M.P., Mohrig, D., 2012, Spatial and temporal needs for water –flow velocity and bed-material sediment transport in the lower Mississippi River: Geological Society of American Bulletin, v. 124, p. 400 – 414.

Paola, C., and Mohrig, D., 1996, Palaeohydraulics revisited: palaeoslope estimation in coarse-grained braided rivers: Basin Research, v. 8, p. 243–254.

Paola, C., Wiele, S. M., and Reinhart, M. A., 1989, Upper−regime parallel lamination as the result of turbulent sediment transport and low−amplitude bed forms: Sedimentology, v. 36, p. 47-59.

Parker, G., 1978, Self-formed straight rivers with equilibrium banks and mobile bed. Part 1. The sand-silt river: Journal of Fluid Mechanics, v. 89, p. 109-125.

Parker, G., 2004, 1D Sediment Transport Morphodynamics with Applications to Rivers and Turbidity Currents: E-book, Minneapolis, St. Anthony Falls Laboratory, University of Minnesota, http://vtchl.uiuc.edu/people/parkerg/morphodynamics_e-book.htm.

Parker, G. and Cm, Y., 1998, The arrested gravel front: Stable gravel-sand transitions in rivers. Part 1: Simplified analytical solutions: Journal Hydraulic Research, v. 36(1), p. 75-100.

Parker, G., J. A. Nittrouer, D. C. Mohrig, M. A. Allison, W. E. Dietrich, and V. R. Voller, 2009, Modeling the morphodynamics of the lower Mississippi River as a quasi-bedrock river, Eos Trans: AGU, v. 90(52), Fall Meet. Suppl., Abstract EP32A-01.

Peakall, J., Ashworth, P. J., and Best, J. L., 2007, Meander-bend evolution, alluvial architecture, and the role of cohesion in sinuous river channels: A flume study. Journal of Sedimentary Research, v. 77, p. 197-212.

Peterson, F., and Ryder, R.T., 1975, Cretaceous rocks in the Henry Mountains region, Utah and their relation to neighboring regions, *in* J. E. Fassett and S. A. Wengerd, eds., Canyonlands Country: Four Corners Geological Society Guidebook, 8th Field Conference, p. 167-189.

Plink-Björklund, P., 2015, Morphodynamics of rivers strongly affected by monsoon precipitation: Review of depositional style and forcing factors: Sedimentary Geology, v. 323, p. 110-147.

Posamentier, H.W., and Vail, P.R., 1988, Eustatic controls on clastic deposition II—sequence and systems tract models, *in* Wilgus, C.K., Hasting, B.S., Kendall, C.G., Posamentier, H. W., Ross, C.A., and Van Wagoner, J.C., eds., Sea level changes – an integrated approach: Society of Economic Paleontologists and Mineralogists: Special Publications, v. 42, p. 125 – 154.

Pranter, M. J., Ellison, A. I., Cole, R. D., and Patterson, P. E., 2007, Analysis and modeling of intermediate-scale reservoir heterogeneity based on a fluvial point-bar outcrop analog, Williams Fork Formation, Piceance Basin, Colorado: American Association of Petroleum Geologists Bulletin, v. 91, p. 1025-1051.

Reijenstein, H.M., H.W. Posamentier, and J.P. Bhattacharya, 2011, Seismic geomorphology and high-resolution seismic stratigraphy of inner-shelf fluvial,

estuarine, deltaic, and marine sequences, Gulf of Thailand: American Association of Petroleum Geologists Bulletin, v. 95, p. 1959-1990.

Reesink, A.J.H. and Bridge, J.S., 2007, Influence of superimposed bedforms and flow unsteadiness on formation of cross strata in dunes and unit bars: Sedimentary Geology, v. 202, p. 281-296.

Roden, J.E., 1998, Sedimentology and Dynamics of Mega-Sand Dunes, Jamuna River, Bangladesh: PhD Dissertation, University of Leeds, 310 p.

Rubin, D.M., 1987, Cross-Bedding, Bedforms, and Paleocurrents: SEPM Concepts in Sedimentology and Paleontology, v. 1, 187 p.

Rubin, D.M., and McCulloch, D.S., 1980, Single and superimposed bedforms: a synthesis of San Francisco Bay and flume observations: Sedimentary Geology, v. 26, p. 207–231.

Rust, B. R., 1984, Proximal braidplain deposits in the Middle Devonian Malbaie formation of eastern Gaspe, Quebec, Canada: Sedimentology, v. 31, p. 675-695.

Salter, T., 1993, Fluvial scour and incision: models for their influence on the development of realistic reservoir geometries, *in* North, C.P., and Prosser, D.J., eds., Characterization of Fluvial and Aeolian Reservoirs: Geological Society of London, Special Publication 73, p. 33–51.

Sambrook-Smith, G.H., Ashworth, P.J., Best, J.L., Woodward, J., and Simpson, C.J., 2005, The morphology and facies of sandy braided rivers: some considerations of scale invariance, *in* Blum, M.D., Marriott, S.B., and Leclair, S., eds., Fluvial

Sedimentology VII, v. 35: International Association of Sedimentologists, Special Publication, p. 145–158.

Sambrook-Smith, G.H., Ashworth, P.J., Best, J.L., Woodward, J., and Simpson, C.J., 2006, The sedimentology and alluvial architecture of the sandy braided South Saskatchewan River, Canada: Sedimentology, v. 53, p. 413-434.

Sarker, M.H., 1996, Morphological Processes in the Jamuna River: MSc thesis, International Institute for Hydraulic and Environmental Engineering, Delft, The Netherlands, 175p.

Schumm, S. A., Mosley, M. P., and Weaver, W. E., 1987, Experimental Fluvial Geomorphology: New York, Wiley, 413 p.

Shanley, K.W., McCabe, P.J., and Hettinger, R.D., 1992, Tidal influence in Cretaceous fluvial strata from Utah, U.S.A.: A key to sequence stratigraphic interpretation: Sedimentology, v. 39, p. 905–930.

Shanley, K.W., and McCabe, P.J., 1994, Perspectives on the sequence stratigraphy of continental strata: American Association of Petroleum Geologists, Bulletin, v. 78, p. 544–568.

Smith, G. H. S., Ashworth, P. J., Best, J. L., Lunt, I. A., Orfeo, O., & Parsons, D. R., 2009, The sedimentology and alluvial architecture of a large braid bar, Río Paraná, Argentina: Journal of Sedimentary Research, v. 79, p. 629-642.

Smith, R.M.H., 1987. Morphology and depositional history of exhumed Permian point bars in the southwestern Karoo, South Africa: Journal of Sedimentary Research, v. 57, p. 19–29.

Smith, C. E., 1998, Modeling high sinuosity meanders in a small flume: Geomorphology, v. 25, p. 19-30.

Smith, D.G., Hubbard, S.M., Leckie, D.A. and Fustic, M., 2009, Counter point bar deposits: lithofacies and reservoir significance in the meandering modern Peace River and ancient McMurray Formation, Alberta, Canada: Sedimentology, v. 56, p. 1655–1669.

Stojic, M., Chandler, J., Ashmore, P., and Luce, J., 1998, The assessment of sediment transport rates by automated digital photogrammetry: Photogrammetric Engineering and Remote Sensing, v. 64, p. 387-395.

Ullah, M.S, Bhattacharya, J.P., Interpreting backwater effects on fluvial style and architecture in a high-gradient compound incised-valley deposit: Examples from the Cretaceous Ferron Notom Delta, Southeastern Utah, USA (in preparation).

Ullah, M.S., Bhattacharya, J.P., and Dupr/e, W.R, 2015, Confluence scours versus incised valleys: examples from the Cretaceous Ferron Notom Delta, South-East Utah, USA. Journal of Sedimentary Research, v. 86 p. 445-458.

Ullah, M.S., Bhattacharya, J.P., Okyay, U., Wu, C., and Browning, B., (in preparation), Reconstructing 2-D fluvial macroform architecture form plan-view data: Examples from the Cretaceous Ferron Sandstone, Notom Delta, Southeastern Utah, U.S.A.

Ullah, M.S., Saylor, J., Bhattacharya, J.P., Fluvial slope calculations from statistical characterization of grain-size distributions (GSDs) in sandy fluvial deposits at a paleo-valley base (in preparation).

Van Dijk, W. M., Lageweg, W. I., and Kleinhans, M. G., 2012, Experimental meandering river with chute cutoffs: Journal of Geophysical Research, v. 117, F03023.

Van Wagoner, J.C., 1995, Sequence stratigraphy and marine to nonmarine facies architecture of foreland basin strata, Book Cliffs, Utah, U.S.A., *in* Van Wagoner, J.C., and Bertram, G.T., eds., Sequence Stratigraphy of Foreland Basin Deposits: American Association of Petroleum Geologists, Memoir 64, p. 137–224.

Van Wagoner, J.C., Mitchum, R.M., Campion, K.M., and Rahmanian, V.D., 1990, Siliciclastic Sequence Stratigraphy in Well-Logs, Cores, and Outcrop: American Association of Petroleum Geologists, Methods in Exploration Series 7, 55 p.

Wang, J., 2013, Plan-view Paleochannel Reconstruction and Paleocurrent Fields of Meander-belts, Cretaceous Ferron Sandstone, Henry Mountains Region: Master's Thesis, University of Houston, p .58.

Williams, G.P., 1986. River meanders and channel size. Journal of Hydrology, v. 88, p. 147–164.

Willis, B.J., 1989, Paleo-channel reconstructions from point-bar deposits: A three-dimensional perspective: Sedimentology, v. 36, p. 757-766.

Willis, B.J., 1993a, Ancient river systems in the Himalayan foredeep, Chinji Village area, northern Pakistan: Sedimentary Geology, v. 88, p. 1-76.

Willis, B.J., 1997, Architecture of fluvial-dominated valley-fill deposits in the Cretaceous Fall River Formation: Sedimentology, v. 44, p. 735–757.

Willis, B.J., and Tang, H., 2010, Three-dimensional connectivity of point-bar deposits: Journal of Sedimentary Research, v. 80, p. 440-454.

Wright, V.P., and Marriott, S.B., 1993, The sequence stratigraphy of fluvial depositional systems: the role of floodplain sediment storage: Sedimentary Geology, v. 86, p. 203–210.

Wright, S.A. and Parker, G., 2004, Flow resistance and suspended load in sand-bed rivers: simplified stratification model: Journal of Hydraulic Engineering, v. 130, p. 796-805.

Wu, C., Bhattacharya, J., and Ullah, S.M., 2015, Paleohydrology and 3D facies architecture of ancient point bars, Ferron Sandstone, Notom Delta, south-central Utah, USA: Journal of Sedimentary Research, v. 85, p. 399–418.

Wu, C., Ullah, M.S, Lu, J., and Bhattacharya, J.P., (submitted) Formation of point bars through rising and falling flood stages: examples from Cretaceous Ferron Sandstone, south-central Utah, U.S.A.: Sedimentology, *in revision*.

Zaitlin, B.A., Dalrymple, R.W., and Boyd, R., 1994, The stratigraphic organization of incised-valley systems associated with relative sea-level change, *in* Dalrymple, R.W., Boyd, R., and Zaitlin, B.A., eds., Incised-Valley Systems, Origin and Sedimentary Sequences: SEPM Special Publication 51, p. 45–60.

Zhu, Y., Bhattacharya, J.P., Li, W., Lapen, T.J., Jicha, B.R., and Singer, B.S., 2012, Milankovitch-scale sequence stratigraphy and stepped forced regressions of the Turonian Ferron Notom Deltaic Complex, South-Central Utah, U.S.A.: Journal of Sedimentary Research, v. 82, p. 723-746.

Appendix

Slope Calculations

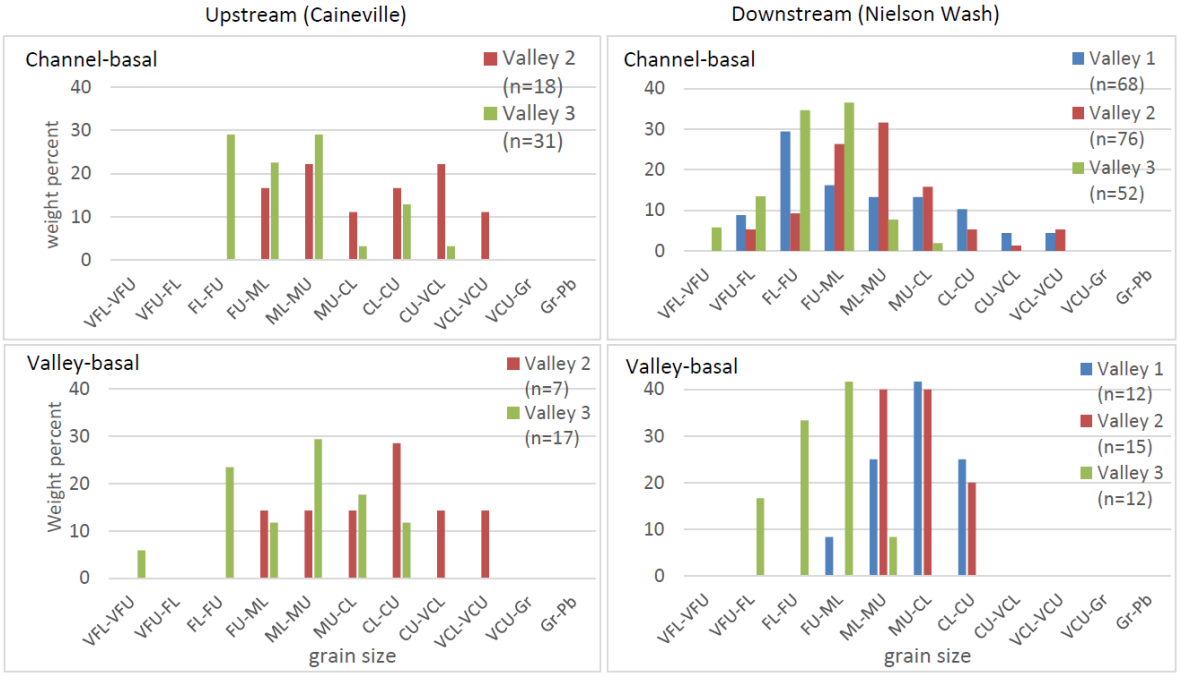

Fig. 1. Histogram of D_{50} grain-sizes of fluvial sandstones at the base of the channels in Valley 1, Valley 2 and Valley 3 (top) and at the base of the valley (bottom).

Table 1: Comparison of average median (D50) grain sizes of the valley-basal and channel basal cross sets among the three valleys in the upstream Caineville and downstream Nielson Wash area.

	Upstream (Caineville)		***Downstream (Nielson Wash)***	
Sample Type	Total Samples	Avg. D50 size (um)	Total Samples	Avg. D50 size (um)
Channel-basal				
Valley 1	–	–	68	559
Valley 2	18	951	76	571
Valley 3	31	494	52	298
Valley-basal				
Valley 1	–	–	12	595
Valley 2	7	883	15	616
Valley 3	17	463	12	273

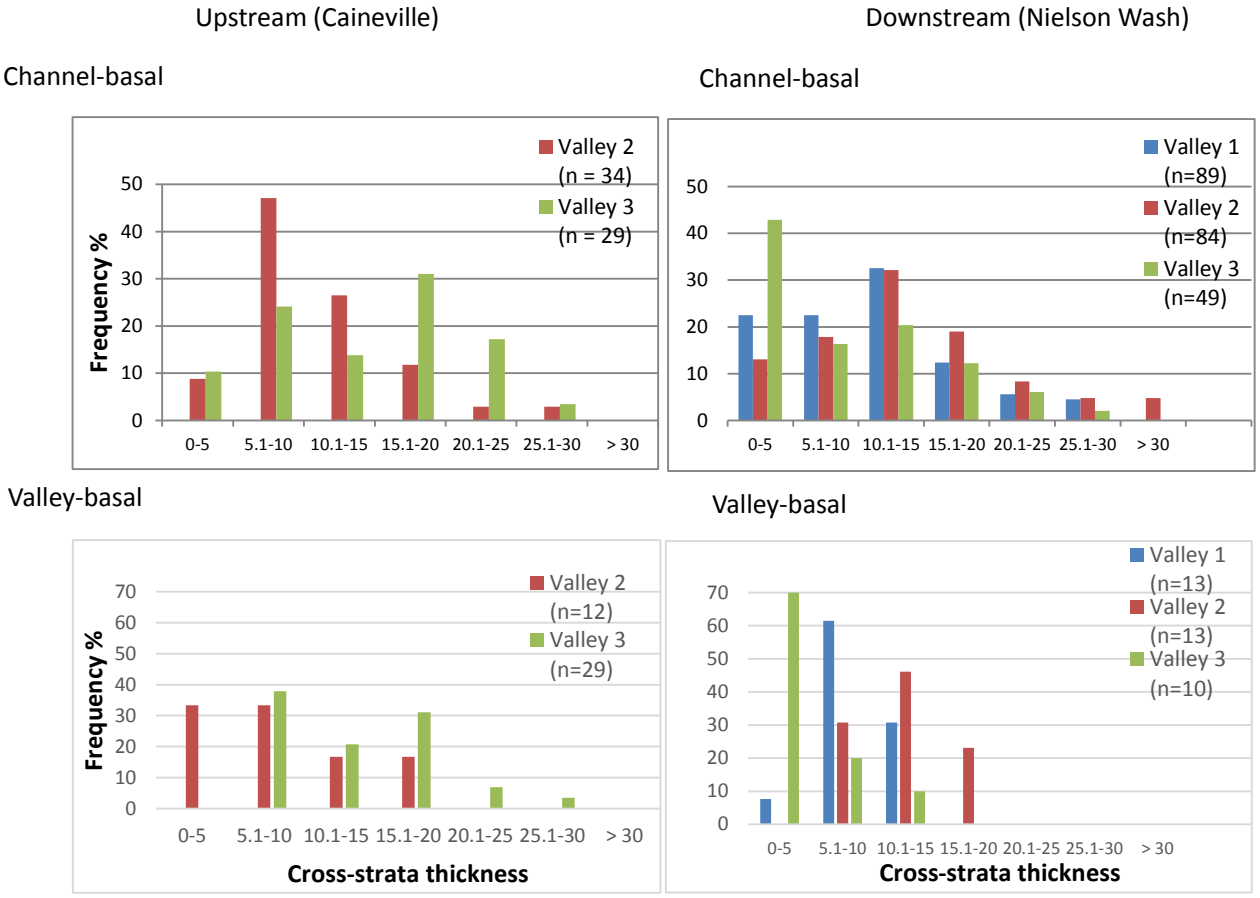

Fig. 2. Histogram of cross-strata thickness of fluvial sandstones at the base of the channels in Valley 1, Valley 2, and Valley 3 (top) and at the base of the valley . Cross-strata thickness at the base of the channels in the valleys is overall larger than that at the base of the valley.

Table 2: Comparison of cross-strata thickness of fluvial sandstones at the base of the channels in Valley 1, Valley 2, and Valley 3 and at the base of the valley in the upstream Caineville and downstream Nielson Wash area.

	Upstream (Caineville)			***Downstream (Nielson Wash)***		
Cross-strata location	Total Samples	Avg. Cross-strata thickness (cm)	Standard deviation	Total Samples	Avg. Cross-strata thickness (cm)	Standard deviation
Channel-basal						
Valley 1	_	_	_	89	12.3	6.8
Valley 2	34	11.9	5.7	84	15.1	8.3
Valley 3	29	15.6	6.3	49	10.2	7.4
Valley-basal						
Valley 1	_	_	_	13	9.9	2.9
Valley 2	12	10.0	5.1	13	13.4	3.6
Valley 3	29	13.9	5.9	10	6.2	3.3

Table 3: Comparison of estimated water depths of the valley-filling and the valley-formative channels in Valley 1, Valley 2, and Valley 3 in the upstream Caineville and downstream Nielson Wash area.

	Upstream (Caineville)		***Downstream (Nielson Wash)***	
	Average dune height (cm) (Eq. 3.1)	Estimated water depth (m)	Average dune height (cm) (Eq. 3.1)	Estimated water depth (m)
Valley-filling channels				
Valley 1	_	_	36 ± 22	2.9 ± 1.9
Valley 2	35 ± 18	2.8 ± 1.6	44 ± 26	3.5 ± 2.3
Valley 3	45 ± 21	3.6 ± 1.9	30 ± 23	2.4 ± 1.9
Valley-formative channels				
Valley 1	_	_	29 ± 11	2.3 ± 1.0
Valley 2	29 ± 17	2.3 ± 1.4	39 ± 14	3.1 ± 1.4
Valley 3	40 ± 20	3.2 ± 1.8	18 ± 11	1.4 ± 0.9

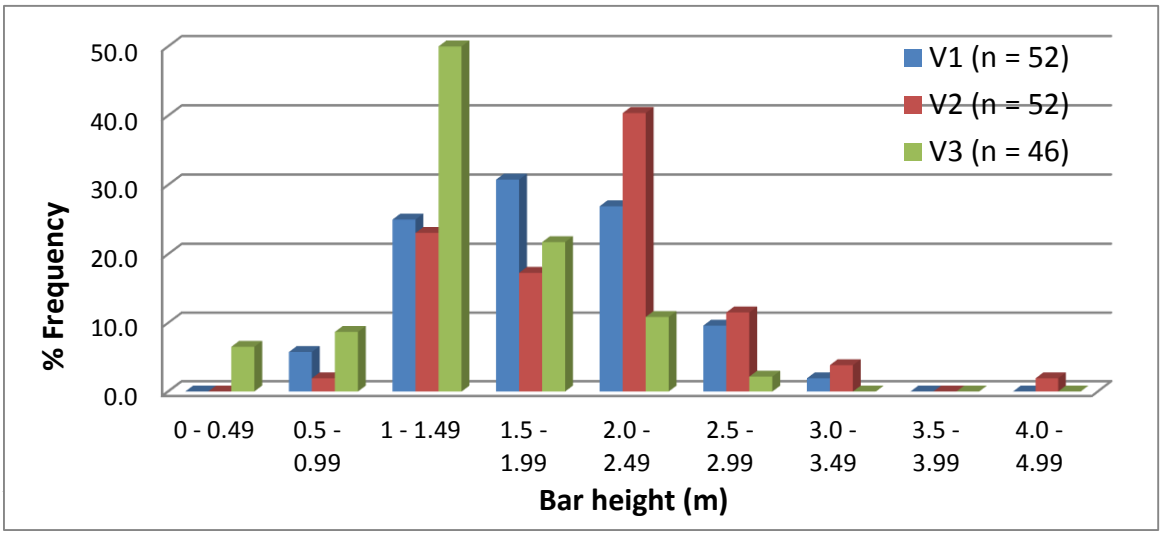

Fig. 3. Histogram of bar thickness of fluvial sandstones in V1, V2 and V3 in Nielson Wash area. Bar thickness in V2 is larger than that in V1 and V3.

Table 4. Analysis of bar thickness and flow depth for the formative rivers within V1, V2, and V3 in Nielson Wash area

Incised valley	Maximum bar thickness from field data (m)	Average bar thickness (m)	Estimated water depth from bar thickness (m)
V1 (N=52)	3	1.7	2.2
V2 (N=52)	4.1	2.0	2.5
V3 (N=46)	2.9	1.3	1.6

Table 5: Comparison of calculated slopes (in degree) of the valley-filling and the valley-formative channels in Valley 1, Valley 2, and Valley 3 in the upstream Caineville and downstream Nielson Wash area. Channel-basal slopes are overall steeper than that of the valley-basal.

	Upstream (Caineville)			***Downstream (Nielson Wash)***		
	Min	Max	Mean	Min	Max	Mean
Channel-basal slope (degree)						
Valley 1	_	_	_	0.02	0.10	0.03
Valley 2	0.04	0.15	0.06	0.02	0.08	0.03
Valley 3	0.02	0.05	0.02	0.01	0.11	0.02
Valley-basal slope (degree)						
Valley 1	_	_	_	0.031	0.08	0.05
Valley 2	0.04	0.18	0.07	0.024	0.06	0.04
Valley 3	0.02	0.06	0.03	0.020	0.09	0.03